Distribution Agreement

In presenting this thesis or dissertation as a partial fulfillment of the requirements for an advanced degree from Emory University, I hereby grant to Emory University and its agents the non-exclusive license to archive, make accessible, and display my thesis or dissertation in whole or in part in all forms of media, now or hereafter known, including display on the world wide web. I understand that I may select some access restrictions as part of the online submission of this thesis or dissertation. I retain all ownership rights to the copyright of the thesis or dissertation. I also retain the right to use in future works (such as articles or books) all or part of this thesis or dissertation.

Signature: _____ _____

Date

Mechanism of Transmembrane Domain Driven Desmoglein Raft Association in Desmosome Assembly

By

Stephanie Zimmer
Doctor of Philosophy

Graduate Division of Biological and Biomedical Science
Biochemistry, Cell and Developmental Biology

_____
Andrew P. Kowalczyk, Ph.D.
Advisor

_____
Victor Faundez, M.D., Ph.D.
Committee Member

_____
John R. Hepler, Ph.D.
Committee Member

_____
Michael Koval, Ph.D.
Committee Member

_____
Winfield S. Sale, Ph.D.
Committee Member

Accepted:

_____
Lisa A. Tedesco, Ph.D.
Dean of the James T. Laney School of Graduate Studies

_____
Date

Mechanism of Transmembrane Domain Driven Desmoglein Raft Association in Desmosome Assembly

By

Stephanie Zimmer
M.Sc., Drexel University, 2015
B.S., Drexel University, 2015

Advisor: Andrew P. Kowalczyk, Ph.D.

An abstract of a dissertation submitted to the Faculty of the James T. Laney School of Graduate Studies of Emory University in partial fulfillment of the requirement for the degree of Doctor of Philosophy in Biochemistry, Cell and Developmental Biology

2021

Abstract

Mechanism of Transmembrane Domain Driven Desmoglein Raft Association in Desmosome Assembly

By Stephanie Zimmer

Desmosomes link cytoskeletal elements of adjacent cells through a series of protein-protein interactions to confer robust mechanical cell adhesion and promote epidermal integrity. Mutations in the genes encoding the desmosomal proteins, such as desmoglein-1 (DSG1), can cause skin fragility diseases such as palmoplantar keratoderma (PPK) or **s**evere dermatitis, multiple **a**llergies, and **m**etabolic wasting (SAM) syndrome. The desmosome has been characterized as a mesoscale lipid raft membrane microdomain whose assembly relies on raft association. Lipid rafts are sphingolipid- and cholesterol-enriched functional ordered plasma membrane regions, yet the relevance of the desmosome as a lipid raft and the mechanism driving raft association of the desmosomal proteins remains unclear. Physical properties of single-pass transmembrane domains (TMDs), including length, exposed surface area, and palmitoylation drive raft association. Furthermore, we have identified disease-causing $DSG1_{TMD}$ mutations in patients with PPK and SAM syndrome which obstruct these properties. Therefore, we hypothesize that $DSG1_{TMD}$ physical properties dictate raft association and desmosome assembly while mutations disrupting these properties cause disease. We designed and expressed a panel of $Dsg1_{TMD}$-GFP variants in DSG-null cells to individually assess the contribution of each physical property towards Dsg1 raft association, desmosome assembly, and function. TMD length and exposed surface area but not palmitoylation contributed to DSG raft association which correlated with desmosome quantity and function. However, we could not rule out whether a motif within the $Dsg1_{TMD}$ sequence contributed to raft association. Furthermore, we identified a $Dsg1_{TMD}$-GFP variant with a scrambled sequence which uncoupled raft association from desmosome assembly and function. We propose an amended model of desmosome assembly in which raft association of desmosomal cadherins in concert with protein-protein interactions drives segregation from adherens junctions while promoting further desmosome assembly by stabilizing nascent desmosomal clusters. We start with a detailed overview of the current understanding of desmosome assembly followed by a description of our DSG-null model and the use of this model to differentiate pathomechanisms of two disease-causing $DSG1_{TMD}$ mutations. We characterize the $Dsg1_{TMD}$ variant panel and then conclude with a series of future directions to address the new questions uncovered by this work.

Mechanism of Transmembrane Domain Driven Desmoglein Raft Association in Desmosome Assembly

By

Stephanie Zimmer

M.Sc., Drexel University, 2015

Advisor: Andrew P. Kowalczyk, Ph.D.

A dissertation submitted to the Faculty of the James T. Laney School of Graduate Studies of Emory University in partial fulfillment of the requirements for the degree of Doctor of Philosophy in Biochemistry, Cell and Development Biology

2021

Table of Contents

List of Figures

Chapter 1

Chapter 2

Chapter 3

Chapter 4

Chapter 5

List of Tables

Chapter 1

Chapter 3

Chapter 4

Chapter 5

CHAPTER 1

The Desmosome as a Model for Lipid Raft Driven Membrane Domain Organization

This chapter is adapted from:

Zimmer, S. E. and Kowalczyk, A. P. (2020). The Desmosome as a Model for Lipid Raft Driven Membrane Domain Organization. BBA Biomembranes.

ABSTRACT

Desmosomes are cadherin-based adhesion structures that mechanically couple the intermediate filament cytoskeleton of adjacent cells to confer mechanical stress resistance to tissues. We have recently described desmosomes as mesoscale lipid raft membrane domains that depend on raft dynamics for assembly, function, and disassembly. Lipid raft microdomains are regions of the plasma membrane enriched in sphingolipids and cholesterol. These domains participate in membrane domain heterogeneity, signaling and membrane trafficking. Structures found to be dependent on raft dynamics include the post-synaptic density in neurons, the immunological synapse, and intercellular junctions, including desmosomes. In this chapter, we discuss the current state of the desmosome field and put forward new hypotheses for the role of lipid rafts in desmosome adhesion, signaling and epidermal homeostasis which will be addressed in subsequent chapters. Furthermore, we propose that differential lipid raft affinity of intercellular junction proteins is a central driving force in the organization of the epithelial apical junctional complex.

INTRODUCTION

1.1 Plasma membrane organization and intercellular junctions

The establishment of plasma membrane heterogeneity represents a fundamental mechanism by which various cellular activities are compartmentalized at the cell surface. This organization is achieved through the formation of membrane domains where specific sets of proteins, lipids, and carbohydrates coalesce to carry out distinct functions such as signaling, transport, and adhesion (2). Prominent examples of these domains include the post-synaptic density in neurons, the immunological synapse, and intercellular junction complexes (3-6). It is widely appreciated that key aspects of plasma membrane heterogeneity are driven by protein-protein interactions that mediate the formation of macromolecular complexes. It is also clear that the lipid composition of the plasma membrane is heterogeneous, and protein-lipid and lipid-lipid associations are central factors in establishing membrane domain specialization.

We recently reported that the desmosome is a specialized membrane domain with properties of a mesoscale (intermediately-sized, 10-1000nm) lipid raft (6). Lipid rafts have emerged as domains essential for membrane organization and specialization (Figure 1.1). Lipid rafts are transient, 10-200nm clusters of protein and lipid nanodomains that can further assemble into larger, more stable microdomains through protein-protein and protein-lipid interactions (2). Lipid rafts are enriched in sphingolipids and cholesterol, are detergent-resistant, and are more ordered than surrounding membrane regions. Importantly, only a specific subset of proteins associate with lipid rafts, thus providing a mechanism for collecting particular proteins into functional scaffolds while selectively excluding non-raft proteins. In cells, lipid rafts have been shown to be essential for numerous processes, including the polarization of the epithelial apical membrane, immunological signaling, and host-pathogen interactions (2, 4, 7, 8). In recent years,

evidence for the involvement of lipid rafts in intercellular junctions, particularly desmosomes, has emerged (6, 9).

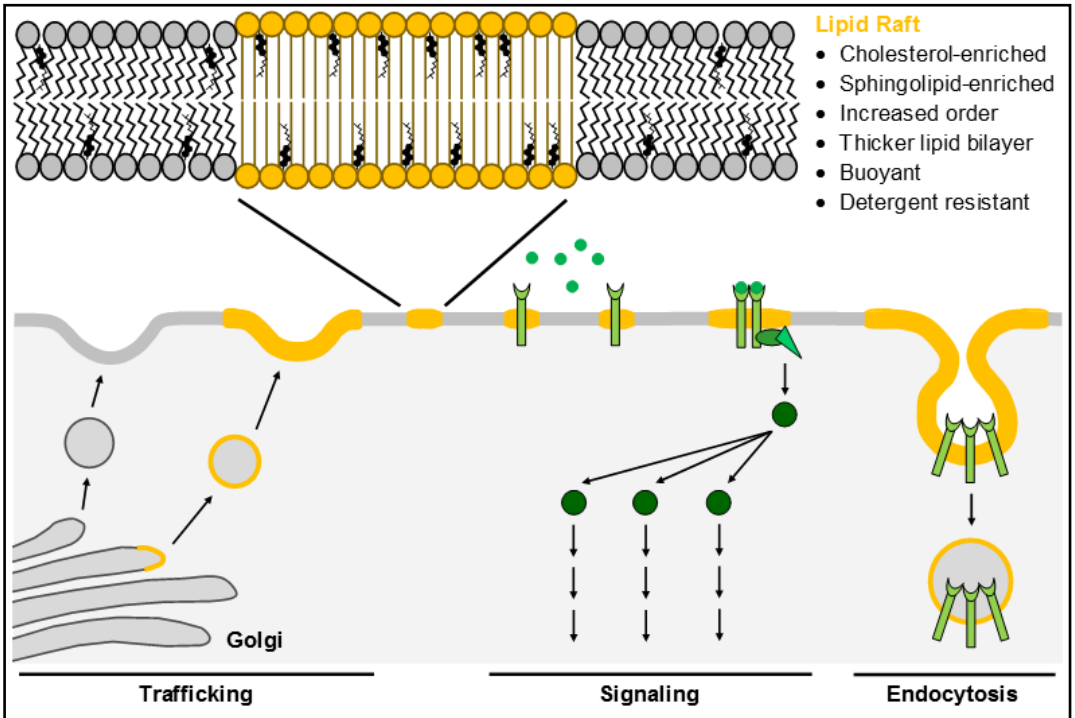

Figure 1.1: **Lipid raft composition and function.** Lipid rafts are cholesterol and sphingolipid-enriched membrane microdomains, which cluster proteins for cell functions such as trafficking, signaling, and endocytosis. Raft membranes are more ordered with thicker lipid bilayers than surrounding membranes and are experimentally characterized by detergent resistance and buoyancy on sucrose gradients.

Intercellular junction complexes, including tight junctions, gap junctions, adherens junctions, and desmosomes, form at sites of cell-cell contact to mediate cell-cell adhesion and communication (Figure 1.2). These junctions exhibit different molecular features that contribute to their differential functions in epithelial biology. Tight junctions are continuous, anastomosing strands of membrane contact that form barriers to establish tissue compartmentalization and to regulate paracellular solute flow (10). Multi-pass transmembrane proteins, including claudins and occludin, associate with the actin cytoskeleton through adaptor proteins, including zona occludens proteins (e.g., ZO-1, ZO-2), cingulin, and others (11, 12). Gap junctions allow solutes to pass between adjacent cells by forming pores composed of two connexons, one in each cell membrane,

which are complexes of six transmembrane proteins called connexins (13). Though functionally and morphologically distinct, adherens junctions and desmosomes are both anchoring junctions that mediate adhesion at sites of cell-cell contact. Adherens Junctions are composed of calcium-dependent classical cadherins and intracellular adaptor proteins, β-catenin and α-catenin, that link the cadherins to the actin cytoskeleton (14). Desmosomes are composed of calcium-dependent desmosomal cadherins and intracellular adaptor proteins, plakoglobin (PG), plakophilin (PKP), and desmoplakin (DP), that link the cadherins to the intermediate filament cytoskeleton (15). Thus, cells assemble a variety of specialized intercellular contacts required for the complex processes that occur during development and adult tissue homeostasis.

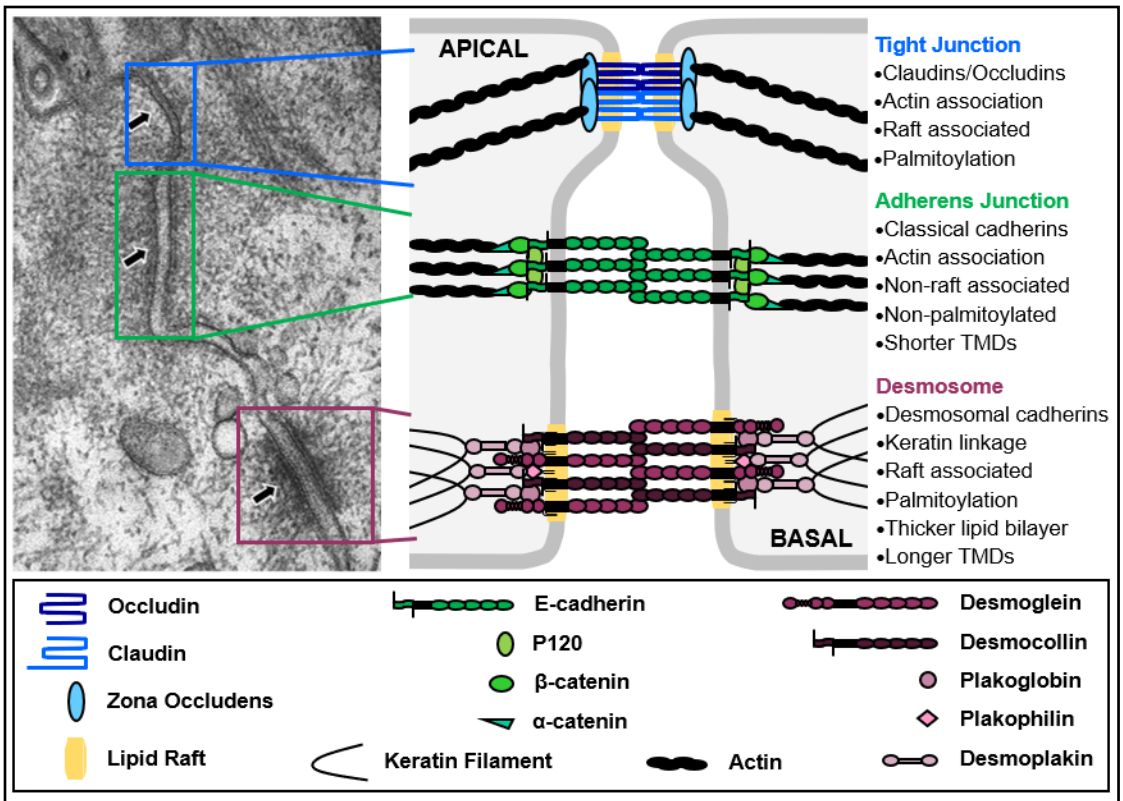

Figure 1.2: **Intercellular junction structure, composition, and characteristics.** Electron micrograph of polarized rat intestinal mucosa [adapted from Farquhar and Palade] show apical tight junctions (blue), adherens junctions (green) and desmosomes (purple). In tight junctions, claudins and occludin link to the actin cytoskeleton through intracellular zona occludens and adaptors to maintain polarity and regulate paracellular ion flow. Adherens junctions mediate calcium-dependent adhesion by anchoring classical cadherin transmembrane proteins to the actin cytoskeleton via intracellular adaptor proteins. Desmosomes also mediate calcium-dependent adhesion but attain a stronger, calcium-independent state, allowing tissues to resist mechanical stress by coupling adjacent cells through desmosomal cadherin transmembrane proteins anchored to intermediate filaments via intracellular adaptor proteins.

We focus on desmosomes with an emphasis on the role of lipid rafts in the formation and function of this unique and important cell junction. We will summarize the current understanding of desmosomal components and how disruption of desmosome function leads to human skin and heart disorders. We then put forward new hypotheses that frame the desmosome as a specialized lipid raft-like membrane domain harboring proteins, lipids, and biophysical features that contribute to both the formation of the desmosome and the exclusion of non-desmosomal proteins.

1.2 Skin and heart require desmosomes to resist mechanical stress

Desmosomes are 0.5μm-1.0μm long protein complexes that anchor keratin filaments to the plasma membrane through a series of protein-protein interactions that mediate robust cell-cell adhesion, thus allowing tissues to resist mechanical stress. The desmosomal cadherins, including desmogleins (DSG) and desmocollins (DSC), are single-pass transmembrane proteins that mediate adhesion through homophilic and heterophilic extracellular interactions between adjacent cells (16-19). The desmosomal cadherins also interact with intracellular armadillo proteins, including PG and PKP, which also bind to DP. DP binds to intermediate filaments, thereby coupling the cytoskeletal elements of adjacent cells. In this manner, desmosomes integrate cytoskeletal networks with adhesive complexes to provide mechanical strength throughout a tissue.

Desmosomes form in all epithelial tissues but are most abundant in the epidermis and heart where their function is crucial. Desmosomal protein composition depends on tissue- and differentiation-specific gene expression (15, 20). In humans, four genes encode DSGs (DSG1-4) and three genes encode DSCs (DSC1-3); expression of at least one DSG and one DSC is necessary for normal desmosome formation (16). DSGs and DSCs each contain five extracellular cadherin repeats, a transmembrane domain, and several intracellular domains, including an intracellular

anchor and a cadherin-like sequence where PG binds (21-23). DSGs also have a proline-rich domain, repeat unit domain, and a DSG terminal domain (24). The function of these unique intracellular domains in DSG is not well understood but may aid in desmosomal cadherin clustering (25, 26).

Desmosomes are essential for epidermal differentiation and barrier formation (27). As a barrier to the external environment, the epidermis is a constantly renewing stratified epithelium composed of proliferating keratinocytes within the basal layer that migrate suprabasally as they differentiate (28). EGFR signaling partly maintains keratinocytes in the basal layer in a proliferative state, where DSG3 and DSC3 are predominantly expressed (29, 30). At the interface between the basal layer and suprabasal layers, DSG1 initiates the differentiation process by interacting with Erbin to inhibit EGFR signaling (31, 32). As keratinocytes differentiate and move suprabasally, DSG3 and DSC3 expression decreases while DSG1 continues to increase, also driving DSC1 expression. Keratin expression switches from keratin-5 and keratin-14 to keratin-1 and keratin-10 and additional epidermal differentiation markers are expressed, such as loricrin and filaggrin (28). These findings suggest that the differential expression pattern of desmosomal cadherin genes is a key driver of the epidermal differentiation process.

Mutations in nearly all desmosomal genes are linked to numerous diseases of the heart and skin. In the heart, desmosomes provide mechanical integrity and cardiomyocyte connectivity in conjunction with adherens junctions and gap junctions in the intercalated discs (33, 34). *DSG2* and *PKP2* mutations cause heart-specific diseases such as arrhythmogenic right ventricular cardiomyopathy/dysplasia and other congenital heart problems while mutations in *DP*, *DSC2*, *PG*, and most other desmosomal genes can cause heart and/or skin disorders (35). Among the many skin-centric desmosomal diseases, common symptoms include woolly hair, hypotrichosis (hair

formation defects), keratoderma (epidermal thickening), and skin fragility due to loss of epidermal integrity. The desmosome is also the target of autoimmune responses and bacterial toxins. Pemphigus vulgaris and pemphigus foliaceus are severe autoimmune epidermal blistering diseases resulting from autoantibodies (IgG) targeting DSG3 and DSG1, respectively (36). These autoantibodies compromise desmosomal adhesion, leading to epidermal fragility and skin blistering. DSG1 can be cleaved by bacterially-produced toxins to cause bullous impetigo and staphylococcal scalded skin syndrome (36), resulting in epidermal blisters that are histologically indistinguishable from pemphigus foliaceus. Collectively, these clinical findings underscore the important role for desmosomes in resisting mechanical stress.

Insight into the importance of individual desmosomal components in epidermal differentiation and homeostasis is also evident from mouse genetic models. Full knockout, conditional knockout, and misexpression of various desmosomal proteins have revealed important roles in both heart and skin function as well as development and differentiation (Table 1.1). Such findings underscore the importance of desmosomal protein expression patterns in driving tissue specific functions and differentiation programs. Thus, many of the desmosomal components are essential not only for epidermal integrity but also for normal development and differentiation.

Table 1.1: Mouse genetic studies reveal important roles for desmosomal proteins in development and homeostasis.

Gene	Expression	Lethality	Observed Defects	References
Dsg1	Knockout	Perinatal	Epidermal water loss, severe blistering	(37)
Dsg2	Knockout	Embryonic	Pre-implantation lethality, potential non-desmosomal role	(38)
	Suprabasal Epidermal Misexpression	Non-lethal	Hyperproliferation, abnormal differentiation, barrier defects	(29)
Dsg3	Knockout	Non-lethal	Separated keratinocytes, weakened desmosomal adhesion in oral mucosa	(39)
	Suprabasal Epidermal Misexpression	Non-lethal	Hyperproliferation, abnormal differentiation, barrier defects	(40)

Dsc1	Knockout	Non-lethal	Epidermal hyperproliferation, loss of cell-cell adhesion	(41)
Dsc3	Knockout	Embryonic	Post-implantation lethality, potentially non-desmosomal role	(42)
	Epidermal Conditional	Non-lethal	Epidermal fragility, hair loss	(43)
	Suprabasal Epidermal Misexpression	Non-lethal	Hyperproliferation, abnormal differentiation, barrier defects	(44)
Pg	Knockout	Embryonic	Heart defects, skin fragility	(45)
Pkp1	Knockout	Postnatal	Epidermal fragility, tight junction defects, growth defects	(46)
Dsp	Knockout	Embryonic	Die at E6.5	(47)
	Epidermal Conditional	Perinatal	Severe skin fragility, disrupted barrier function	(48)

1.3 The desmosome has features characteristic of a lipid raft-like membrane domain

The molecular mechanisms of desmosome formation are not fully understood. Desmosomal cadherin adhesion is necessary for the assembly process, but the mechanisms by which desmosomal cadherins and plaque components coalesce into a densely-packed membrane domain are not clear. A number of studies have now shown that desmosomal proteins associate with lipid rafts and that desmosome assembly, cell-cell adhesion, and desmosome disassembly are all raft-dependent processes (49, 50). Several previous studies have examined the role of raft domains in desmosome assembly (50, 51); this work is reviewed elsewhere (36) and will not be discussed here. Early studies of desmosomes showed that cholesterol and sphingolipids, both of which are enriched in lipid raft membrane domains, are enriched in desmosomes isolated from bovine snout (52, 53). More recently, evidence for lipid raft association has come from sucrose gradient fractionations in which desmosomal components were identified in detergent-resistant membrane (DRM) fractions, starting with the identification of DSG2 (54). Later studies revealed that DSG1, DSG3, DSC2, PG, PKP2, DP, and keratins are all present in DRM fractions (6, 49, 50). These studies also found that depleting cholesterol in cells with methyl-β-cyclodextrin

(mβCD) redistributed desmosomal cadherins along cell borders, reduced adhesion strength, and prevented assembly of desmosomal components without disrupting adherens junction formation (49, 50, 55). Additionally, desmosomal components were shown to colocalize with certain raft markers, including ostreolysin, CD59, and caveolin but not clathrin (49, 50). For ostreolysin, transmission immunoelectron microscopy was used to further show an association with desmosomes which was reduced when cells were treated with mβCD (55). Furthermore, siRNA knockdown of the raft marker, flotillin-2, reduced cell-cell adhesion (56). Collectively, these studies strongly link desmosome assembly and function with lipid rafts.

Studies in model membranes have shown that lipid bilayers composed of longer and saturated acyl chains such as those found in lipid rafts are thicker than those with unsaturated or shorter acyl chains found in non-raft membrane domains (57). In addition, the presence of higher levels of cholesterol in raft domains thickens the bilayer, increases order, and stiffens the membrane (58-61). Using cryo-electron tomography, we found that the lipid bilayer of the plasma membrane within the desmosome is thicker than non-desmosome and desmosome-adjacent bilayers (6). These findings represent the first evidence that a plasma membrane domain known to contain lipid raft associating proteins is thicker than other regions of the plasma membrane. Because desmosomal proteins associate with lipid rafts, disruption of rafts prevents desmosome assembly, and the desmosomal lipid bilayer is thicker than surrounding membrane, we concluded that desmosomes represent a mesoscale, or intermediately-sized, raft-like plasma membrane domain.

1.4 Mechanism of desmosomal protein association with lipid raft membrane microdomains

Association with raft or non-raft lipid microdomains occurs by incompletely understood mechanisms but has been proposed to involve protein-lipid (62) and/or protein-cholesterol (63) interactions mediated by the transmembrane domain (TMD) of integral membrane proteins (64). Recently, three physical properties of TMDs have been shown to dictate the raft affinity of single-pass transmembrane proteins. Collectively termed physiochemical properties, these include TMD length, TMD surface area, and palmitoylation (64-66). Lorent et al. (65) combined these properties into a model that can predict the free energy required for a single-pass transmembrane protein to associate with rafts (Figure 1.3). This model for raft affinity is highly predictive across a wide range of single-pass transmembrane proteins and incorporates TMD length, surface area and palmitoylation as key driving factors in lipid raft association.

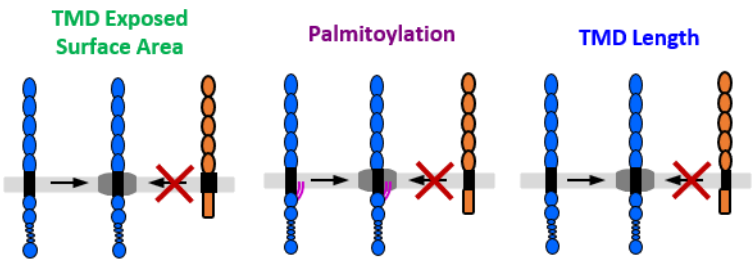

Figure 1.3: TMD physical properties drive raft association. Collectively considering the physical properties of a single-pass transmembrane protein TMD predicts the energy required for that protein to be targeted to a lipid raft membrane microdomain. Long, non-bulky, palmitoylated TMDs yield smaller predicted energies which are more favorable for raft association.

1.4.1 TMD Length

Cholesterol and sphingolipid content increases as membranes are modified along the secretory pathway, leading to thicker lipid bilayers at the plasma membrane compared to the ER and Golgi (67). Similarly, the amino acid (AA) length of TMDs of single-pass transmembrane proteins increases through the secretory pathway such that proteins localized to the ER have the shortest TMDs at about 16AA while those that localize to the plasma membrane are longer at about 21AA (68). Consistent with the predicted increased thickness of raft bilayers in the plasma

membrane, those proteins that partition into lipid rafts possess TMDs that are even longer (about 24AA or more) than a typical non-raft associated plasma membrane protein (64, 65). This feature allows the extended hydrophobic TMD α-helix of raft proteins to associate with extended acyl chains and cholesterol present in lipid raft domains while excluding proteins with shorter TMDs due to hydrophobic mismatch (69, 70). Interestingly, the DSG TMDs are all 24AA in length whereas the DSC TMDs are only 21AA in length even though DSCs are associated with raft domains. These observations highlight the importance of other protein features in regulating raft association, including TMD surface area and palmitoylation.

1.4.2 TMD Surface Area

The exposed surface area of a TMD refers to the area of the collective residue side chains (71). Single-pass transmembrane proteins bearing TMDs with smaller surface areas can partition into rafts to a greater degree due to a smaller energy barrier; these proteins pack into the more ordered environment of the lipid raft more readily than those with larger surface areas. DSG TMDs contain a number of bulky leucine residues such that the surface area may be larger than anticipated for a raft-associated protein. The E-cadherin TMD also contains numerous leucines. These residues have been shown to mediate TMD-TMD dimerization via a leucine zipper-like motif which is important for cell adhesion through mechanisms that are not fully understood (72). Because oligomerization via TMD-TMD dimerization can also increase raft affinity (66), leucine residues in DSGs could be important for DSG dimerization or oligomerization, as well as raft association. This possibility remains to be tested. Likewise, leucine residues are also present in the DSC TMD. These observations raise the possibility of heterodimerization between DSG and DSC, which, when coupled with the longer DSG TMD, could support raft association of DSCs as

well as segregation of nascent adherens junctions and desmosomes. Additional experiments are needed to fully understand how the leucine-rich TMDs of these various cadherins contribute to dimerization, raft association and overall cadherin function for both classical and desmosomal cadherins.

1.4.3 Palmitoylation

The presence of a palmitoyl group on cysteine residues adjacent to TMDs in single-pass transmembrane proteins has also been shown to increase raft association. Palmitoylation is a reversible post-translational modification that adds a 16C saturated acyl chain to cysteine residues (73). For soluble cytoplasmic proteins, palmitoylation localizes a protein to the plasma membrane and is important in regulation, stability, and function (74, 75). Integral membrane proteins are commonly palmitoylated on cysteine residues on the cytoplasmic face of the TMD (73), and this posttranslational modification is recognized as a key raft protein modification (66). All desmosomal cadherins possess membrane proximal cysteines which are well conserved between species (Figure 1.4). Interestingly, palmitoylation of DSG2 regulates trafficking as well as stability of the protein but is not necessary for raft association (76). DSG3, also, does not require palmitoylation for raft association (6). Thus, palmitoylation appears to be important in regulating desmosomal cadherin dynamics, but it does not appear to be necessary for raft association.

Proteins are palmitoylated by palmitoyl acyl transferases (PATs), of which there are 23 in humans (77). Named for their conserved DHHC (Asp-His-His-Cys) motif, the DHHC proteins are multimeric transmembrane proteins with differential tissue expression that can localize throughout membrane compartments, including ER, Golgi, and plasma membrane to palmitoylate targets (78, 79). While the PAT(s) responsible for palmitoylating desmosomal proteins remain to be identified,

DHHC13 and DHHC21 have been shown to be important in keratinocyte proliferation and hair follicle differentiation in the epidermis (80-82). There is some promiscuity among DHHC targets as many have been shown to be palmitoylated by multiple DHHC forms in cultured cells, raising the possibility that multiple DHHC proteins are capable of palmitoylating desmosomal proteins.

In contrast to the desmosomal cadherins, palmitoylation of the cytoplasmic PKPs is necessary for raft association and for desmosome assembly. Loss of membrane association and reduced Triton X-100 insolubility were seen in palmitoylation-deficient PKP2 and PKP3 mutants. Furthermore, expression of these mutants resulted in the loss of desmosome assembly and adhesion in a dominant-negative fashion. PKPs are thought to function by recruiting and clustering other desmosomal proteins. This is accomplished through actively guiding DP and intermediate filaments to sites of cell-cell contact and clustering desmosomal cadherins at the cell surface (83-85). Though PKP1 is also palmitoylated, no studies have been done to address the impact of the modification on PKP1 function. Though similar, the PKP proteins serve different purposes. For example, PKP1 but not PKP3 regulates desmoglein clustering (86). Disease-causing truncation mutations in PKP1 lead to reduced size and number of desmosomes in patients (87, 88) while overexpression of PKP1 can increase desmosome length and adhesion strength (89). PKP3 overexpression also increases desmosome size and stability by upregulating the expression of other

Figure 1.4: Desmosomal cadherins are palmitoylated at intracellular membrane-proximal cysteine residues. Human sequences for DSG1-4 and DSC1-3 showing TMD residues in blue and palmitoylated cysteines highlighted in yellow. Palmitoylation at DSG2 cysteine residues has been experimentally verified while only presence of palmitoyl groups on DSG1-DSG3 and DSC2-3 but not exact sites has been shown.

desmosomal proteins (90). PKP palmitoylation likely enhances membrane association during clustering of desmosomal cytoplasmic plaque proteins, thereby promoting the lateral packing of desmosomal proteins along the two-dimensional plane of the plasma membrane.

1.5 Role of raft association in disease

Lipid raft associated proteins have been implicated in a variety of human diseases. Well-studied examples of diseases in which raft protein function is disrupted include Alzheimer's Disease and Prion Diseases (91). Various pathogens also have been shown to utilize rafts for various steps in their life cycles (91). A possible link between lipid raft disruption and atopic dermatitis has been identified as genes involved in lipid biosynthesis were found to be down-regulated in patient skin relative to healthy skin (92). Furthermore, expression profiles were similar between patient skin and cultured keratinocytes in which lipid rafts were disrupted by mβCD treatment, including the same lipid biosynthesis genes downregulated in patient skin (93). These findings raise the possibility that altered raft function or the inability of proteins to associate with rafts could represent an underlying disease pathomechanism.

Recently, we identified a dominantly-inherited disease-causing mutation in the *DSG1* gene that causes a glycine-to-arginine substitution in the transmembrane spanning region of the DSG1 protein (6). The individuals carrying this mutation were diagnosed with **s**evere dermatitis, multiple **a**llergies, and **m**etabolic wasting (SAM) syndrome. SAM syndrome is characterized by epidermal thickening, fragility, and barrier defects (27). Studies of this TMD mutation revealed that the mutant DSG1 protein was excluded from lipid rafts and failed to assemble into desmosomes both in patient skin and in cell culture models (6). Molecular modeling predicts that the glycine-to-arginine substitution in the DSG1 TMD shortens the run of hydrophobic amino acids, resulting in

hydrophobic mismatch with the thicker lipid bilayer present in the raft-like desmosomal membrane domain. This mutation appears to be the first example of a mutation that compromises raft association as part of the disease pathomechanism.

The mutation in the DSG1 TMD that causes SAM syndrome may represent a newly appreciated class of mutations that disrupt raft association and cause human disease, particularly among proteins bearing mutations in the TMD. Disease-causing glycine-to-arginine substitutions have been identified in the TMDs of other single-pass transmembrane proteins including myelin protein zero (MPZ) and FGFR3 which cause Marie-Charcot-Tooth Syndrome (94, 95) and Achondroplasia (96), respectively. Both proteins have been identified in proteomic screens assaying raft association (97, 98). Though raft association of FGFR3 has not been further verified, MPZ has been identified in DRMs from adult peripheral nerve myelin (99, 100). In both examples, the mutation was found to disrupt TMD-TMD mediated interactions. As oligomerization is known to increase raft affinity (101), loss of lipid raft association could be central to the disease mechanisms of these mutations. Further investigation is warranted for these and other mutations that might involve loss of raft association as part of an underlying disease pathomechanism.

1.6 A new model for epithelial intercellular junction organization: lipid rafts as a driving force for the assembly and segregation of junctional complexes

The association of desmosomes with lipid rafts is emerging as a mechanism fundamental to the organization of the desmosomal membrane domain. A key question emerging from this work is how raft association of desmosomal components integrates with the assembly mechanisms of other junctional complexes, including adherens junctions. In contrast to desmosomes, adherens junction components do not associate with lipid rafts biochemically (5, 50). However, desmosome

assembly requires E-cadherin-based adhesion (102-105). The mechanisms by which adherens junctions regulate desmosome assembly are not fully understood, although adherens junctions and desmosomal proteins engage in a number of overlapping protein-protein interactions (106). Recently, Shafraz et al. (107) showed that the requirement of adherens junction components for desmosome assembly may be driven by a direct interaction between E-cadherin and desmosomal cadherins. Using a combination of atomic force microscopy and cell biological approaches, E-cadherin trans-homodimerization was found to initiate both adherens junction and desmosome assembly by allowing for the brief cis-heterodimerization of E-cadherin and DSG2 (107). Concurrently, short-lived DSC2 homodimers give way to DSG2:DSC2 heterodimers when the E-cadherin:DSG heterodimers disengage. In line with these findings, others have shown that the relative cell surface levels of DSGs and DSCs regulate the adhesion process (16), but the recruitment of desmosomal cadherins begins with DSC clustering at the cell surface (108, 109). DSG and associated armadillo proteins then stabilize the DSC clusters (108, 109).

If adherens junction and desmosomal proteins can associate, how do these structures resolve into distinct membrane domains? One explanation is differential protein affinities. Both PG and PKPs are required for the formation of distinct, non-continuous desmosomes (83). Mixed adherens/desmosome junctions were identified in cardiac tissue from mice lacking Pg (110). PG is unstable in the absence of a desmosomal cadherin (111), yet is also capable of binding E-cadherin and α-catenin in place of β-catenin. However, due to overlapping binding sites, PG cannot bind α-catenin if it is bound to a desmosomal cadherin, thus excluding the desmosomal cadherin:PG complex and likely contributing to segregation of the two junctions (106). These

examples highlight how differential protein affinities contribute to the assembly of different junctions.

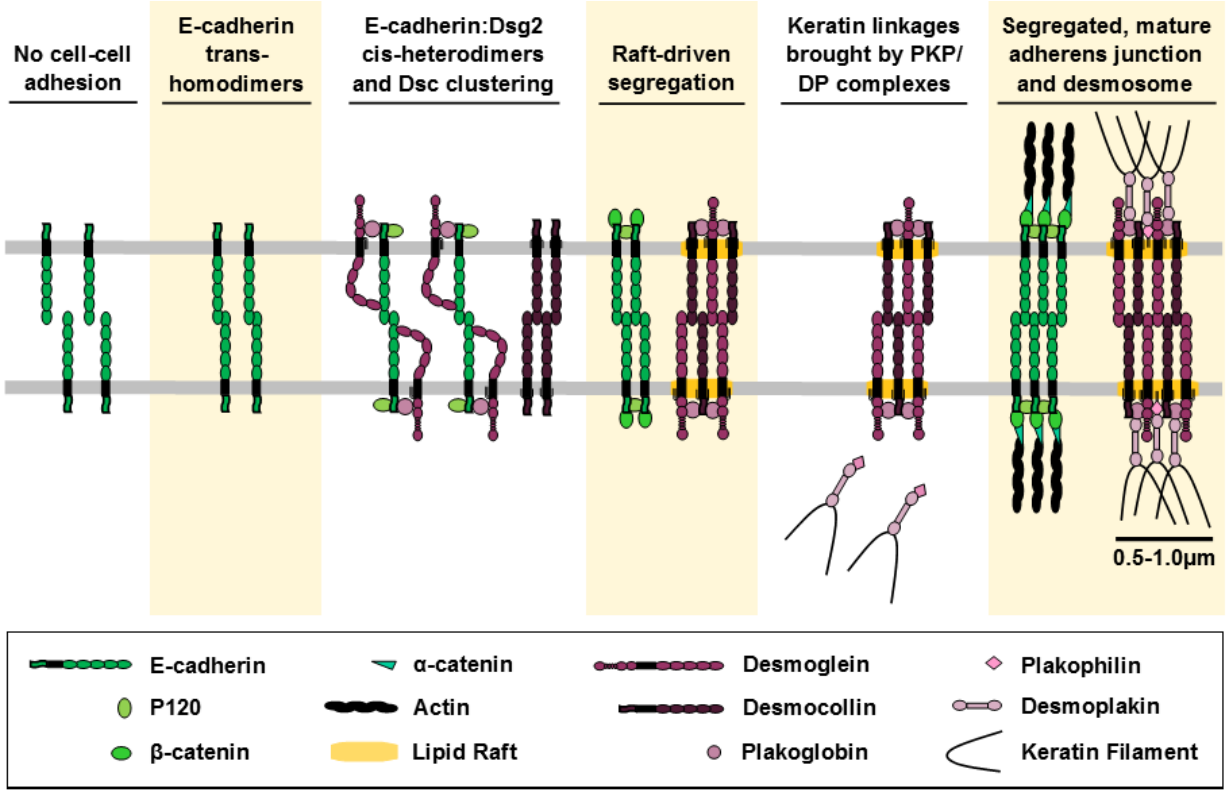

Figure 1.5: Lipid rafts drive segregation of adherens junctions and desmosomes during junction assembly. Transient interactions between desmosomal and classical cadherins coordinate cadherin clustering at the cell surface. Adaptor proteins stabilize nascent cadherin clusters. Interplay between cadherins and membrane lipids leads to accumulation of cholesterol and raft lipids around desmosomal cadherin clusters and drives segregation of adherens junction and desmosome components. PKPs further enhance desmosome formation and segregation from adherens junctions by promoting raft-associated clustering and by promoting DP and keratin linkages.

We propose that a second driving force to segregate adherens junctions and desmosomes is differential affinity for lipid rafts (Figure 1.5). In contrast to desmosomal proteins, adherens junction components show poor affinity for raft fractions (5, 6, 50). For example, when the DSG TMD is replaced with the E-cadherin TMD, the chimeric cadherin fails to associate with lipid rafts (6). In addition, unlike desmosomal cadherins, E-cadherin is not palmitoylated (112), further reducing raft affinity. As discussed above, E-cadherin and DSG associate at the plasma membrane during initial cell-cell contact formation. Super-resolution imaging shows that these nascent complexes then resolve into separate membrane domains as junction formation matures (107). It

is likely that desmosomal cadherin association with raft lipids harboring longer acyl chains and with higher levels of cholesterol leads to thickening of the lipid bilayer and the formation of a membrane environment energetically unfavorable for the shorter E-cadherin TMD. Through this mechanism, E-cadherin and cytoplasmic plaque proteins associated with E-cadherin would be excluded from the desmosome as junction formation proceeds. Similarly, the palmitoylated desmosomal plaque proteins, particularly PKPs, would further drive coalescence into a raft domain and further exclude adherens junction components. Such a mechanism would allow for coordinated assembly of the two junctions followed by subsequent resolution into distinct membrane domains.

For these proposed mechanisms to work, we would expect the DSG TMD to be critical for the raft association mechanism while loss of DSG raft association would be expected to affect normal processes of desmosome assembly and function. Therefore, we hypothesize that DSG TMD physical properties dictate lipid raft domain association and desmosome assembly while mutations disrupting these properties cause disease. We have already discussed the existence of a disease-causing glycine-to-arginine substitution in the DSG1 TMD identified in a patient with SAM syndrome. In Chapter 2, we will establish a new DSG-null model system for the study of DSGs. In Chapter 3, we will explore the effects of a different glycine-to-arginine substitution in the DSG1 TMD identified in a patient with palmoplantar keratoderma in comparison to that of the SAM syndrome patient. The findings in Chapter 3 further establish an important role for the DSG1 TMD in raft association, desmosome assembly, and function. Chapter 4 will continue in this vein by exploring the properties of the DSG1 TMD that drive DSG raft association and the consequences of losing DSG1 raft association. This will be explored by using $DSG1_{TMD}$ variants in which one of the physical properties discussed above will be altered to individually address the

contribution of TMD length, exposed surface area, and palmitoylation. In both chapters, we will utilize the DSG-null cells described in Chapter 2 to stably express our disease-causing DSG1 mutations and $DSG1_{TMD}$ variants. With these stable cell lines, we will determine the ability of these various constructs to drive raft association, how that affects the raft association of other desmosomal proteins, overall desmosomal assembly, and desmosome function. Through these experiments, we will further our understanding of the relationship between raft association and desmosome assembly and function as well as uncover new potential mechanisms. Our findings support an alteration to the model of desmosome assembly described above where raft association nucleates DSC clusters which are joined by raft-associated DSG and PG complexes segregating from adherens junctions. This dissertation will be concluded with a discussion of future directions and conclusions.

1.7 ACKNOWLEDGEMENTS

The authors would like to thank members of the Kowalczyk lab as well as Drs. Kathleen J. Green and Sara N. Stahley for helpful suggestions in the preparation of this manuscript. Work in the Kowalczyk lab is supported by grants R01AR050501 and R01AR048266 from the National Institutes of Health. SEZ was supported by a training grant from the National Institutes of Health T32GM008367.

CHAPTER 2

Establishing a New Model System to Study Desmoglein Function

ABSTRACT

Desmosome assembly is driven by a series of protein-protein interactions involving both adherens junction and desmosomal components that results in independent mature junctions and robust cell-cell adhesion, yet these interactions remain poorly understood. We created a desmoglein (DSG)-null A431 cell line to better understand early stages of desmosome assembly and study the raft associating mechanisms of desmogleins. Desmosomal proteins are mislocalized in these cells resulting in little desmosome-mediated cell-cell adhesion, but exogenous expression of Dsg species rescues these phenotypes. These cells can be used for expressing disease-causing DSG mutants or other DSG variants to better understand the role of the different DSG domains during desmosomal processes, including assembly and disassembly and to determine the mechanism of adherens junction-desmosome segregation during junction assembly.

2.1 INTRODUCTION

Desmosome assembly requires the presence of both desmogleins (DSG) and desmocollins (DSC) (16). The four genes that encode the DSG species in humans are differentially expressed (15, 20). While DSG2 is ubiquitous through epithelial and cardiac tissues, DSG1, DSG3, and DSG4 are confined to different layers of the epidermis where their expression is regulated by differentiation state (20). DSG3 is predominantly expressed in the basal, proliferating layers but decreases as DSG1 levels increase through the upper, differentiating layers (30-32). DSG4 is largely restricted to hair follicles (113).

Much remains unknown about desmosomal processes and how desmosomal proteins and their differential expression drive those processes. Prior work with desmosomal proteins has often involved transient or stable transfection of a tagged protein of interest in a variety of cell lines alongside the endogenous protein of interest (6, 76, 112). Our earlier work with Dsg1 and Dsg3 TMD constructs has also used this method (6), but the possible masking or muting of biological effects by the presence of endogenous protein raised concerns about the continued use of this method.

To reduce the potential contributions of endogenous desmosomal protein, we used CRISPR-Cas9 to knockout DSG2 in A431 cells. Characterization of these DSG2-KO A431 cells revealed total loss of DSG2 with no change in expression levels of other desmosomal proteins. As DSG2 is the sole DSG species in A431 cells, desmosomal proteins, particularly desmoplakin (DP), were mislocalized, raft association of DP and PG reduced, and cell-cell adhesion weakened by the loss of DSG2. Exogenous expression of DSG species rescued these defects. With a strong, rescuable desmosomal phenotype, these DSG-null cells are well-suited for understanding the role that DSGs play in desmosomal processes.

2.2 RESULTS

2.2.1 DSG-null cell characterization reveals desmosomal defects

We chose A431 cells to create a DSG-null cell line. A431 cells are an immortal human epidermoid carcinoma cell line commonly used in desmosomal studies (76, 114, 115). We first determined the DSG expression profile of A431s using immunofluorescence and western blot analysis and found that DSG2 was predominantly expressed with no evidence of DSG1 or DSG3 at the protein level (Figure 2.1A). In contrast, positive controls for the DSG1, DSG2, and DSG3 antibodies used readily detected Dsg1 in A431 cells transfected with a Dsg1 construct and detected both DSG2 and DSG3 in HaCaTs, an immortal human keratinocyte cell line (20, 116). Our collaborator, Daniel Conway, used CRISPR-Cas9 to knockout DSG2 in these A431 cells, and we characterized them.

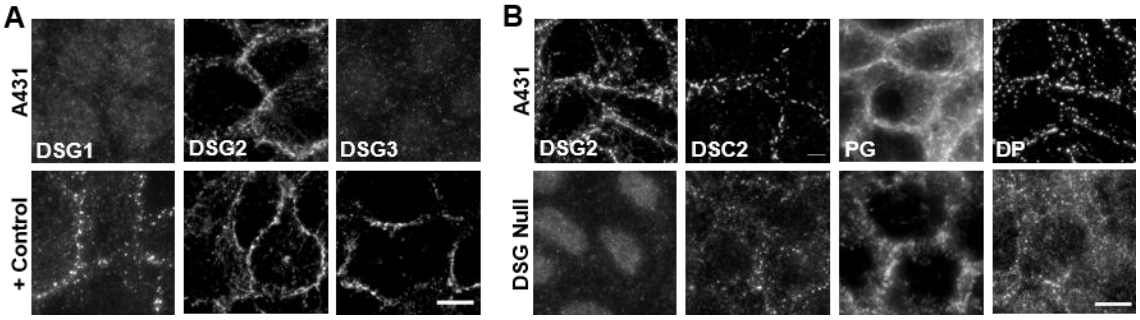

Figure 2.1: DSG2 knockout in A431 cells causes desmosomal protein mislocalization. A) Widefield immunofluorescence images show DSG2 but not DSG1 or DSG3 is highly expressed in A431 cells. DSG1 positive control is A431s transfected with an mDsg1 construct. DSG2 and DSG3 are endogenously expressed in HaCaTs. B) Widefield immunofluorescence images show lack of DSG2 staining in DSG2 KO cells and altered localization of DSC2, PG, and DP. Scale bars = 10 μm.

We verified the loss of DSG2 expression by both immunofluorescence (Figure 2.1B) and western blot analysis of whole cell lysates (Figure 2.2A). We also detected low DSG3 levels that were absent in the parental A431 cells by immunofluorescence (data not shown). However, in the absence of DSG2, DP, plakoglobin (PG), and DSC2 all experienced altered localization. In normal conditions, DP appears in discrete, border-localized desmosomal puncta, but this localization is lost in the DSG-null cells. While DSC2 appeared to form border-localized desmosomal puncta,

these were smaller in size and less organized than in the parental cells. PG maintained border localization but appeared reduced in intensity. PG also interacts with components of adherens junctions (117), so this observation may be due to enhanced localization with adherens junctions. Though the dispersal of several desmosomal components away from border puncta gave the appearance of reduced protein expression, western blot analysis of whole cell lysates revealed no statistically significant difference between the expression levels of DP, DSC2, PG, or E-cadherin (Figure 2.2). Therefore, even in the presence of slightly upregulated DSG3, loss of DSG2 expression alters localization but not expression of desmosomal proteins; we consider these cells to be DSG-null.

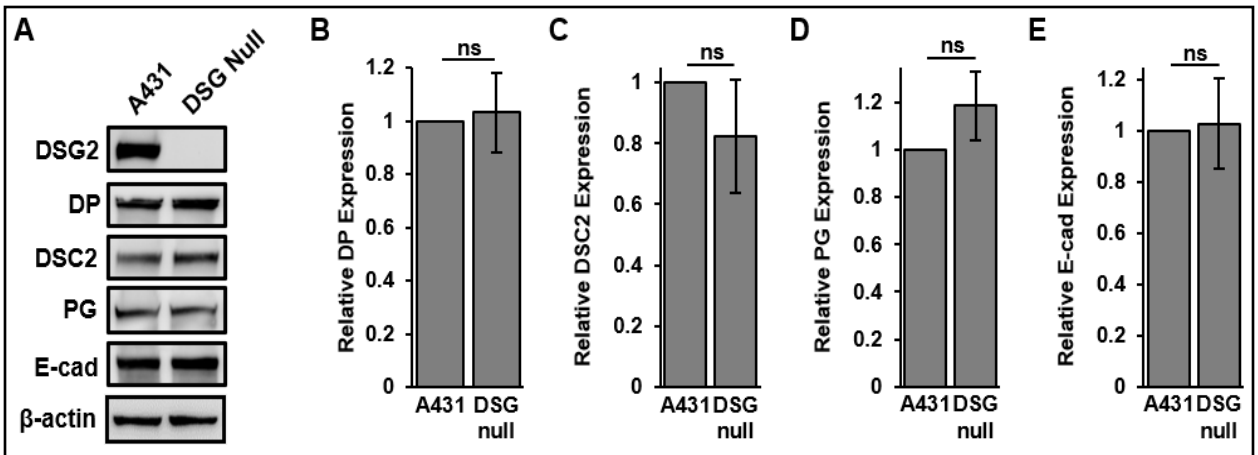

Figure 2.2: DSG2 knockout in A431 cells does not affect expression levels of other desmosomal proteins or E-cadherin. A) Western blots showing DSG2-KO in A431 cells with no change in levels of DP, DSC2, PG, or E-cadherin. β-actin used as loading control. B) Quantification of DP expression levels in A431 parental cells versus DSG2-KO cells. C) Quantification of DSC2 expression levels in A431 parental cells versus DSG2-KO cells. D) Quantification of PG expression levels in A431 parental cells versus DSG2-KO cells. E) Quantification of E-cadherin expression levels in A431 parental cells versus DSG2-KO cells. Error bars show mean +/- SEM (n=4).

Mislocalization of desmosomal proteins in the DSG-null cells suggests that these cells may not assemble desmosomes. The components of mature desmosomes are detergent resistant and associate with rafts (49, 50). Therefore, we can use raft association as a proxy for desmosome formation. We used sucrose gradient fractionations to separate buoyant, detergent-resistant membranes (DRMs) from non-buoyant, non-detergent resistant membranes (non-DRMs) (118).

We found that raft association of DP and PG but not DSC2 were significantly reduced in DSG-null cells compared to A431s (Figure 2.3). This loss of raft association suggests that DSG-null cells do not assemble mature desmosomes.

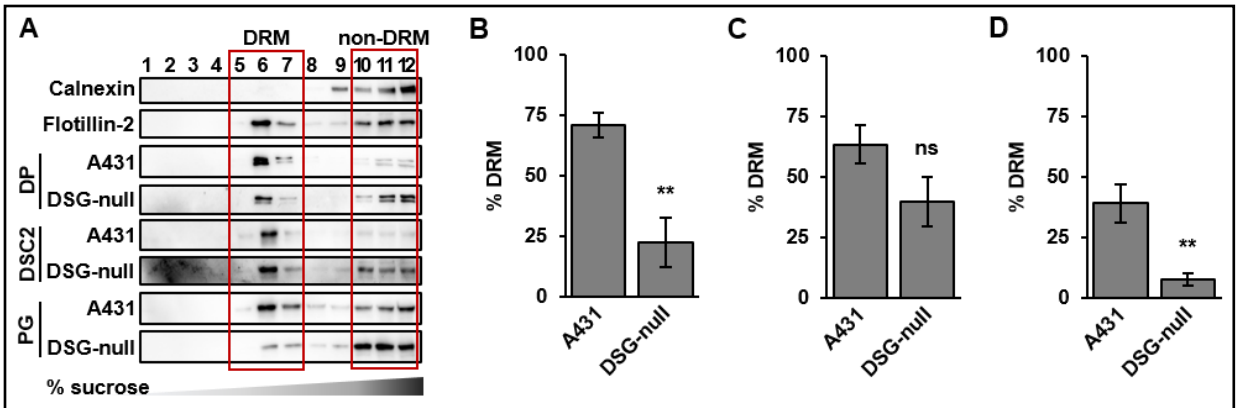

Figure 2.3: Desmosomal proteins exhibit reduced raft association in DSG-null cells. A) Western blots of sucrose gradient fractionations show distribution of DP, DSC2, and PG between DRM and non-DRM fractions in A431 vs DSG-null cells. Calnexin = non-DRM marker. Flotillin-2 = DRM marker. B) Quantification of DP distribution between DRM and non-DRM fractions. C) Quantification of DSC2 distribution between DRM and non-DRM fractions. D) Quantification of PG distribution between DRM and non-DRM fractions. Error bars show mean +/- SEM (n=4). **p < 0.01

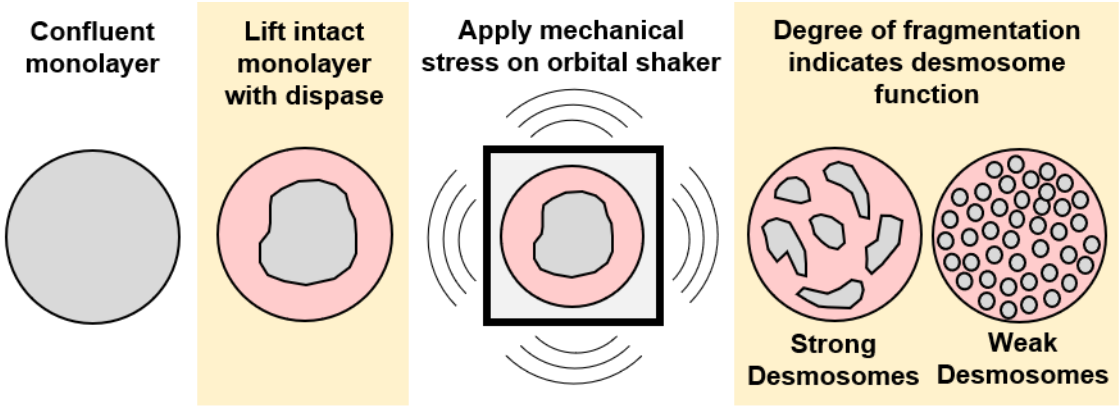

Figure 2.4: Dispase cell dissociation assay tests desmosome strength. Confluent monolayers treated with dispase are lifted from the substrate and undergo mechanical stress on an orbital shaker. Monolayers fragment based on desmosome strength. Few fragments indicate strong desmosomes while many fragments indicate weak desmosomes.

With mislocalized desmosomal components exhibiting reduced raft association indicative of reduced desmosome formation, we next asked if the DSG-null cells formed functional desmosomes. We used a dispase cell dissociation assay which assesses desmosome function by degree of mechanical stress-induced monolayer fragmentation (119). A monolayer of confluent

cells is lifted off its substrate with the enzyme dispase which cleaves cell-substrate interactions while maintaining cell-cell interactions. Monolayers are subjected to mechanical stress on an orbital shaker and the resulting monolayer fragments are counted such that minimal fragmentation correlates with strong, functional desmosomes while extensive fragmentation suggests the presence of weak or non-functional desmosomes (Figure 2.4). DSG-null cell monolayers fragmented significantly more than A431 cell monolayers (Figure 2.5), indicating that desmosome function is reduced in these cells.

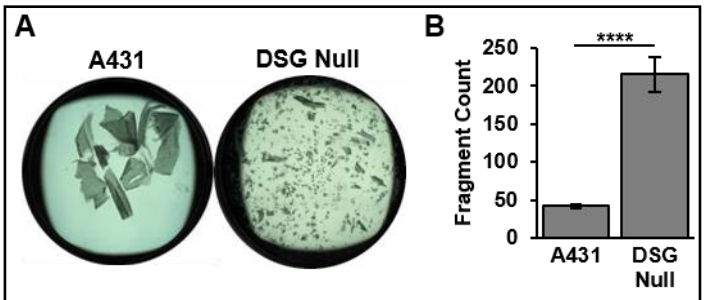

Figure 2.5: DSG-null A431 cells have reduced desmosome function. A) Images show monolayer fragmentation of A431 cells versus DSG-null cells. B) Quantification of A. Error bars show mean +/- SEM (n = 7). ****p < 0.0001

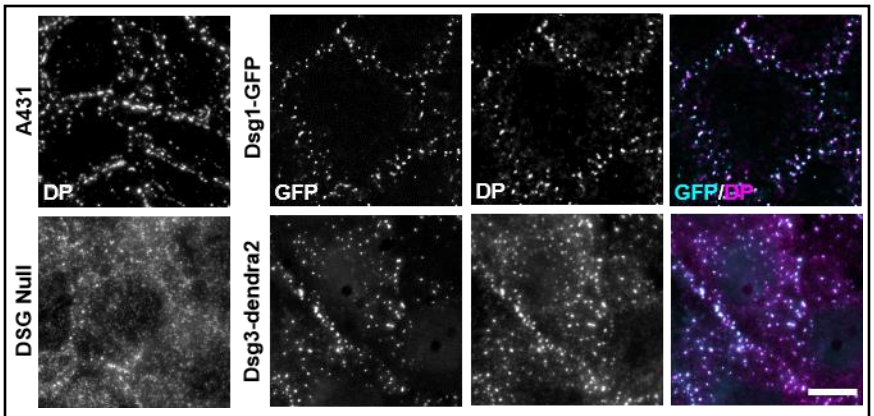

Figure 2.6: Exogenous expression of Dsg species rescues desmosomal protein localization. Widefield immunofluorescence images show expression of Dsg1-GFP or Dsg3-dendra2 and DP localization in DSG-null cells. DP staining in A431 and DSG-null cells for reference. Scale bar = 10 μm.

2.2.2 Exogenous expression of Dsg species rescues desmosomal defects in DSG-null cells

Having seen that the DSG-null cells exhibited altered desmosomal protein localization and reduced desmosome formation, we sought to rescue these characteristics by expression of

exogenous DSG species. We stably expressed Dsg1-GFP or Dsg3-dendra2 by lentiviral transduction and bulk sorted cells to create cell populations with similar expression distributions while removing cells that expressed either Dsg species at very high levels or not at all. We found that re-expression of either Dsg species showed renewed desmosome assembly with DP localization returning to desmosomal puncta along cell-cell borders (Figure 2.6).

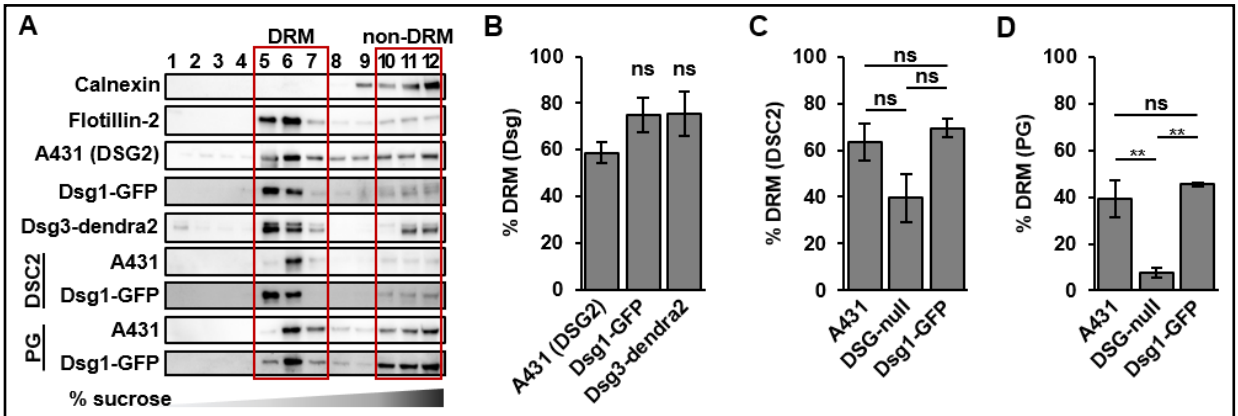

Figure 2.7: Exogenous expression of Dsg species recovers raft association of desmosomal proteins. A) Western blots show sucrose gradient fractionations of DSG-null cells expressing Dsg1-GFP or Dsg3-dendra2 as well as DRM segregation of DSC2 or PG in parental A431 cells versus DSG-null cells expressing Dsg1-GFP. Calnexin = non-DRM marker. Flotillin-2 = DRM marker. B) Quantification of DSG blots in A in parental A431 cells versus Dsg1-GFP or Dsg3-dendra2 in DSG-null cells. C) Quantification of DSC2 blots in A in parental A431 cells versus DSG-null cells or DSG-null cells expressing Dsg1-GFP. D) Quantification of PG blots in A in parental A431 cells versus DSG-null cells and DSG-null cells expressing Dsg1-GFP. Error bars in B show mean +/- standard deviation (n = 2 (A431 (DSG2), Dsg3-dendra2), n = 4 (Dsg1-GFP)). Error bars in C, D show SEM +/- standard deviation (n = 4). **p < 0.01

Additionally, sucrose gradient fractionations revealed that Dsg1-GFP and Dsg3-dendra2 segregated into DRMs similarly to DSG2 in A431 parental cells (Figure 2.7A, B). There was no significant change in the DRM segregation of DSC2 between A431 parental cells, DSG-null cells, and DSG-null cells expressing Dsg1-GFP (Figure 2.7A, C). Reduced PG segregation into DRMs observed in DSG-null cells was also rescued by the exogenous expression of Dsg1-GFP (Figure 2.7A, D). This indicates that Dsg1-GFP is capable of driving raft association and desmosome assembly and that the presence of the GFP tag does not appear to affect Dsg1 behavior. Lastly, we repeated the dispase cell dissociation assay and found that expression of either Dsg1-GFP or Dsg3-

dendra2 rescued desmosome function (Figure 2.8). Therefore, the DSG-null cells exhibit a dysfunctional desmosome phenotype which can be rescued by exogenous expression of Dsg species.

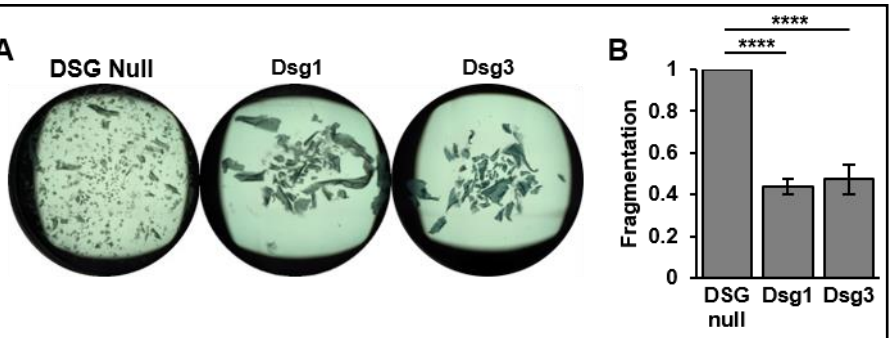

Figure 2.8: Exogenous expression of Dsg species in DSG-null cells rescues desmosome function. A) Images show fragmentation of DSG-null cell monolayers expressing Dsg1-GFP or Dsg3-dendra2. B) Quantification of A. Error bars show mean +/- SEM (n=6). ****p < 0.0001

2.3 DISCUSSION

We characterized a newly established DSG-null A431 cell line with defective desmosome assembly and function that could be rescued with exogenous expression of Dsg species. In these cells, loss of DSG2 expression resulted in mislocalization of DP, DSC2, and PG and reduced desmosome formation and function.

Prior to using A431s for this purpose, we found that DSG2 was the sole DSG species expressed at the protein level in these cells (Figure 2.1). Some have reported DSG2 to be the only expressed DSG species in A431s (20) while others have reported DSG3 expression in addition to DSG2 (112). Though DSG3 was absent in the parental A431s, we observed low DSG3 levels in the DSG2-KO cells (data not shown). This may be the result of a compensatory mechanism which has been observed following the loss of a desmosomal cadherin in some cases (120, 121). However, these levels were insufficient to maintain normal localization of desmosomal proteins or desmosome function. Therefore, we consider these cells to be DSG-null.

The use of CRISPR-Cas9 has become widespread since its development. Others are also using this technique in desmosomal studies. For example, Wanuske et al used HaCaT cells, an immortalized keratinocyte cell line, to create PG-null and DP-null cell lines (122). In this way, they identified that loss of PG altered desmosome morphology and reduced strength, but loss of DP, the link between the desmosomal plaque and the cytoskeleton, caused complete loss of adhesion, though the desmosomal cadherins still formed small clusters. With these cells, they established a role for DP in stabilizing nascent clusters of desmosomal components into mature junctions. Our DSG-null cells will be useful in untangling the interactions necessary for forming these nascent clusters in the early stages of desmosome assembly. Furthermore, considering the success of these DSG-null cells, additional knockout cell lines can be created to further explore the roles of DSCs, PG, PKPss, and even the classical cadherins during desmosome assembly.

In the subsequent chapters, we use these DSG-null cells to compare two disease-causing glycine-to-arginine mutations in the $DSG1_{TMD}$ and to explore the $Dsg1_{TMD}$ physical properties that drive raft association and the cost of reduced raft association on desmosomal processes.

2.4 MATERIALS AND METHODS

Generation of constructs and lentivirus

Cloning of plasmid expressing Dsg1-GFP has been previously described (6). Lentivirus for Dsg1-GFP and Dsg3-dendra2 was purchased from Cyagen VectorBuilder.

Cell line generation, culture, and reagents

A431 cells were cultured in DMEM (Corning 10-013-CV) with 10% fetal bovine serum (Hyclone SH30071.03) and 1X antibiotic-antimycotic solution (Corning 30-004-CI). CRISPR/cas9 was used to knockout DSG2 (DSG2 gRNA target sequence GTTACGCTTTGGATGCAAG) as

previously described (123). Cells were stably infected with lentiviruses expressing murine desmoglein constructs. Blasticidin (5μg/ml) was used to select for infected cells. No clonal isolation was performed. Cell lines expressing Dsg-GFP species were subjected to fluorescence-activated cell sorting to obtain populations with roughly equal Dsg-GFP expression levels.

Immunofluorescence

Cells were cultured to 70% confluence on glass coverslips and fixed in 3.7% paraformaldehyde (PFA) in PBS+ on ice for 10 min. Cells were blocked and permeabilized in PBS+ containing 0.1% Triton X-100 and 3% BSA for 10 min. Primary and secondary antibodies (listed below) were diluted into blocking solution (PBS+ containing 3% BSA and 0.05% Triton X-100). Cells were rinsed using PBS+ containing 0.05% Triton X-100. Cells were mounted to glass microscope slides using Prolong Gold mounting medium (ThermoFisher Scientific).

Antibodies

Antibodies used were as follows: mouse-anti-DSG2 (6D8, courtesy of Dr. Jim Wahl), mouse anti-GFP (Abcam ab1218); rabbit anti-DP (Bethyl A303-356A); mouse anti-PG (BD Trans Lab 610253); mouse anti-Dsc2/3 (Life Technologies 326200); mouse anti-DSG3 5G11 (Invitrogen 32-6300); mouse anti-β-actin (Sigma A5451); mouse anti-E-cadherin (Abcam1416 (immunofluorescence); BD Trans Lab 610182 (immunoblots)). Mouse anti-Dsg1 (PF1-8-15 IgG1) was a kind gift from Dr. Aimee Payne. Secondary antibodies conjugated to Alexa Fluors were purchased from Invitrogen. Horseradish peroxidase-conjugated secondary antibodies were purchased from BioRad.

Image acquisition

Widefield microscopy was performed using a Nikon Ti-E inverted microscope (100x/1.49 NA oil immersion objective) equipped with a motorized stage and a Hamamatsu C11440-22CU digital

camera. Images were deconvolved using Microvolution (124) in ImageJ. All microscopy was performed at room temperature. Results are representative of three independent replicates with 10 cells per condition.

Isolation of DRM

DRMs were isolated as described previously (118). Briefly, cells were cultured in 10-cm^2 dishes and washed with PBS+. Cells were collected by scraping in TNE buffer supplemented with protease inhibitors (Roche 11836153001) and pelleted by centrifugation at 0.4xg at 4°C for 5 min (5415R; Eppendorf). Cells were resuspended in TNE buffer and homogenized using a 25-gauge needle. TNE buffer containing 1% Triton X-100 was added and cells were incubated on ice for 30 min. Four hundred-twenty microliters of detergent extract were mixed with 840µl of 56% sucrose in TNE and placed at the bottom of a centrifuge tube. Volumes (1.9µl) of 35 and 5% sucrose were layered on top of the sample. Following an 18-hr centrifugation at 4°C (44,000 rpm, SW55 rotor, Beckman Opima LE-80 K Ultracentrifuge), 420-µl fractions (1-11, remaining volume combined to make up fraction 12) were removed from top to bottom of the gradient and stored at -20°C until processed for western blot analysis. Flotillin-2 and calnexin were used as raft and non-raft markers, respectively.

Dispase-based fragmentation assay

Cells were cultured until confluent in 24-well tissue culture plates and treated with 1 U/ml dispase (Corning) for 15 min at 37°C. Cell sheets released from the plate were rinsed with PBS+, transferred to 1.5 ml Eppendorf tubes in 500µl PBS+, and then subjected to mechanical stress on an orbital shaker on its highest setting for 45 sec. Fragments were transferred to a fresh 24-well plate, fixed with 1% PFA, and stained with methylene blue (Sigma). Plates were imaged on an Elispot scanner (Cellular Technologies, Ltd) and fragments counted with ImageJ.

Statistics

Error bars represent standard error of the mean. Significance was determined using one-way ANOVA followed by Dunnett's post-hoc and p-values have been indicated. Statistical analysis of immunofluorescence results was conducted on at least 3 independent experiments with 10 images per condition per replicate. For all experiments involving western blotting, statistical analysis was conducted on results from four independent experiments. Statistical analysis of dispase assays was conducted on results from seven independent experiments.

2.5 ACKNOWLEDGEMENTS

The author would like to thank Dr. Daniel Conway for generating the DSG-null A431 cell line. Work in the Kowalczyk lab is supported by grants R01AR050501 and R01AR048266 from the National Institutes of Health. SEZ was supported by a training grant from the National Institutes of Health T32GM008367. This research project was also supported in part by the Emory Flow Cytometry Core (EFCC).

CHAPTER 3

Differential Pathomechanisms of Desmoglein-1 Transmembrane Domain Mutations in Skin Disease

This chapter is adapted from:

Zimmer, S. E., Takeichi, T., Conway, D., Kubo, A., Suga, Y., Akiyama, M., Kowalczyk, A. P. Differential pathomechanisms of DSG1 transmembrane domain mutations in skin disease. (Revisions submitted to Journal of Investigative Dermatology).

ABSTRACT

Dominant and recessive mutations in the desmosomal cadherin, desmoglein-1 (DSG1), cause the skin diseases palmoplantar keratoderma (PPK) and **s**evere dermatitis, multiple **a**llergies, and **m**etabolic wasting (SAM) syndrome, respectively. Here, we compare two dominant missense mutations in the DSG1 transmembrane domain (TMD), G557R and G562R, causing PPK ($DSG1_{PPK}$) and SAM syndrome ($DSG1_{SAM}$), respectively, to determine the differing pathomechanisms of these mutants. Expressing the $DSG1_{TMD}$ mutants in a DSG-null background, we use cellular and biochemical assays to reveal differences in the mechanistic behavior of each mutant. Super resolution microscopy and functional assays showed a failure by both mutants to assemble desmosomes due to reduced membrane trafficking and lipid raft targeting. $DSG1_{SAM}$ maintained normal expression levels and turnover relative to $DSG1_{WT}$, but $DSG1_{PPK}$ lacked stability, leading to increased turnover through lysosomal and proteasomal pathways and reduced expression levels. These results differentiate the underlying pathomechanisms of these disorders, suggesting that $DSG1_{SAM}$ acts dominant negatively while $DSG1_{PPK}$ is a loss-of-function mutation

causing the milder PPK disease phenotype. These mutants portray the importance of the DSG TMD in desmosome function and suggest that a greater understanding of the desmosomal cadherin TMDs will further our understanding of the role that desmosomes play in epidermal pathophysiology.

3.1 INTRODUCTION

Epidermal integrity relies on the formation of intercellular junctions to protect against abrasion, infection, and water loss. Among these junctions, desmosomes mediate strong cell-cell adhesion by mechanically coupling adjacent cells through a series of protein-protein interactions involving desmosomal cadherins and intercellular adaptor proteins that anchor intermediate filaments to the plasma membrane (125, 126). Desmosomes are targeted in numerous skin fragility diseases caused by autoantibodies, bacterially-produced toxins, and gene mutations (36, 127-130). Among genetically-inherited diseases, haploinsufficiency of the desmosomal cadherin, desmoglein-1 (DSG1), causes a relatively mild disorder called palmoplantar keratoderma (PPK) in which epidermal thickening occurs along the palms of the hands and soles of the feet (131). In contrast, **s**evere dermatitis, multiple **a**llergies, and **m**etabolic wasting (SAM) syndrome has broader effects arising from epidermal thickening, fragility, and barrier defects typically caused by recessively-inherited DSG1 loss of function mutations (27).

DSG1 is critical in the epidermis where it promotes differentiation and becomes the main DSG mediator of desmosomal adhesion in the upper epidermal layers (31, 32). The differences in severity between PPK and SAM syndrome are thought to be due to gene dosage; PPK arises from DSG1 haploinsufficiency while the complete loss of functional DSG1 in SAM syndrome causes a more severe clinical presentation (132). Recently, we reported an unusual case of SAM syndrome (referred to as $DSG1_{SAM}$) in which a dominantly-inherited missense mutation in *DSG1* caused a glycine-to-arginine substitution at residue 562 in the DSG1 transmembrane domain (TMD) (6). Here and in a related study (Takeichi et al, in preparation), we report a second instance of a missense mutation in the *DSG1* TMD. This novel mutation also causes a glycine to arginine substitution, occurring at position 557 within the $DSG1_{TMD}$, but the patient presents with PPK

(referred to as DSG1$_{PPK}$). Despite the genetic similarities between these cases, the phenotypic disparity suggests differing pathomechanisms underlying an important role for the DSG TMD in desmosome assembly and function.

Here, we sought to determine the disease mechanisms of DSG1$_{PPK}$ versus DSG1$_{SAM}$ mutations and to determine the role of the DSG TMD in desmosome assembly and function. By expressing these mutants in a DSG-null background, we identified defects in membrane trafficking and lipid raft targeting which resulted in reduced desmosome assembly and function. Both DSG1$_{PPK}$ and DSG1$_{SAM}$ mutants failed to support normal desmosome formation and were deficient in cell-cell adhesion strength. Mechanistically, DSG1$_{PPK}$ was rapidly degraded in a lysosome- and proteasome-dependent manner, while DSG1$_{SAM}$ maintained normal protein and cell surface stability. These findings reveal that different mutations within the DSG1$_{TMD}$ cause different types of inherited human skin disease by distinct mechanisms and suggest that different therapeutic strategies should be explored for treating these related disorders.

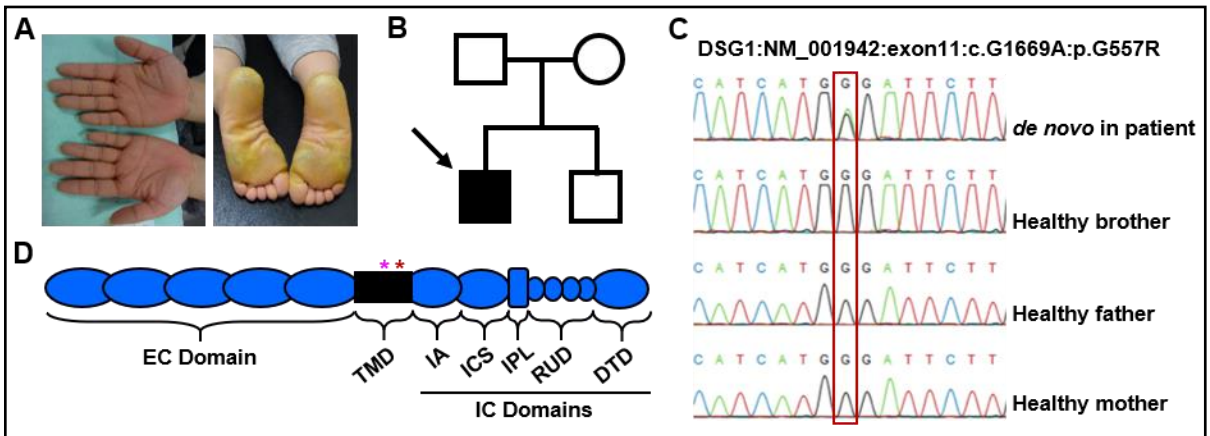

Figure 3.1: PPK patient with DSG1$_{TMD}$ glycine-to-arginine substitution. A) Photographs of patient's hands and feet. **B)** Pedigree of patient's immediate family. Arrow indicates proband. **C)** Chromatogram of patient and patient's relatives. **D)** Model of DSG1 domains with pink asterisk depicting location of DSG1$_{PPK}$ and red asterisk depicting location of DSG1$_{SAM}$. IA = intracellular anchor, ICS = intracellular cadherin segment, IPL = intracellular proline-rich linker, RUD = repeating unit domains, DTD = desmoglein terminal domain.

3.2 RESULTS

3.2.1 Dsg1$_{TMD}$ mutants support the formation of fewer, smaller, and weaker desmosomes.

We previously reported a heterozygous mutation in the DSG1$_{TMD}$ (G562R) that disrupts DSG1 association with lipid rafts, causing SAM syndrome (6). Here and in related work (Takeichi et al, in preparation) we report a second DSG1$_{TMD}$ missense mutation, G1669A, resulting in a different glycine-to-arginine substitution in the DSG1$_{TMD}$ (G557R) (Figure 3.1, Figure 3.2A), which causes PPK rather than SAM syndrome. To understand how these two DSG1$_{TMD}$ mutations cause different skin diseases, we stably expressed mouse desmoglein (Dsg1a) ORF with the corresponding disease-causing TMD mutations (Dsg1$_{WT}$, Dsg1$_{PPK}$, or Dsg1$_{SAM}$) in the DSG-null A431 cells described in Chapter 2. Dsg1a shares 78% sequence identity with DSG1; most differences are in the extracellular anchor. DSG-null A431 cells stably expressing Dsg1$_{WT}$-GFP, Dsg1$_{PPK}$-GFP, or Dsg1$_{SAM}$-GFP were established using a lentiviral system and bulk sorted to create populations with roughly equal expression patterns (Table 3.1). Immunofluorescence (Figure 3.2B) and western blot analysis (see additional analysis below) revealed reduced expression of the Dsg1$_{PPK}$-GFP mutant relative to Dsg1$_{WT}$-GFP or Dsg1$_{SAM}$-GFP. Therefore, the brightness and contrast for Dsg1$_{PPK}$-GFP images were adjusted to allow for assessment of localization differences between the Dsg1 variants. Desmocollin-2 (DSC2), plakoglobin (PG), and E-cadherin levels were unaffected (see Figure 3.8). We found that both Dsg1$_{TMD}$ mutants could be detected with desmoplakin (DP) in cell border-localized puncta. However, while DP is properly localized at borders in cells expressing Dsg1$_{WT}$-GFP, it remained mislocalized in cells expressing Dsg1$_{PPK}$-GFP or Dsg1$_{SAM}$-GFP. Quantifying the number of puncta positive for Dsg1-GFP and DP revealed fewer puncta per border in the mutant-expressing cells relative to those expressing Dsg1$_{WT}$-GFP

(Figure 3.2C). These findings suggest that G:R substitutions in the $DSG1_{TMD}$ compromise the ability of DSG1 mutants to support desmosome formation.

Table 3.1: Percentage of cells stably expressing $Dsg1_{WT}$-GFP, $Dsg1_{PPK}$-GFP, or $Dsg1_{SAM}$-GFP, based on post-sort data from FACS sorting.

Cell Line	GFP+ Cells
$Dsg1_{WT}$-GFP	89.2%
$Dsg1_{PPK}$-GFP	96.0%
$Dsg1_{SAM}$-GFP	86.6%

To assess the adhesive potential of the various cell lines, we utilized a dispase cell fragmentation assay in which increased monolayer fragmentation correlates with decreased cell-cell adhesion strength (119). $Dsg1_{WT}$-GFP expression restored adhesion in the DSG-null A431 cells whereas the $Dsg1_{SAM}$-GFP mutant failed to rescue desmosome function. The $DSG1_{PPK}$-GFP mutant exhibited an intermediate adhesive phenotype (Figure 3.2D, E). These results suggest that the $DSG1_{SAM}$ mutation compromises desmosomal adhesion more than the $DSG1_{PPK}$ mutation.

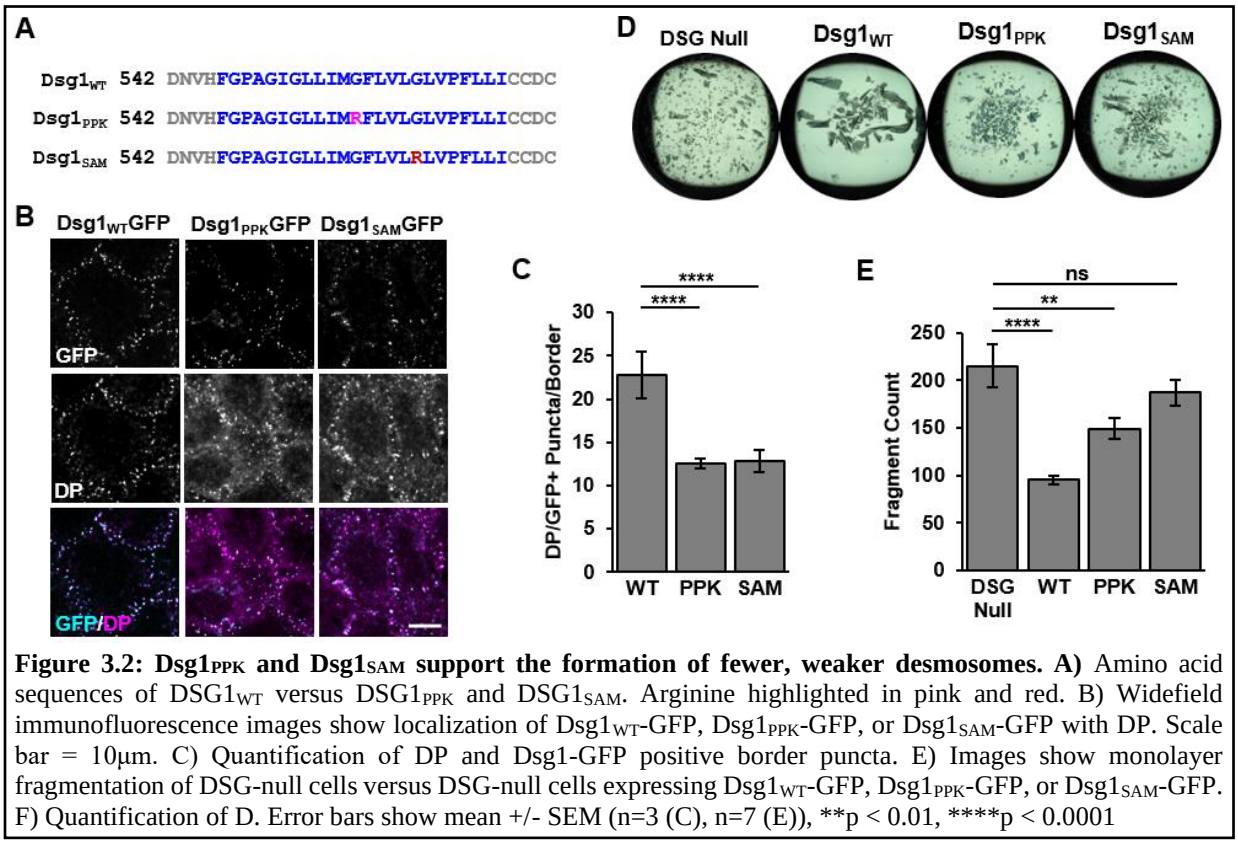

Figure 3.2: $Dsg1_{PPK}$ and $Dsg1_{SAM}$ support the formation of fewer, weaker desmosomes. A) Amino acid sequences of $DSG1_{WT}$ versus $DSG1_{PPK}$ and $DSG1_{SAM}$. Arginine highlighted in pink and red. B) Widefield immunofluorescence images show localization of $Dsg1_{WT}$-GFP, $Dsg1_{PPK}$-GFP, or $Dsg1_{SAM}$-GFP with DP. Scale bar = 10μm. C) Quantification of DP and Dsg1-GFP positive border puncta. E) Images show monolayer fragmentation of DSG-null cells versus DSG-null cells expressing $Dsg1_{WT}$-GFP, $Dsg1_{PPK}$-GFP, or $Dsg1_{SAM}$-GFP. F) Quantification of D. Error bars show mean +/- SEM (n=3 (C), n=7 (E)), $^{**}p < 0.01$, $^{****}p < 0.0001$

Desmosomes are characterized by the formation of mirror image cytoplasmic plaque structures that appear as "railroad track" staining patterns when resolved by super-resolution optical imaging (133, 134). To determine the cause of the reduced function in desmosomes formed from Dsg1$_{PPK}$-GFP and Dsg1$_{SAM}$-GFP, we used structured illumination microscopy (SIM) to examine desmosome organization (Figure 3.3A). We localized the Dsg1-GFP variants with DP, a mature desmosome marker, and quantified images by measuring desmosome length and desmosomes per border. Cells expressing Dsg1$_{WT}$-GFP formed more, longer desmosomes than cells expressing Dsg1$_{PPK}$-GFP or Dsg1$_{SAM}$-GFP (Figure 3.3B, C). Together, these findings suggest that Dsg1$_{PPK}$-GFP and Dsg1$_{SAM}$-GFP support the formation of desmosomes that are fewer, smaller, and weaker than desmosomes formed from Dsg1$_{WT}$-GFP.

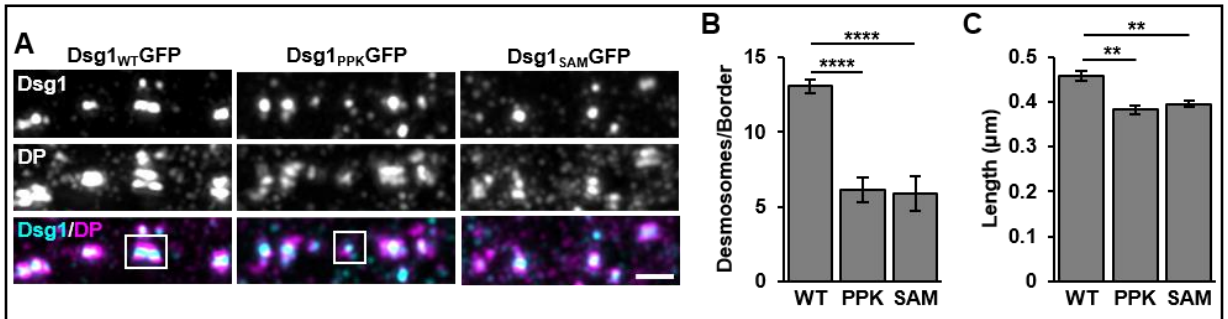

Figure 3.3: Dsg1$_{PPK}$ and Dsg1$_{SAM}$ desmosomes are smaller than Dsg1$_{WT}$ desmosomes. A) SIM images show resolved DP railroad tracks in DSG-null cells expressing Dsg1$_{WT}$-GFP, Dsg1$_{PPK}$-GFP, or Dsg1$_{SAM}$-GFP. Scale bar = 10µm. B) Quantification of desmosome number per border. C) Quantification of desmosome length. Desmosome = DP railroad tracks sandwiching Dsg1-GFP; example of desmosomes versus non-desmosomes shown in white boxes in A. Error bars show mean +/- SEM (n=3), **p < 0.01, ****p < 0.0001

3.2.2 Dsg1$_{TMD}$ mutants reduce desmosome assembly by disrupting raft association.

Triton X-100 insolubility of desmosomal proteins is an indication of cytoskeletal attachment and overall desmosome assembly status (6, 50, 135). Using a Triton X-100 solubility assay, we found that Dsg1$_{PPK}$-GFP and Dsg1$_{SAM}$-GFP exhibited increased solubility compared to Dsg1$_{WT}$-GFP (Figure 3.4A, B). E-cadherin solubility remained unchanged across the cell lines

(Figure 3.4A, C). This finding suggests that Dsg1$_{PPK}$-GFP and Dsg1$_{SAM}$-GFP do not readily assemble into cytoskeleton-attached desmosomes.

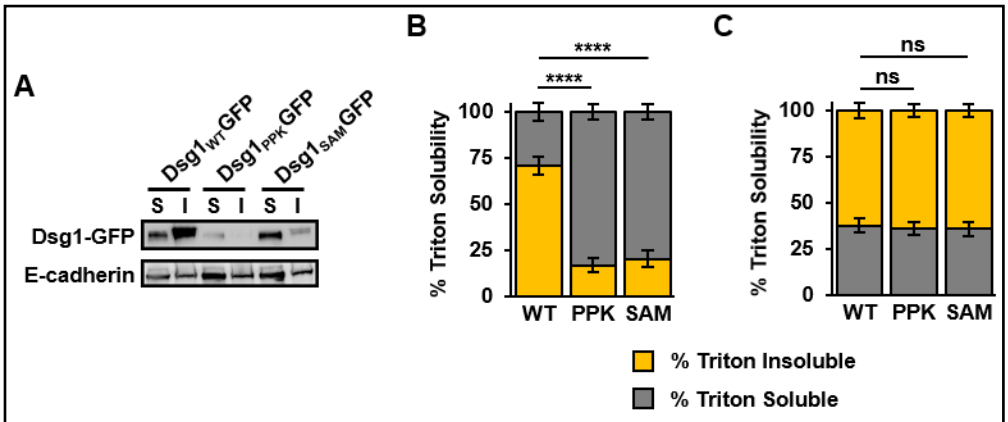

Figure 3.4: Dsg1$_{PPK}$ and Dsg1$_{SAM}$ reduce cytoskeletal attachment. A) Western blots show distribution of Dsg1-GFP or E-cadherin between Triton X-100 soluble and insoluble fractions. S = soluble fraction; I = insoluble fraction. B) Quantification of Dsg1-GFP blots showing Triton X-100 solubility of Dsg1-GFP in DSG-null cells expressing Dsg1$_{WT}$-GFP, Dsg1$_{PPK}$-GFP, or Dsg1$_{SAM}$-GFP. C) Quantification of E-cadherin blots showing Triton X-100 solubility of E-cadherin in DSG-null cells expressing Dsg1$_{WT}$-GFP, Dsg1$_{PPK-TMD}$-GFP, or Dsg1$_{SAM-TMD}$-GFP. Error bars show mean +/- SEM (n=4), ****p<0.0001

Desmosomes are intermediately-sized lipid rafts (6), highly ordered, cholesterol- and sphingolipid-enriched regions of the cell membrane important in various cell processes (2). Certain TMD properties target single-pass transmembrane proteins, like desmogleins, to lipid rafts (65). To determine how the arginine residues in DSG1$_{PPK}$ and DSG1$_{SAM}$ could alter the TMD properties that drive raft association of membrane proteins, we modeled each TMD α-helix using the Robetta server (136) (Figure 3.5A). Whereas the DSG1$_{WT}$ TMD is predicted to neatly traverse the membrane, the DSG1$_{PPK}$ and DSG1$_{SAM}$ models predict that arginine breaks the α-helix, effectively shortening the TMD from the normal 24 residues to 11 residues for DSG1$_{PPK}$ and 16 residues for DSG1$_{SAM}$. Length is one of several TMD properties used to predict TMD raft affinity by calculating the energy needed for raft association (65). We used this raft affinity model to predict the energy necessary for DSG1$_{WT}$, DSG1$_{PPK}$, and DSG1$_{SAM}$ to associate with lipid rafts and found that DSG1$_{PPK}$ and DSG1$_{SAM}$ would require more energy for raft association than DSG1$_{WT}$.

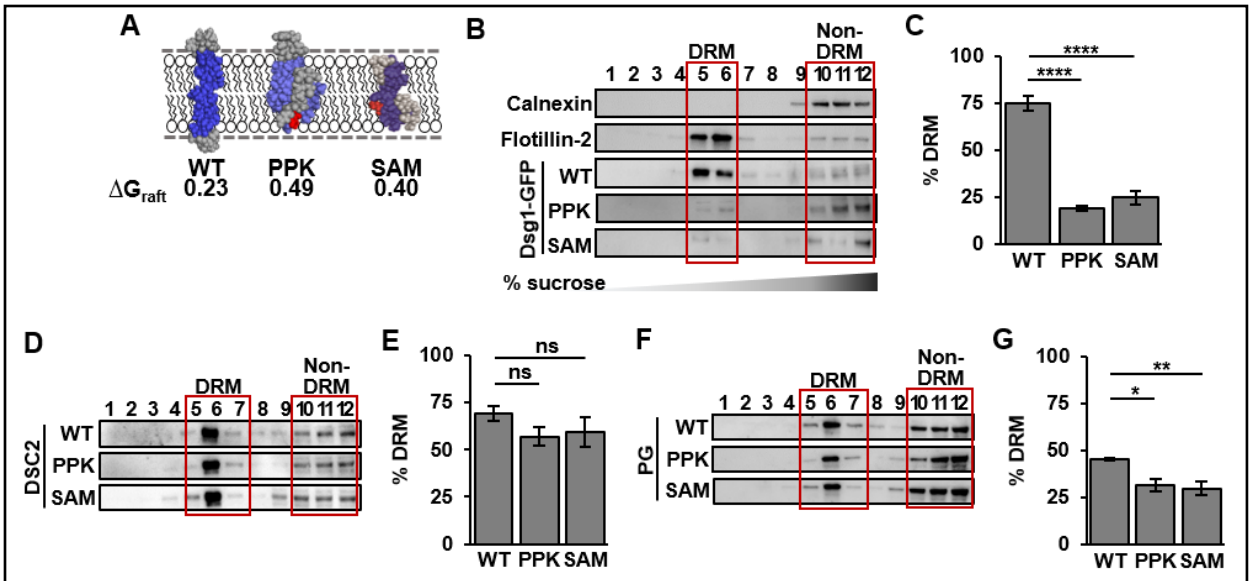

Figure 3.5: Dsg1$_{TMD}$ mutants reduce raft association. A) Robetta server modeling of DSG1$_{WT}$, DSG1$_{PPK}$, and DSG1$_{SAM}$. Blues = TMD residues. Gray = non-TMD residues. Red = arginine. Raft affinities (ΔG_{raft}) shown beneath models. DSG1$_{SAM}$ adapted from (6). B) Western blots show DRM isolation by sucrose gradient fractionation. Calnexin = marker of non-DRM fractions. Flotillin-2 = marker of DRM fractions. Remaining blots depict Dsg1-GFP from cells expressing Dsg1$_{WT}$-GFP, Dsg1$_{PPK}$-GFP, or Dsg1$_{SAM}$-GFP. C) Quantification of Dsg1-GFP blots in B. D) Western blots showing DRM isolation by sucrose gradient fractionation of DSC-2. E) Quantification of DSC2 blots in D. F) Western blots showing DRM isolation by sucrose gradient fractionation of PG. G) Quantification of PG blots in F. Error bars show mean +/- SEM (n=4), *p < 0.05, **p < 0.01, ****p < 0.0001

To verify this predicted loss of raft association in the DSG1$_{TMD}$ mutants, we used sucrose gradient fractionations to isolate detergent-resistant, raft membranes (DRMs) from non-detergent, non-raft membranes (non-DRMs). Raft association was verified by blotting for the DRM marker, flotillin-2, and the non-DRM marker, calnexin (Figure 3.5B). Significantly more Dsg1$_{WT}$-GFP fractionated with DRMs, suggesting defective raft targeting of both Dsg1$_{PPK}$-GFP and Dsg1$_{SAM}$-GFP (Figure 3.5B, C). Assessing the raft association of other desmosomal proteins, we found that DSC2 raft association was unaffected (Figure 3.5D, E), while less PG associated with rafts in cells expressing Dsg1$_{PPK}$-GFP or Dsg1$_{SAM}$-GFP compared to Dsg1$_{WT}$-GFP (Figure 3.5F, G), suggesting that DSC2 but not PG associates with rafts independently of desmogleins. Together, these findings suggest that the reduced number, size, and strength of desmosomes formed by Dsg1$_{PPK}$-GFP and Dsg1$_{SAM}$-GFP may be due to defective raft targeting of the Dsg1$_{TMD}$ mutants and the sequestration of PG away from desmosomal raft domains.

3.2.3 Dsg1$_{PPK}$ and Dsg1$_{SAM}$ exhibit distinct trafficking defects.

The difference in TMD length predicted by modelling would also be expected to affect Dsg1 subcellular localization (68). At steady state, we found increased colocalization of Dsg1$_{PPK}$-GFP and Dsg1$_{SAM}$-GFP with the ER marker, VAPB, relative to Dsg1$_{WT}$-GFP (Figure 3.6A, B). We had previously observed that the Dsg1$_{SAM}$-GFP mutant was retained in the Golgi following a calcium switch (6). Here, we observed increased colocalization of both the Dsg1$_{SAM}$-GFP and the Dsg1$_{PPK}$-GFP mutants with the Golgi marker, GM130, at steady state (Figure 3.6C, D). These observations suggest that Dsg1$_{TMD}$ mutants exhibit delayed trafficking through the biosynthetic pathway to the cell surface.

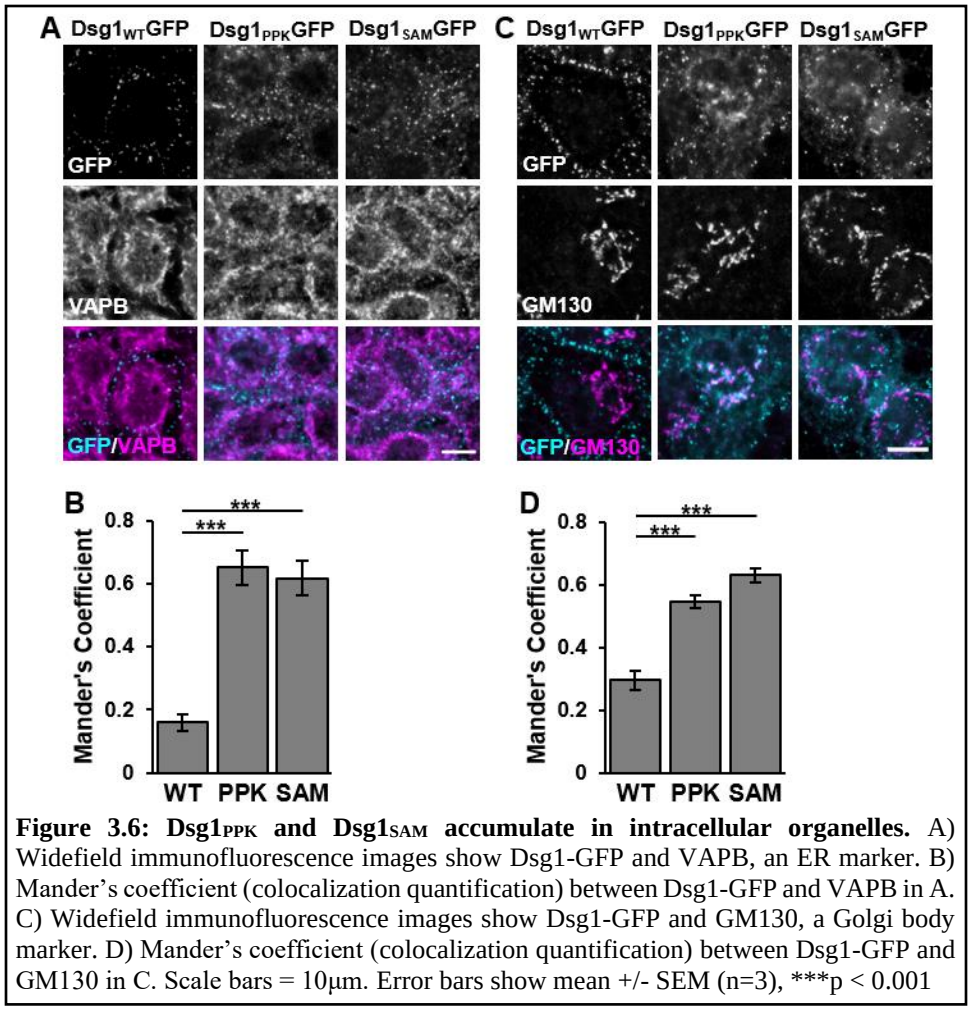

Figure 3.6: Dsg1$_{PPK}$ and Dsg1$_{SAM}$ accumulate in intracellular organelles. A) Widefield immunofluorescence images show Dsg1-GFP and VAPB, an ER marker. B) Mander's coefficient (colocalization quantification) between Dsg1-GFP and VAPB in A. C) Widefield immunofluorescence images show Dsg1-GFP and GM130, a Golgi body marker. D) Mander's coefficient (colocalization quantification) between Dsg1-GFP and GM130 in C. Scale bars = 10μm. Error bars show mean +/- SEM (n=3), ***p < 0.001

Despite apparent trafficking defects, immunofluorescence images show plasma membrane localization of $Dsg1_{PPK}$-GFP and $Dsg1_{SAM}$-GFP (Figure 3.2B). Our previous work showed that steady state surface levels of $Dsg1_{SAM}$-GFP are equal to that of $Dsg1_{WT}$-GFP (6). Using surface biotinylation, we found reduced steady state surface levels of $Dsg1_{PPK}$-GFP (Figure 3.7A, B). To determine whether this was due to differences in surface stability, we performed a pulse-chase using an antibody against the Dsg1 ectodomain. Cells were fixed but not permeabilized 0, 1, 3, or 6 hours after antibody treatment and imaged to compare remaining cell surface levels between

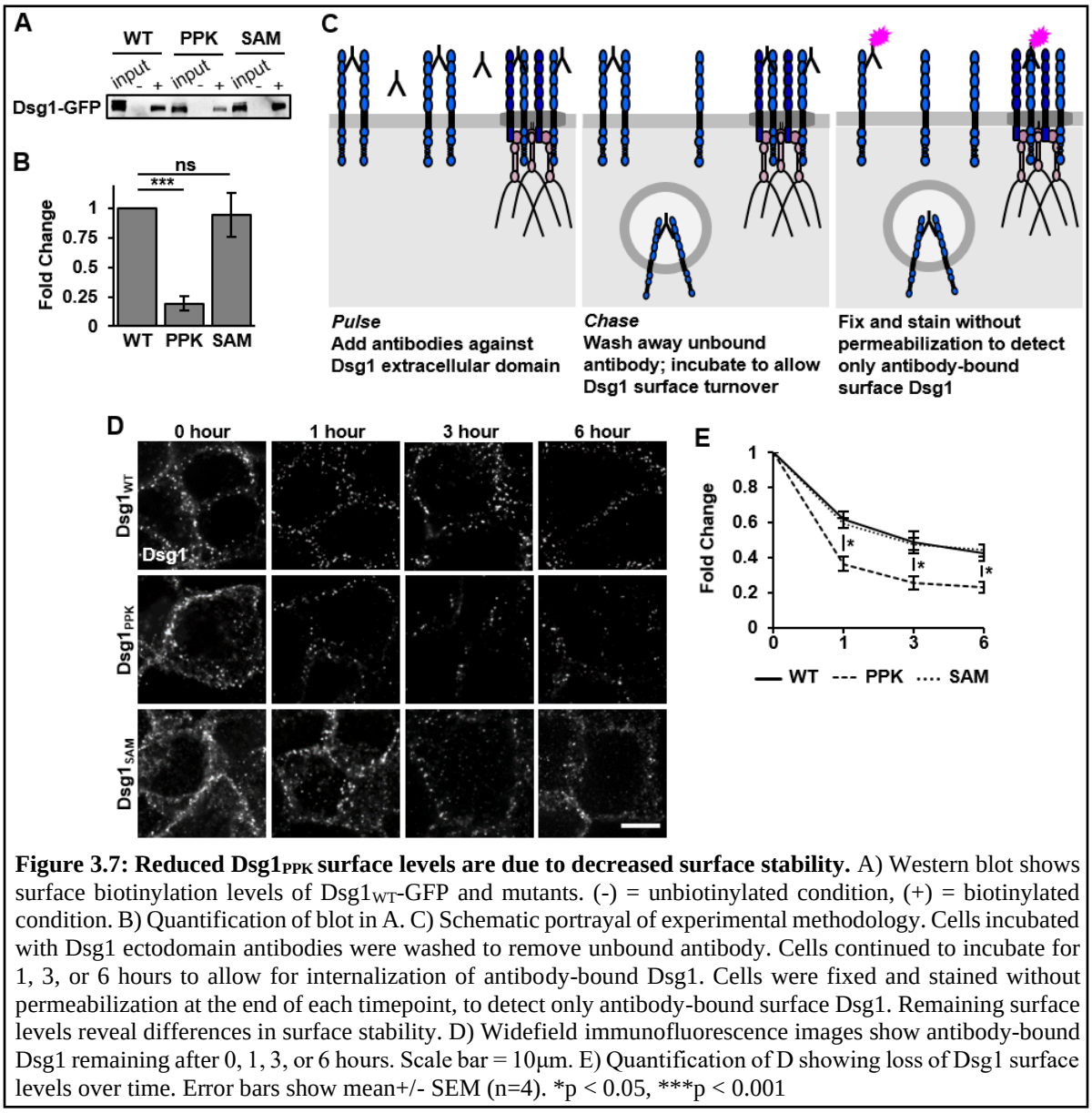

Figure 3.7: Reduced $Dsg1_{PPK}$ surface levels are due to decreased surface stability. A) Western blot shows surface biotinylation levels of $Dsg1_{WT}$-GFP and mutants. (-) = unbiotinylated condition, (+) = biotinylated condition. B) Quantification of blot in A. C) Schematic portrayal of experimental methodology. Cells incubated with Dsg1 ectodomain antibodies were washed to remove unbound antibody. Cells continued to incubate for 1, 3, or 6 hours to allow for internalization of antibody-bound Dsg1. Cells were fixed and stained without permeabilization at the end of each timepoint, to detect only antibody-bound surface Dsg1. Remaining surface levels reveal differences in surface stability. D) Widefield immunofluorescence images show antibody-bound Dsg1 remaining after 0, 1, 3, or 6 hours. Scale bar = 10μm. E) Quantification of D showing loss of Dsg1 surface levels over time. Error bars show mean+/- SEM (n=4). *$p < 0.05$, ***$p < 0.001$

Dsg1$_{WT}$-GFP and the two mutants (Figure 3.7C-E). More Dsg1$_{PPK}$-GFP was lost after the first hour than Dsg1$_{WT}$-GFP or Dsg1$_{SAM}$-GFP; this trend continued up to six hours, suggesting that Dsg1$_{PPK}$-GFP is less stable at the cell surface.

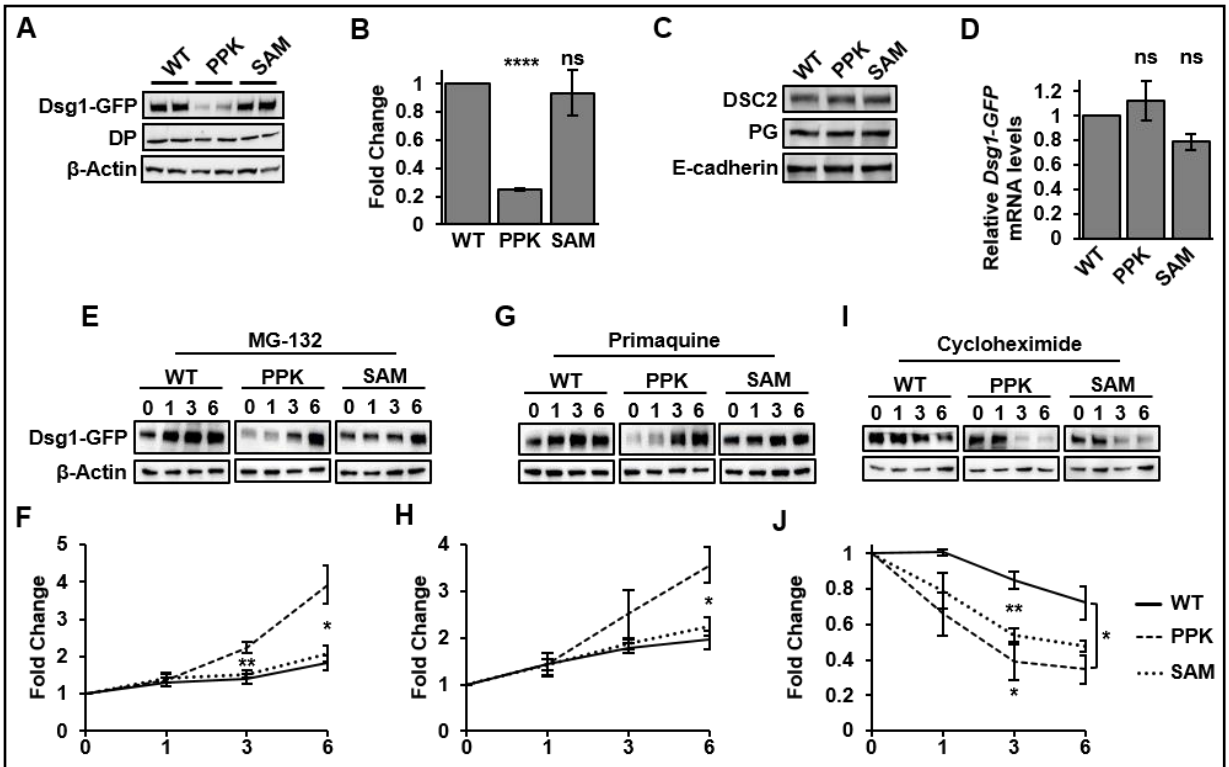

Figure 3.8: Inhibiting protein degradation rescues Dsg1(PPK) levels. A) Western blot of whole cell lysates showing reduced Dsg1$_{PPK}$-GFP levels. DP levels are unchanged. β-actin shows equal loading. Two lanes per sample. B) Quantification of Dsg1-GFP blot in A. C) Additional western blots of whole cell lysates showing that DSC2, PG, and E-cadherin levels are unchanged in DSG-null cells expressing Dsg1$_{WT}$-GFP, Dsg1$_{PPK}$-GFP, or Dsg1$_{SAM}$-GFP. D) Quantification of qRT-PCR analysis showing that mRNA levels of *Dsg1-GFP* does not differ between cell lines. *Dsg1-GFP* levels normalized to *GAPDH* levels. E) Western blots depicting Dsg1-GFP levels after 0, 1, 3, or 6 hours of MG-132 treatment. β-actin shows equal loading. F) Quantification of E. G) Western blots depicting Dsg1-GFP levels after 0, 1, 3, or 6 hours of primaquine treatment. β-actin shows equal loading. H) Quantification of E. I) Western blots depicting Dsg1-GFP levels after 0, 1, 3, or 6 hours of cycloheximide treatment. β-actin shows equal loading. J) Quantification of I. Error bars show mean +/- SEM (n=4 (A-C, E-J), n=3 (D)), *p < 0.05, **p < 0.01, ****p < 0.0001

3.2.4 Low Dsg1$_{PPK}$ expression levels are caused by increased protein turnover rates.

To determine if retention in the ER and increased surface turnover of the Dsg1$_{PPK}$-GFP mutant resulted in reduced steady state protein levels, qRT-PCR and western blot analysis was conducted for whole cell lysates of cells expressing Dsg1$_{WT}$-GFP or the Dsg1$_{SAM}$-GFP and Dsg1$_{PPK}$-GFP mutants. Dsg1$_{PPK}$-GFP protein levels were reduced compared to Dsg1$_{WT}$-GFP and

$Dsg1_{SAM}$-GFP, but mRNA levels were consistent across cell lines (Figure 3.8A, B, D). In addition, cells were treated for various amounts of time with MG132 or primaquine to inhibit proteasomal or lysosomal degradation, respectively (Figure 3.8E-H). MG132 and primaquine treatments increased steady state levels of each Dsg1 variant over a 6-hour time course. However, the effects were most dramatic for $Dsg1_{PPK}$-GFP, restoring $Dsg1_{PPK}$-GFP to levels similar to those seen for $Dsg1_{WT}$-GFP and $Dsg1_{SAM}$-GFP. Similarly, cycloheximide treatment resulted in more rapid loss of $Dsg1_{PPK}$-GFP levels compared to $Dsg1_{WT}$-GFP (Figure 3.8I, J). These data indicate that the low levels of the $Dsg1_{PPK}$-GFP mutant are caused by increased protein degradation rates relative to $Dsg1_{WT}$-GFP and $Dsg1_{SAM}$-GFP.

3.3 DISCUSSION

The *DSG1* mutations reported here are unique among >30 known *DSG1* mutations causing PPK or SAM syndrome (137). The *DSG1* extracellular domain harbors the majority of currently known mutations, most of which cause premature translation termination and transcript degradation by nonsense-mediated mRNA decay (138). The $DSG1_{PPK}$ and $DSG1_{SAM}$ mutations studied here both occur in the TMD but cause disease by different mechanisms. Using a DSG-null background, we find that neither mutant supports normal desmosome formation. However, while the $DSG1_{SAM}$ mutant is expressed at the cell surface and accumulates at steady state levels similar to $DSG1_{WT}$, the $DSG1_{PPK}$ mutant exhibits lower expression levels due to rapid turnover that is dependent upon lysosomal and proteasomal pathways. Our findings suggest that $Dsg1_{PPK}$ undergoes primarily proteasomal degradation that likely occurs in ER compartments where the mutant accumulates after biosynthesis. $Dsg1_{PPK}$ that escapes ER retention or degradation mechanisms traffics to the cell surface and assembles with other desmosomal proteins. However,

the Dsg1$_{PPK}$ pool at the cell surface is unstable, presumably due to increased endocytic rates and subsequent lysosomal degradation. In contrast, Dsg1$_{SAM}$ escapes proteasomal degradation and traffics slowly to the cell membrane where its stability at the cell surface permits a dominant negative activity that may occur through competition with wildtype desmosomal cadherins for the binding of intracellular adaptor proteins such as PG. These findings explain in part the mechanisms by which these two unique DSG mutations cause different types of skin disease (Figure 3.9).

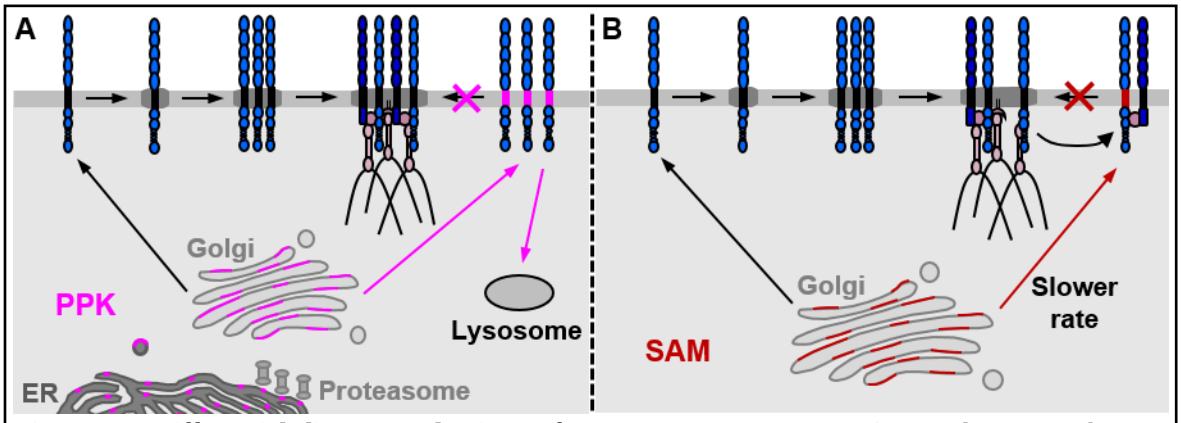

Figure 3.9: Differential disease mechanisms of two DSG1$_{TMD}$ mutants. A) PPK disease mechanism model. Based on current evidence, most DSG1$_{PPK}$ is degraded by the proteasome soon after synthesis. Some traffics to the plasma membrane where its instability leads to rapid internalization and lysosomal degradation. In the context of the patient, cells must rely solely on protein produced from the WT allele. **B)** SAM disease mechanism model. Based on current evidence (here and from previous publication), the SAM mutant traffics to the plasma membrane more slowly than WT. Stable at the membrane, it is less capable of associating with rafts or assembling into functional desmosomes. However, it can interact with other desmosome proteins, either preventing their assembly into desmosomes, or pulling them out of other desmosomes, leading to a dominant negative effect.

TMDs are stretches of hydrophobic residues which allow proteins to traverse lipid bilayers in an energetically-favorable manner. Uncommon within TMDs, arginines mostly occur at the cytoplasmic-facing end of the α-helix where they interact with phospholipid headgroups, terminate TMDs, and determine membrane protein topology (68, 139-141). The inappropriate presence of an arginine can disrupt normal TMD behavior (142) from synthesis to trafficking and stability. Our modelling of DSG1$_{PPK}$ and DSG1$_{SAM}$ predict that the arginine residues present in the mutants "snorkel" (143, 144) at the membrane:cytoplasmic interface where they may stabilize the mutant TMDs in a trade-off that reduces the energetic costs of arginine and disrupts both protein-lipid

associations and TMD behavior. This snorkeling is predicted to create kinks in the α-helix to maintain the remaining hydrophobic residues within the hydrophobic region of the lipid bilayer, effectively shortening the 24-residue $DSG1_{TMD}$ to just 11 residues for $DSG1_{PPK}$ and 16 residues for $DSG1_{SAM}$. ER membranes can conform to TMDs down to 10 residues (145), but arginine decreases the efficiency of translocon-mediated TMD insertion into ER membranes, with the greatest effect occurring in the middle (146-148). The increased proteasomal degradation of $DSG1_{PPK}$ that we observed may be the result of inefficient ER insertion. The $DSG1_{SAM}$ arginine is sufficiently distant from the TMD center that its impact on insertion efficiency would be substantially less. Therefore, the effect of arginine on TMD behavior is position-dependent, likely forming the basis for the differing disease mechanisms of $DSG1_{PPK}$ versus $DSG1_{SAM}$.

Though $Dsg1_{PPK}$ and $Dsg1_{SAM}$ trafficked to the plasma membrane, both mutants exhibited retention in the ER and Golgi (Figure 3.6). TMD physical properties, including TMD length and residue asymmetry, guide subcellular localization. Single-pass transmembrane proteins with shorter, uniform TMDs localize to ER and Golgi while those with longer, asymmetric TMDs localize to the cell membrane (68, 149). The asymmetry in plasma membrane-localized TMDs manifests as bulky cytoplasmic residues and thin exoplasmic residues which allows TMDs to conform to differential lipid packing between leaflets (149). Consistent with this, bulky leucines in the $DSG1_{TMD}$ are prevalent in the cytoplasmic half while smaller glycines and alanines are prevalent in the outer half. Our models suggest that this asymmetry is maintained in $DSG1_{SAM}$ but not in $DSG1_{PPK}$. While interactions with other desmosomal proteins may contribute to the localization of $DSG1_{PPK}$ at the plasma membrane, its instability due to local membrane distortions, shortness, and even loss of symmetry may result in the rapid internalization and subsequent lysosomal degradation observed in our experiments.

Our previous work with $Dsg1_{SAM}$ showed that the $DSG1_{TMD}$ is important in desmosome assembly and function through its ability to drive raft association (6). The kinks introduced by arginine in our models increase the exposed surface area of the TMD residue sidechains which likely affects lipid packing around $DSG1_{PPK}$ and $DSG1_{SAM}$. Both exposed surface area and TMD length have been shown to guide raft association of single-pass transmembrane proteins (64); TMDs with longer helices and less exposed surface area pack more readily into the ordered, longer-chained acyl groups of lipid raft domains. We observed decreased raft association of $Dsg1_{PPK}$ and $Dsg1_{SAM}$ in isolated DRMs which also reduced raft association of PG but not DSC2. Raft association of desmosomal proteins is required for desmosome assembly and function (49, 50). This loss of raft association is likely a major factor in the reduced desmosome size and number, along with reduced cell-cell adhesion strength, observed in cells expressing the $Dsg1_{SAM}$ or $Dsg1_{PPK}$ mutants.

Many of our experiments showed apparently similar behavior between $Dsg1_{PPK}$ and $Dsg1_{SAM}$, so how might one mutation cause a mild disorder while the other causes a severe disorder? In the context of patient skin, both $DSG1_{PPK}$ and $DSG1_{SAM}$ are expressed alongside wildtype DSG1. Desmosomal protein levels are elevated in palm and sole skin relative to skin in other parts of the body allowing for larger desmosomes to form (150). The key behavioral differences we identified between $Dsg1_{PPK}$ and $Dsg1_{SAM}$ involved stability. Increased protein turnover and decreased cell surface stability of $DSG1_{PPK}$ would ultimately lead to a haploinsufficient disease mechanism in which $DSG1_{WT}$ protein levels are sufficient for normal desmosome assembly throughout most of the body, but insufficient for the assembly of larger desmosomes needed to maintain epidermal integrity in the palms and soles. Furthermore, DSG1 expression is not only critical for desmosome adhesive strength in the upper epidermis but also for

initiating epidermal differentiation by decreasing RAS/MAPK pathway activity (31, 32). In the presence of $DSG1_{PPK}$, $DSG1_{WT}$ protein levels may be insufficient to drive appropriate epidermal differentiation in the palms and soles. Indeed, elevated RAS/MAPK signaling has been observed in PPK patient skin (32) and PPK symptoms have been observed in individuals diagnosed with RASopathies (151). How $Dsg1_{SAM}$ might affect the RAS/MAPK pathway is unclear, though patient skin samples showed epidermal thickening consistent with differentiation defects (6). In contrast to $Dsg1_{PPK}$, $Dsg1_{SAM}$ maintains normal turnover rates and cell surface stability, allowing this mutant to interfere with normal desmosomal processes regardless of location, resulting in the more severe phenotype. Therefore, this mutant is well-poised to act dominant negatively, though the exact mechanism requires further experiments to parse out.

In summary, our findings demonstrate a key role for the $DSG1_{TMD}$ in desmosome assembly and function as well as the differential effects of glycine to arginine mutations based on TMD residue position. Additional work with the $DSG1_{TMD}$ will further our understanding of desmosome assembly mechanisms and their contribution to epidermal differentiation and disease.

3.4 MATERIALS AND METHODS

Generation of mutants and lentivirus

Cloning of plasmids expressing $Dsg1_{WT}$-GFP and $Dsg1_{SAM}$-GFP was previously described (6). The plasmid expressing $Dsg1_{PPK}$-GFP was cloned by the Cloning Division within the Emory Integrated Genomics Core. Lentivirus for $Dsg1_{WT}$-GFP and $Dsg1_{SAM}$-GFP was purchased from Cyagen VectorBuilder. Lentivirus for $Dsg1_{PPK}$-GFP was made by transfection into HEK-293T cells together with necessary lentiviral regulatory genes. Lentivirus was collected from culture supernatants 48-72 h after transfection and concentrated by high-speed centrifugation.

Structural predictions

TMD sequences were analyzed using the Robetta structure prediction server (136). Raft affinities were calculated using the following formula:

$$\Delta G_{raft} = \Delta\gamma_{TMD,Lo\text{-}Ld}(ASA) + n_{palm}(\Delta G_{palm}) - 2B_{LP}(d_{TMD} - 0.5(d_{Lo}+d_{LD})) \quad (65)$$

Cell line generation, culture, and reagents

A431 cells were cultured in DMEM (Corning 10-013-CV) with 10% fetal bovine serum (Hyclone SH30071.03) and 1X antibiotic-antimycotic solution (Corning 30-004-CI). CRISPR/cas9 was used to knockout DSG2 (DSG2 gRNA target sequence GTTACGCTTTGGATGCAAG) as previously described (123). Cells were stably infected with lentiviruses expressing murine desmoglein constructs. Blasticidin (5μg/ml) was used to select for infected cells. No clonal isolation was performed. Cell lines expressing $Dsg1_{WT}$-GFP and mutants were subjected to fluorescence-activated cell sorting to obtain populations with roughly equal Dsg1-GFP expression levels.

Immunofluorescence

Cells were cultured to 70% confluence on glass coverslips and fixed in 3.7% paraformaldehyde (PFA) in PBS+ on ice for 10 min. Cells were blocked and permeabilized in PBS+ containing 0.1% Triton X-100 and 3% BSA for 10 min. Cells were not permeabilized for the surface turnover assay and Triton was excluded from all buffers. Saponin was used in place of Triton for intracellular organelle colocalization studies. Primary and secondary antibodies (listed below) were diluted into blocking solution (PBS+ containing 3% BSA and 0.05% Triton X-100). Cells were rinsed using PBS+ containing 0.05% Triton X-100. Cells were mounted to glass microscope slides using Prolong Gold mounting medium (ThermoFisher Scientific).

Antibodies

Antibodies used were as follows: rabbit anti-calnexin (Enzo Life Sciences ADI-SPA-860); mouse anti-flotillin-2 (BD Trans Lab610383); rabbit anti-GFP (Life A11122); mouse anti-GFP (Abcam ab1218); rabbit anti-DP (Bethyl A303-356A); mouse anti-PG (BD Trans Lab 610253); mouse anti-Dsc2/3 (Life Technologies 326200); mouse anti-E-cadherin (BD Trans Lab 610182); mouse anti-GM130 (BD TransLab 610822); rabbit anti-VAPB (Invitrogen PA5-53023); mouse anti-β-actin (Sigma A5451); mouse anti-DSG3 5G11 (Invitrogen 32-6300). Mouse anti-Dsg1 (PF1-8-15 IgG1) was a kind gift from Dr. Aimee Payne. Secondary antibodies conjugated to Alexa Fluors were purchased from Invitrogen. Horseradish peroxidase-conjugated secondary antibodies were purchased from BioRad.

Image acquisition

Widefield microscopy was performed using a Nikon Ti-E inverted microscope (100x/1.49 NA oil immersion objective) equipped with a motorized stage and a Hamamatsu C11440-22CU digital camera. Images were deconvolved using Microvolution (124) in ImageJ. SIM was performed using a Nikon N-SIM system on an Eclipse Ti-E microscope system equipped with a 100x/1.49 NA oil immersion objective, 488- and 561-nm solid-state lasers in three-dimensional SIM mode. Images were captured using an EM charge-couple device camera (DU-897; Andor Technology) and reconstructed using NIS-Elements software with the N-SIM module (version 5.02; Nikon). All microscopy was performed at room temperature.

Triton solubility assay

Cells were cultured until confluent in six-well tissue culture plates. Cells were washed twice with ice-cold PBS+. The Triton-soluble pool was isolated by incubating cells with Triton lysis buffer (1% Triton X-100, 10 mM Tris, pH7.5, 140 mM NaCl, 5 mM EDTA, 2 mM EGTA, with protease

inhibitor [Roche 11836170001]) for 10 min on ice. Lysate was then centrifuged at 13,200xg for 10 min at 4°C to pellet the Triton-insoluble fraction. The Triton-soluble supernatant was collected and mixed 1:1 with 2x Laemmli sample buffer containing 5% β-mercaptoethanol. The Triton-insoluble pellet was resuspended in 2x Laemmli sample buffer (Bio-Rad 161-0737) containing 5% β-mercaptoethanol. All samples were heated to 95°C for 10 min and vortexed half-way through, prior to being run on a gel for western blotting.

Isolation of DRM

DRMs were isolated as described previously (118). Briefly, cells were cultured in 10-cm^2 dishes and washed with PBS+. Cells were collected by scraping in TNE buffer supplemented with protease inhibitors (Roche 11836153001) and pelleted by centrifugation at 0.4xg at 4°C for 5 min (5415R; Eppendorf). Cells were resuspended in TNE buffer and homogenized using a 25-gauge needle. TNE buffer containing 1% Triton X-100 was added and cells were incubated on ice for 30 min. Four hundred-twenty microliters of detergent extract were mixed with 840µl of 56% sucrose in TNE and placed at the bottom of a centrifuge tube. Volumes (1.9µl) of 35 and 5% sucrose were layered on top of the sample. Following an 18-hr centrifugation at 4°C (44,000 rpm, SW55 rotor, Beckman Opima LE-80 K Ultracentrifuge), 420-µl fractions (1-11, remaining volume combined to make up fraction 12) were removed from top to bottom of the gradient and stored at -20°C until processed for western blot analysis. Flotillin-2 and calnexin were used as raft and non-raft markers, respectively.

Dispase-based fragmentation assay

Cells were cultured until confluent in 24-well tissue culture plates and treated with 1 U/ml dispase (Corning) for 15 min at 37°C. Cell sheets released from the plate were rinsed with PBS+, transferred to 1.5 ml Eppendorf tubes in 500µl PBS+, and then subjected to mechanical stress on

an orbital shaker on its highest setting for 45 sec. Fragments were transferred to a fresh 24-well plate, fixed with 1% PFA, and stained with methylene blue (Sigma). Plates were imaged on an Elispot scanner (Cellular Technologies, Ltd) and fragments counted with ImageJ.

Surface Biotinylation

Cells were grown until confluent in a 6-well tissue culture plate and then biotinylated for 30 min at 37°C using PBS+ containing 0.5mg/ml EX-Link Sulfo-NHS-SS-Biotin (Thermo Scientific 21331). Unbound biotin was quenched in cold PBS+ containing 50mM Tris-HCl for 1 min on ice. After washing in cold 1X PBS+, cells were lysed in RIPA (PBS+ containing 1% Triton X-100, 0.1% SDS, 0.1% sodium deoxycholate, 10 mM Tris-HCl, 140 mM NaCl, 1 mM EDTA, 0.5 mM EGTA, and protease inhibitor cocktail [Roche 11836153001]), scraped to collect, transferred to an Eppendorf tube, and incubated on ice for 10 minutes. Biotinylated protein was captured on streptavidin-coated beads (Thermo Scientific 20349) during 1 hour rotation at 4°C. Beads were collected by centrifugation at 2500 xg at 4°C for 1 min and washed three times with cold PBS+. Protein was released from beads using 2X Laemmli buffer containing 5% β-mercaptoethanol.

Protein turnover assays

Cells were cultured until confluent in 12-well tissue culture plates and treated with 10 μM MG132 (Millipore 474790) or 200 μM primaquine bisphosphate (Sigma 160393) for 0, 1, 3, or 6 hours at 37°C. On ice, cells were washed with cold PBS+ and lysed in RIPA (PBS+ containing 1% Triton X-100, 0.1% SDS, 0.1% sodium deoxycholate, 10 mM Tris-HCl, 140 mM NaCl, 1 mM EDTA, 0.5 mM EGTA, and protease inhibitor cocktail [Roche 11836153001]), scraped to collect, transferred to an Eppendorf tube, and mixed 1:1 with 2X Laemmli buffer containing 5% β-mercaptoethanol. All samples were heated to 95°C for 10 min and vortexed half-way through, prior to being run on a gel for western blotting.

qRT-PCR

Cells were grown to 90% confluency in 6-well plates. Total RNA was isolated using Trizol (Life Technologies) and reverse transcribed using the iScript cDNA Synthesis kit (Bio-Rad). We used the PerfeCta SYBR Green FastMix kit (Quantabio) for qPCR and ran reactions in 96-well plates on a Lightcycler. Primer pairs (IDT; 5'-GAACCGCATCGAGCTGAA-3') were used to amplify part of the GFP tag. Primer pairs for human GAPDH and β-actin were used as reference genes.

Statistics

Error bars represent standard error of the mean. Significance was determined using one-way ANOVA followed by Dunnett's post-hoc and p-values have been indicated. Statistical analysis of immunofluorescence results was conducted on at least 3 independent experiments with 10 images per condition per replicate. For all experiments involving western blotting, statistical analysis was conducted on results from four independent experiments. Statistical analysis of dispase assays was conducted on results from seven independent experiments.

3.5 ACKNOWLEDGEMENTS

The author would like to thank Dr. Ryan Hobbs and Natella Maglakelidze for their help in running qRT-PCR as well as the use of their Lightcyler instrument. Work in the Kowalczyk lab is supported by grants R01AR050501 and R01AR048266 from the National Institutes of Health. SEZ was supported by a training grant from the National Institutes of Health T32GM008367. DEC was supported by grants R03AR068096 and R35GM119617 from the National Institutes of Health. MA was supported by funding from Advanced Research and Development Programs for Medical Innovation (AMED-CREST) (19gm0910002h0105) from the Japan Agency for Medical Research and Development (AMED) and by a Grant-in-Aid for Scientific Research (B) (18H02832) from the Japan Society for the Promotion of Science (JSPS) and by Health and Labor Sciences Research

Grants, Research on Intractable Diseases (20FC1052) from the Ministry of Health, Labor and Welfare of Japan. This research project was also supported in part by the Emory University Integrated Cellular Imaging Microscopy Core, the Emory Flow Cytometry Core (EFCC), and the Emory Integrated Genomics Core (EIGC).

CHAPTER 4

The Desmoglein-1 Transmembrane Domain Drives Raft Association during Desmosome Assembly

ABSTRACT

The desmosome is a mesoscale lipid raft membrane microdomain which mediates robust cell adhesion through a series of protein-protein interactions to link cytoskeletal elements of adjacent cells. Desmosome assembly requires raft association of the desmosomal proteins, but this mechanism remains unknown. Physical properties of transmembrane domains (TMDs) of single-pass transmembrane proteins, including length, exposed surface area, and palmitoylation, drive raft association. We hypothesize that these TMD physical properties drive raft association of the desmosomal cadherin, desmoglein-1 (DSG1), while the abrogation of raft association will hinder desmosome assembly and function. Using the DSG-null cells from Chapter 2, we expressed a panel of $Dsg1_{TMD}$-GFP variants to individually assess the contribution of each physical property towards Dsg1 raft association and assembling functional desmosomes. We find that TMD length and exposed surface area but not palmitoylation drive raft association, but we could not rule out the possible contribution of unidentified motifs. Furthermore, while reduced Dsg1 raft association impacts desmosome assembly and function, these processes can be uncoupled. We propose an amended model of desmosome assembly in which raft association simultaneously drives segregation from adherens junctions and promotes clustering of desmosomal proteins.

4.1 INTRODUCTION

Essential for epidermal integrity, desmosomes are intercellular junctions that mechanically couple adjacent cells to mediate robust cell-cell adhesion by linking cytoskeletal elements through a series of protein-protein interactions (15). Extensively discussed in Chapter 1, desmosomes have been characterized as a type of highly ordered, intermediately-sized lipid raft membrane microdomain into which the desmosomal proteins partition (6). Though the lipid raft partitioning mechanism of desmosomal proteins remains unknown, our work with the two disease-causing DSG1 mutants characterized in Chapter 3 points to the transmembrane domain (TMD) as a likely driver of desmosomal cadherin raft association as both mutants notably had missense mutations in the TMD-encoding portion of *DSG1*. In general, mechanisms guiding the partitioning of raft-associating membrane proteins into lipid rafts is incompletely understood, but this mechanism has been proposed to involve protein-lipid (62) and/or protein-cholesterol interactions (63) mediated by the TMD. Indeed, three structural features of TMDs that dictate raft affinity of single-pass transmembrane proteins have been identified. Collectively termed TMD physical properties, these include TMD length, TMD surface area, and palmitoylation status (64-66), all of which are thoroughly described in Chapter 1.

We hypothesize that one or more of these $DSG1_{TMD}$ physical properties dictate lipid raft association, desmosome assembly, and desmosome function while mutations disrupting these properties cause disease. To address the contribution of each of the physical properties, we created a panel of $Dsg1_{TMD}$ variants designed to individually assess the contribution of each TMD physical property towards raft association. We used this panel of differentially-behaving $Dsg1_{TMD}$ variants to parse out the relationship between Dsg1 raft association and desmosome assembly and function. We find that both TMD length and TMD surface area but not palmitoylation are involved in Dsg1

raft association. This involvement extends to desmosome assembly and function, as none of the $Dsg1_{TMD}$ variants are able to assemble functional desmosomes as well as $Dsg1_{WT}$. Furthermore, we find that the ability of Dsg1 to associate with rafts strongly correlates with desmosome function, suggesting that raft partitioning of Dsg1 is vitally important for desmosome assembly and strength. We put forth a mechanism whereby raft partitioning of Dsg1 is an essential nucleating step in desmosome assembly that allows for clustering of desmogleins and desmocollins.

4.2 RESULTS

4.2.1 $Dsg1_{TMD}$ variants are predicted to maintain α-helical structures characteristic of TMDs

In order to dissect the contribution of each TMD physical property towards raft association of Dsg1 and its relationship to desmosome assembly and function, we designed a panel of GFP-tagged $Dsg1_{TMD}$ variants in which one of the TMD properties is altered (Figure 4.1). To address TMD length, we shortened the Dsg1 TMD by removing seven residues from either the N- or C-terminal end ($Dsg1_{\Delta 7N}$-GFP, $Dsg1_{\Delta 7C}$-GFP) or by introducing a glycine-to-arginine substitution ($Dsg1_{G552R}$-GFP) in a similar fashion to the disease-causing SAM mutant ($Dsg1_{SAM}$-GFP) (6). In these variants, the 24-residue Dsg1 TMD is shortened to 16 or 17 residues, depending on variant. To address TMD surface area, we decreased exposed surface area by substituting alanines for the normal Dsg1 TMD residues ($Dsg1_{Ala}$-GFP). We increased exposed surface area by substituting in leucines ($Dsg1_{Leu}$-GFP). The potential importance of surface area was also addressed through chimeras in which the Dsg1 TMD was swapped with TMDs from the raft associating membrane protein LAT ($Dsg1_{LAT}$-GFP) or the non-raft associating protein E-cadherin ($Dsg1_{Ecad}$-GFP). To address TMD palmitoylation, we substituted the palmitoylated cysteines with alanines ($Dsg1_{AADA}$-GFP). Considering the additional possibility that specific motifs within the TMD sequence could be important, we also scrambled the Dsg1 TMD residues in two ways ($Dsg1_{scr1}$-GFP, $Dsg1_{scr2}$-

GFP). For each variant, we predicted whether it would maintain raft association similarly to $Dsg1_{WT}$-GFP when expressed in cells. Working on the assumption that any one or all of these physical properties could be relevant for raft association, we predicted that $Dsg1_{Ala}$-GFP, $Dsg1_{LAT}$-GFP, $Dsg1_{scr1}$-GFP, and $Dsg1_{scr2}$-GFP would maintain raft association while the other variants would not.

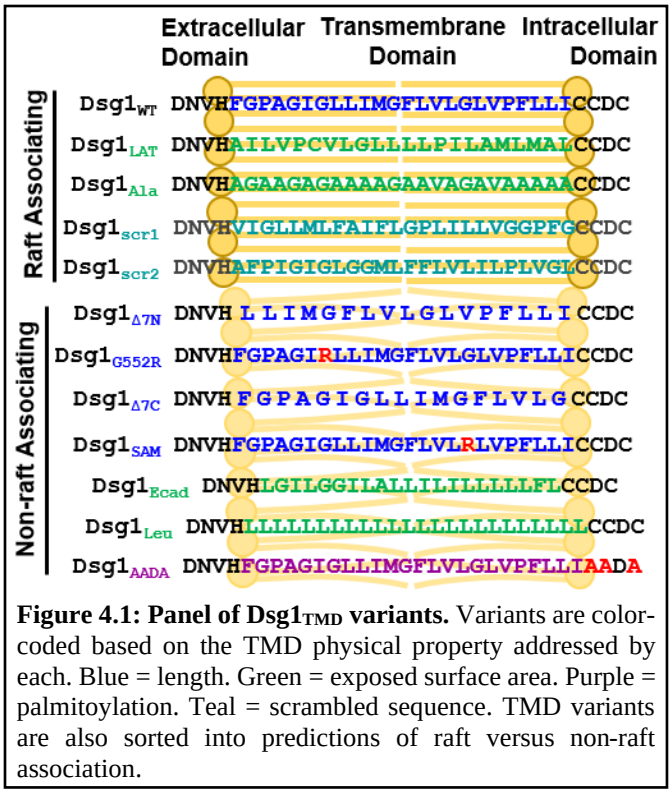

Figure 4.1: Panel of $Dsg1_{TMD}$ variants. Variants are color-coded based on the TMD physical property addressed by each. Blue = length. Green = exposed surface area. Purple = palmitoylation. Teal = scrambled sequence. TMD variants are also sorted into predictions of raft versus non-raft association.

Prior to expressing the $Dsg1_{TMD}$ variants in cells, we modeled each $Dsg1_{TMD}$ variant using the Robetta server (136) and Pymol (152) (Figure 4.2). We found that all TMD variants are predicted to maintain α-helical structures through the region expected to interact with membranes (Figure 4.2a). On further analysis with space-filling models of the Dsg1 TMD variants, we noted potentially important differences between certain variants relative to $Dsg1_{WT}$ (Figure 4.2b). $Dsg1_{scr1}$ is predicted to have a kink on the intracellular end of the TMD which may affect its predicted raft associating behavior by affecting how the lipids interact with the TMD residues. In contrast, $Dsg1_{scr2}$, with its differing sequence, does not have this kink. $Dsg1_{LAT}$ also has a kink on

the extracellular end of the TMD. $Dsg1_{Ala}$ displays an unbroken and narrow α-helix. $Dsg1_{\Delta 7N}$ and $Dsg1_{\Delta 7C}$ have shorter helices, consistent with the TMD length reduction while $Dsg1_{G552R}$ has apparently normal length, but the arginine is in a predicted position where it would be expected to "snorkel" at the interface between the hydrophobic bilayer and the outside of the cell (143, 144). Similarly, the arginine in $Dsg1_{SAM}$ is predicted to both snorkel and introduce a kink to the α-helix, as discussed more thoroughly in Chapter 3. This may suggest that $Dsg1_{G552R}$ will be able to function better than $Dsg1_{SAM}$. $Dsg1_{Ecad}$ and $Dsg1_{Leu}$ have extra bulk relative to $Dsg1_{WT}$ as planned. Lastly, $Dsg1_{AADA}$, which is displayed at a different angle from $Dsg1_{WT}$ to increase visibility of the cysteine-to-alanine substitutions, is very similar to $Dsg1_{WT}$.

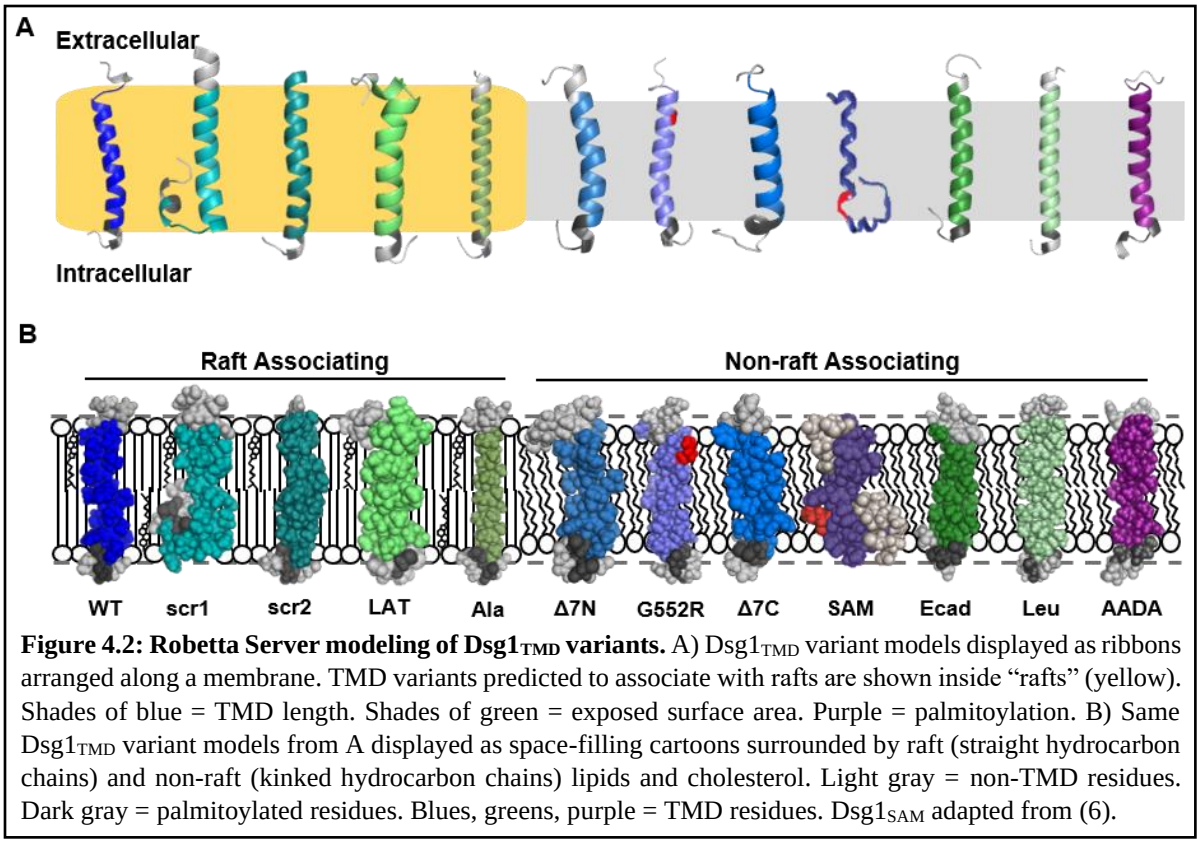

Figure 4.2: Robetta Server modeling of $Dsg1_{TMD}$ variants. A) $Dsg1_{TMD}$ variant models displayed as ribbons arranged along a membrane. TMD variants predicted to associate with rafts are shown inside "rafts" (yellow). Shades of blue = TMD length. Shades of green = exposed surface area. Purple = palmitoylation. B) Same $Dsg1_{TMD}$ variant models from A displayed as space-filling cartoons surrounded by raft (straight hydrocarbon chains) and non-raft (kinked hydrocarbon chains) lipids and cholesterol. Light gray = non-TMD residues. Dark gray = palmitoylated residues. Blues, greens, purple = TMD residues. $Dsg1_{SAM}$ adapted from (6).

In assembling and analyzing the $Dsg1_{TMD}$ variants, we determined the number of residues and expected length of each as well as calculated the raft affinity (ΔG_{raft}) (Table 4.1) (65). Raft affinity was calculated using the formula described in Chapter 1, taking into account the differing

TMD length, surface area, and palmitoylation sites of each of the $Dsg1_{TMD}$ variants. These calculations further help us predict how each $Dsg1_{TMD}$ variant will behave as they are predictions of the energy required for a single-pass transmembrane protein to associate with rafts. Therefore, lower raft affinity calculations correlate with increased likelihood of raft association. $Dsg1_{scr1}$, $Dsg1_{scr2}$, and $Dsg1_{LAT}$ have similar raft affinities to $Dsg1_{WT}$ while $Dsg1_{Ala}$ has a higher raft affinity in line with our raft associating predictions for those variants. In contrast, $Dsg1_{G552R}$, $Dsg1_{SAM}$, $Dsg1_{Ecad}$, $Dsg1_{Leu}$, and $Dsg1_{AADA}$ are predicted to require more energy to associate with rafts than $Dsg1_{WT}$. Again, this is consistent with our predictions for those variants. The raft affinity calculations for $Dsg1_{\Delta 7N}$ and $Dsg1_{\Delta 7C}$ are not consistent with our predictions for these two variants. Removing residues from the Dsg1 TMD artificially reduced the calculated surface area of these TMD variants, resulting in an apparently reduced energy required for raft association. For prediction purposes, these calculations were disregarded.

Table 4.1: Number of residues in TMD, predicted TMD length (residue number multiplied by 1.5Å), and calculated raft affinity (ΔG_{raft}) for each $Dsg1_{TMD}$ variant.

	WT	**scr1**	**scr2**	**LAT**	**Ala**	**Δ7N**	**G552R**	**Δ7C**	**SAM**	**Ecad**	**Leu**	**AADA**
Residues	24	24	24	22	24	17	17	17	16	21	24	24
Length (nm)	3.6	3.6	3.6	3.3	3.6	2.55	2.55	2.55	2.4	3.15	3.6	3.6
ΔG_{raft}	0.23	0.23	0.23	0.21	-0.34	0.16	0.37	-0.02	0.40	0.30	0.64	1.2

4.2.2 $Dsg1_{TMD}$-GFP variants mostly localize to cell borders.

To test our predictions regarding the ability of each of the $Dsg1_{TMD}$ variants to associate with rafts and assemble into functional desmosomes, we stably expressed each $Dsg1_{TMD}$-GFP variant in the DSG-null A431 cells described in Chapter 2. Stable expression using a lentiviral system resulted in a set of 12 cell lines, each expressing one of the $Dsg1_{TMD}$-GFP variants described above. Each cell line was bulk sorted using the same gating to remove very high and very low expressing cells, resulting in populations with fairly equivalent expression levels. The similarity of the expression levels was verified by immunoblot of whole cell lysates (Figure 4.3A,

B). We found that the Dsg1$_{TMD}$-GFP variants were largely expressed at similar levels to Dsg1$_{WT}$-GFP. While some were expressed a little more highly or lowly, none were significantly different from Dsg1$_{WT}$-GFP. We also assessed the protein levels of DP, DSC2, and PG in cells expressing each Dsg1$_{TMD}$-GFP variant and found some variation, but none were significantly different from cells expressing Dsg1$_{WT}$-GFP (Figure 4.3A, C-E).

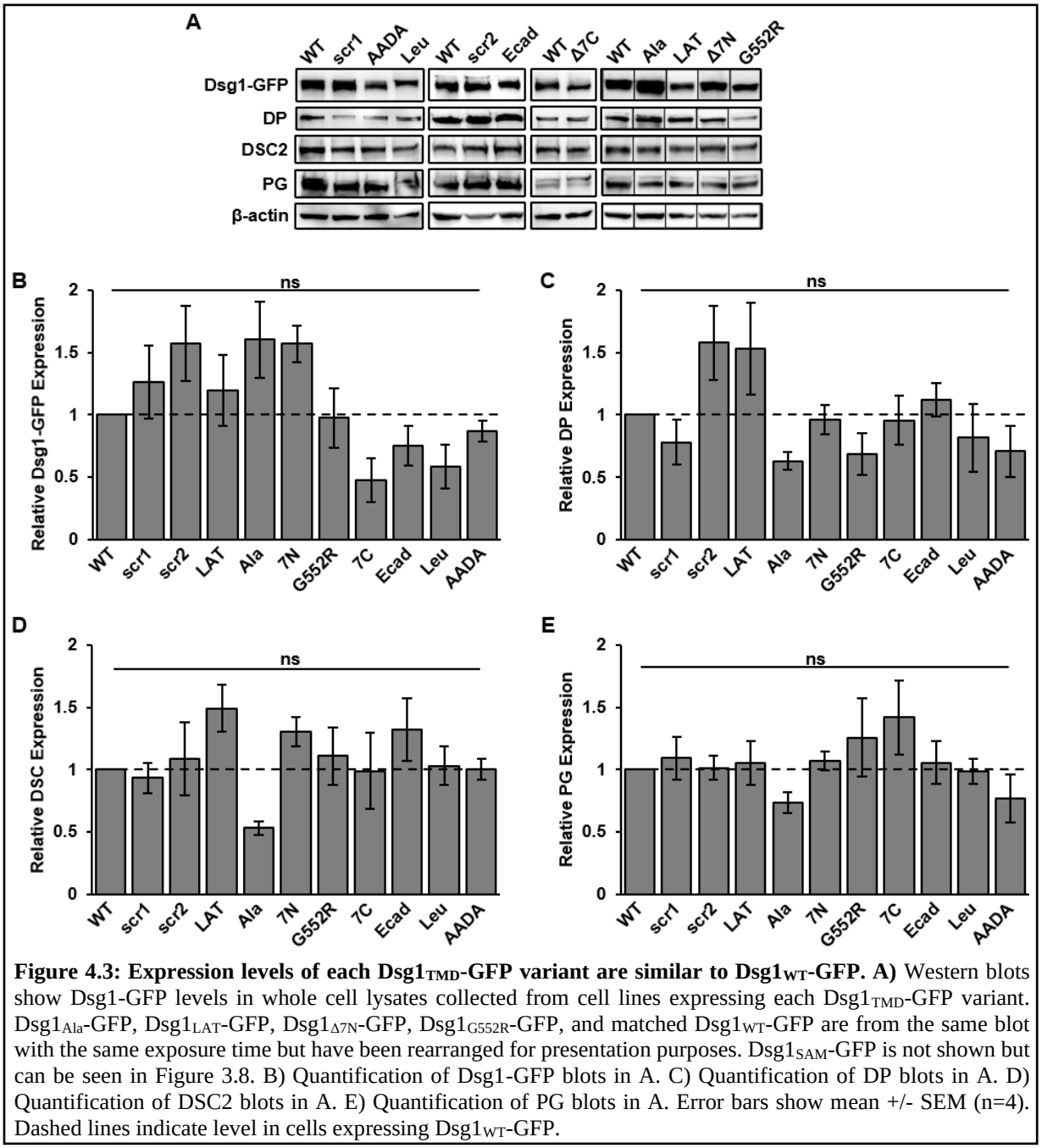

Figure 4.3: Expression levels of each Dsg1$_{TMD}$-GFP variant are similar to Dsg1$_{WT}$-GFP. A) Western blots show Dsg1-GFP levels in whole cell lysates collected from cell lines expressing each Dsg1$_{TMD}$-GFP variant. Dsg1$_{Ala}$-GFP, Dsg1$_{LAT}$-GFP, Dsg1$_{\Delta 7N}$-GFP, Dsg1$_{G552R}$-GFP, and matched Dsg1$_{WT}$-GFP are from the same blot with the same exposure time but have been rearranged for presentation purposes. Dsg1$_{SAM}$-GFP is not shown but can be seen in Figure 3.8. B) Quantification of Dsg1-GFP blots in A. C) Quantification of DP blots in A. D) Quantification of DSC2 blots in A. E) Quantification of PG blots in A. Error bars show mean +/- SEM (n=4). Dashed lines indicate level in cells expressing Dsg1$_{WT}$-GFP.

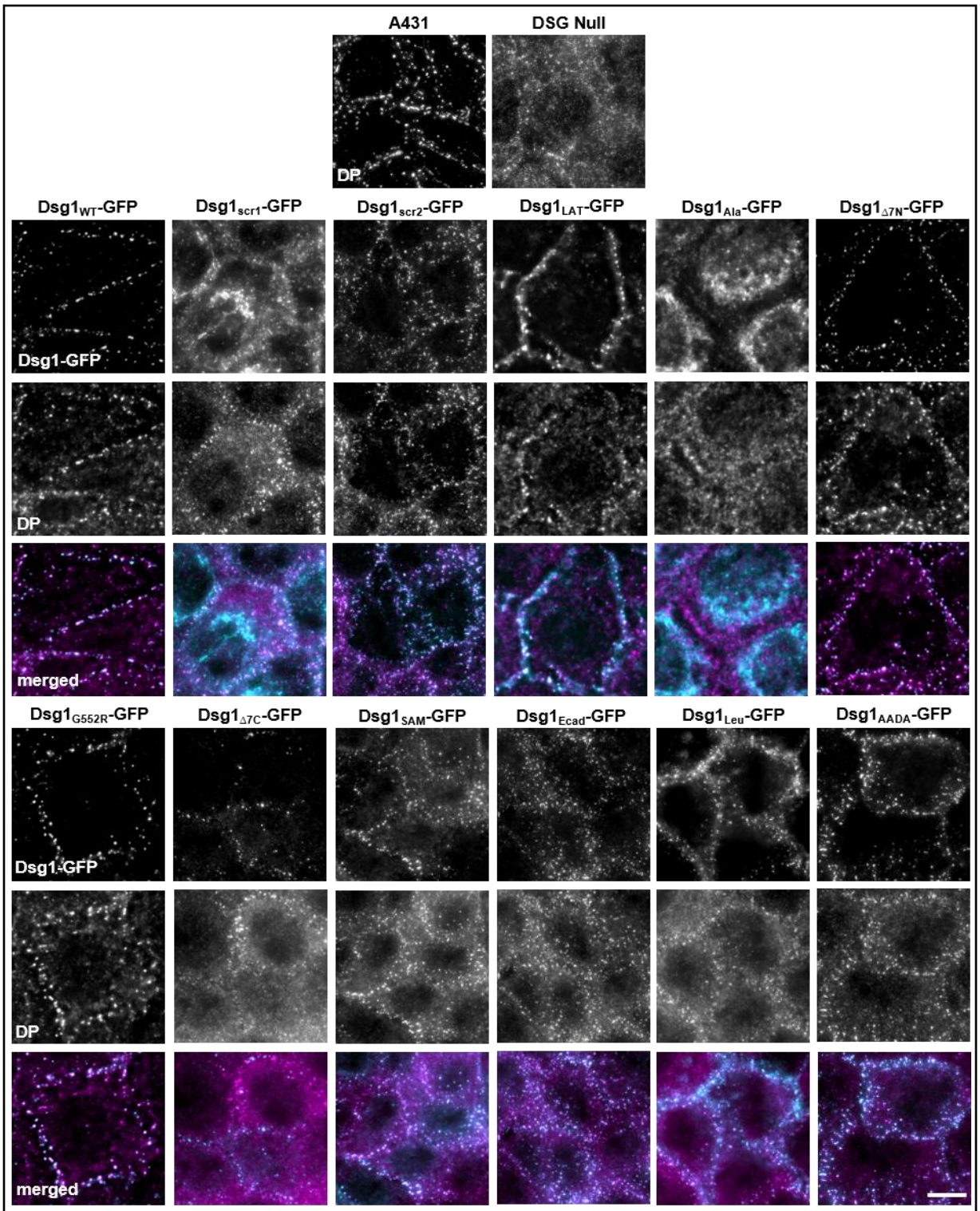

Figure 4.4: Most $Dsg1_{TMD}$-GFP variants localize to borders similarly to $Dsg1_{WT}$-GFP. Widefield immunofluorescence images show localization of each $Dsg1_{TMD}$-GFP variant in DSG-null cells. Most variants localize to cell borders. Cells were also stained for DP. DP localization in A431s and DSG-null cells included for reference. Most variants form discrete puncta containing both Dsg1-GFP and DP. Magenta = DP. Cyan = Dsg1-GFP. Scale bar = 10 µm.

Desmogleins localize to the plasma membrane where they assemble into desmosomes with other desmosomal proteins at cell-cell borders. We used immunofluorescence to verify that the $Dsg1_{TMD}$-GFP variants maintained normal localization and found that most of the $Dsg1_{TMD}$-GFP variants appeared to localize normally (Figure 4.4). However, $Dsg1_{Ala}$-GFP and $Dsg1_{scr1}$-GFP appeared predominantly in intracellular organelles, although some $Dsg1_{scr1}$-GFP also showed membrane localization. Of note, $Dsg1_{LAT}$-GFP appeared diffuse around the plasma membrane rather than in discrete puncta observed in many of the other cell lines.

As previously described in Chapter 2, desmoplakin (DP) is mislocalized in DSG-null A431 cells but can be rescued by expression of wildtype desmogleins but not disease-causing $Dsg1_{SAM}$-GFP or $Dsg1_{PPK}$-GFP mutants (see Figures 2.6, 3.2). Therefore, we also stained for DP to determine if expression of the $Dsg1_{TMD}$-GFP variants could rescue DP localization (Figure 4.4). We found strongly reduced intracellular DP staining in cells expressing $Dsg1_{scr2}$-GFP and $Dsg1_{AADA}$-GFP similar to $Dsg1_{WT}$-GFP, somewhat reduced intracellular staining in cells expressing $Dsg1_{\Delta 7N}$-GFP and $Dsg1_{G552R}$-GFP, and no reduction in intracellular DP staining in cells expressing the other $Dsg1_{TMD}$-GFP variants. Additionally, among those $Dsg1_{TMD}$-GFP variants that show apparently normal desmoglein localization, we see colocalization with DP in discrete desmosome-like puncta which may indicate that these variants are capable of desmosome assembly. Together, based on the variability in localization of the $Dsg1_{TMD}$-GFP variants, colocalization with DP, and rescue of DP localization, we have a diverse panel of mutants. In the next sections, we characterize the ability of each $Dsg1_{TMD}$-GFP variant to associate with rafts and assemble into functional desmosomes.

4.2.3 A full-length TMD is required for Dsg1 raft association, desmosome assembly, and desmosome function.

To further characterize the $Dsg1_{TMD}$-GFP variants, we categorized each variant based on the physical property being addressed. Our previous work with $Dsg1_{SAM}$-GFP suggested that the presence of the arginine residue created a 16-residue TMD from the normal 24 residues ((6), Chapter 2). As TMD length is one of the identified physical properties that has been shown to drive raft partitioning (64), we pursued this line to further evaluate the effect of TMD length on Dsg1 raft association and function. Towards this, we created the following $Dsg1_{TMD}$-GFP variants: $Dsg1_{\Delta 7N}$-GFP, $Dsg1_{\Delta 7C}$-GFP, and $Dsg1_{G552R}$-GFP and compared their behavior to that of $Dsg1_{WT}$-GFP and $Dsg1_{SAM}$-GFP.

We used sucrose gradient fractionations to assess the raft association capabilities of these $Dsg1_{TMD}$-GFP variants. Sucrose gradient fractionations allow for the segregation of buoyant, detergent-resistant membranes (DRMs) containing raft-associated proteins from non-buoyant, non-detergent-resistant membranes (non-DRMs) (118). We verified the successful segregation of these fractions by immunoblotting for the raft associating protein, flotillin-2, and the non-raft associating protein, calnexin (Figure 4.5A). In sucrose gradient fractionations, we routinely find that about 75% of $Dsg1_{WT}$-GFP segregates with DRMs (Figure 4.5A, B). However, none of the $Dsg1_{TMD}$-GFP variants addressing length maintained that level of DRM segregation (Figure 4.5A, B). We took this observation another step further to see if this loss in raft association had any effect on other desmosomal proteins. DRM segregation of DSC2 was not affected by the expression of these $Dsg1_{TMD}$-GFP variants (Figure 4.5C, D) suggesting that raft association of desmocollins may occur independently of DSG raft association, an observation we also made in Chapter 3 (Figure 3.5D, E). In contrast, significantly less plakoglobin (PG) segregated into DRMs for all $Dsg1_{TMD}$-

GFP variants except for Dsg1$_{\Delta 7N}$-GFP (Figure 4.5E, F). As PG is a cytoplasmic protein whose ability to partition into rafts would be dependent on other raft associating proteins, such as the desmosomal cadherins, this finding is unsurprising.

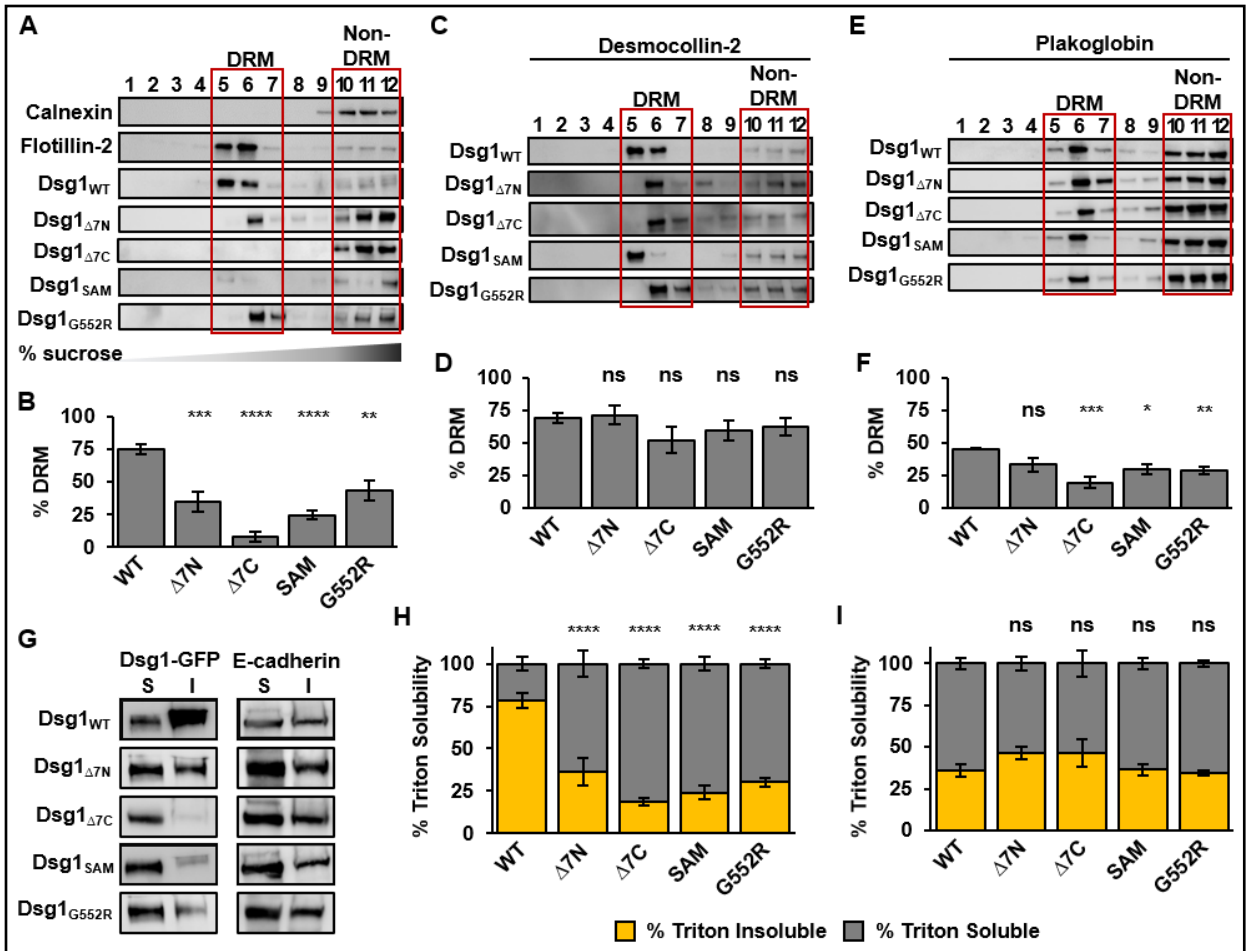

Figure 4.5: TMD length guides Dsg1 raft association. A) Western blots show segregation of Dsg1$_{TMD}$-GFP between DRM and non-DRM fractions. Calnexin = non-DRM marker. Flotillin-2 = DRM marker. Remaining blots show Dsg1-GFP in DSG-null cells expressing Dsg1$_{WT}$-GFP, Dsg1$_{\Delta 7N}$-GFP, Dsg1$_{\Delta 7C}$-GFP, Dsg1$_{SAM}$-GFP, or Dsg1$_{G552R}$-GFP. B) Quantification of A. C)Western blots show segregation of DSC2. D) Quantification of C. E) Western blots show segregation of PG. F) Quantification of E. G) Western blots show distribution of Triton X-100 soluble versus insoluble Dsg1-GFP or E-cadherin in DSG-null cells expressing Dsg1$_{WT}$-GFP, Dsg1$_{\Delta 7N}$-GFP, Dsg1$_{\Delta 7C}$-GFP, Dsg1$_{SAM}$-GFP, or Dsg1$_{G552R}$-GFP. H) Quantification of Dsg1-GFP blots in G. I) Quantification of E-cadherin blots in G. Error bars = mean +/- SEM (n=4). *p < 0.05, **p < 0.01, ***p < 0.001, ****p < 0.0001

The reduction in DRM segregation of PG and Dsg1$_{\Delta 7N}$-GFP, Dsg1$_{\Delta 7C}$-GFP, Dsg1$_{G552R}$-GFP, and Dsg1$_{SAM}$-GFP relative to Dsg1$_{WT}$-GFP in cells expressing these variants may result in reduced cytoskeletal attachment of desmosomes formed from those variants. Segregation of whole cell lysates into Triton X-100 insoluble and soluble fractions can be used as an indication of

cytoskeletal attachment and overall desmosome assembly where greater Triton X-100 insolubility equates to greater levels of cytoskeletal attachment and assembled desmosomes (6, 50, 135). Most $Dsg1_{WT}$-GFP is found in the insoluble fraction. However, the $Dsg1_{TMD}$-GFP variants were significantly more soluble in Triton X-100 than $Dsg1_{WT}$-GFP (Figure 4.5G, H). This effect appeared to be specific to Dsg1 rather than a global impact on Triton X-100 solubility, as E-cadherin solubility in Triton X-100 was unchanged across the cell lines (Figure 4.5G, I). Therefore, these results suggest that these $Dsg1_{TMD}$-GFP variants are less capable of assembling cytoskeletally-attached desmosomes which may be the result of reduced raft partitioning.

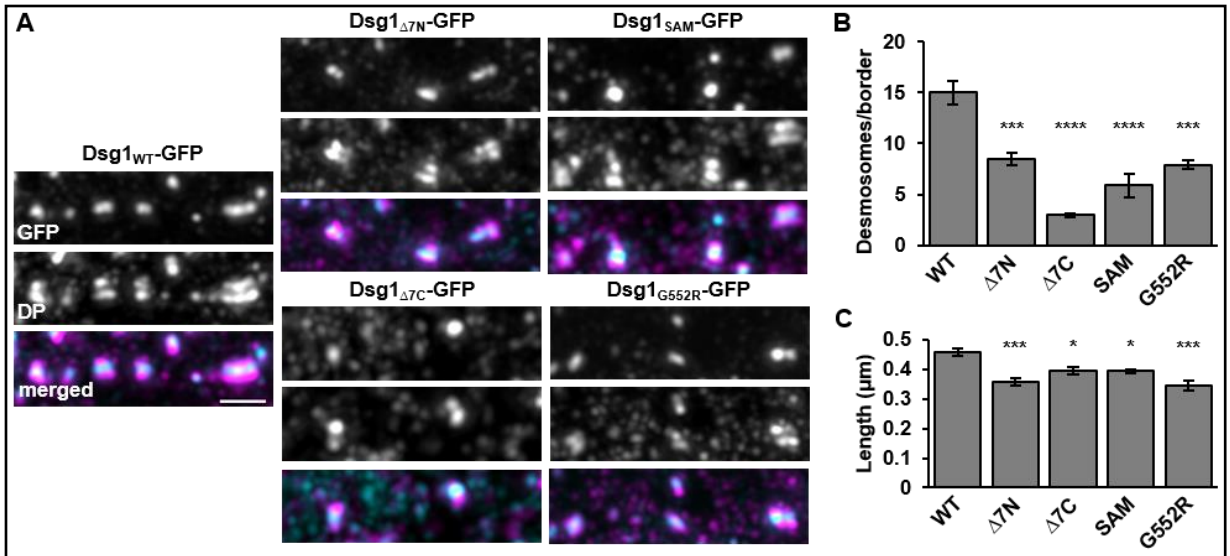

Figure 4.6: Short $Dsg1_{TMD}$ variants support the formation of fewer, smaller desmosomes. A) SIM images show resolved desmosomes in DSG-null cells expressing $Dsg1_{WT}$-GFP, $Dsg1_{\Delta 7N}$-GFP, $Dsg1_{\Delta 7C}$-GFP, $Dsg1_{SAM}$-GFP, or $Dsg1_{G552R}$-GFP. Magenta = DP. Cyan = Dsg1-GFP. Scale bar = 1 μm. B) Quantification of desmosome number per border. C) Quantification of desmosome length. Error bars = mean +/- SEM (n=3, 10 images per replicate). *$p < 0.05$, ***$p < 0.001$, ****$p < 0.0001$

Desmosomes assemble into characteristic mirror-imaged, railroad track patterns which can be observed with super-resolution microscopy (133, 134). Having already seen by immunofluorescence and widefield microscopy (Figure 4.4) that these $Dsg1_{TMD}$-GFP variants display some level of border localization with DP, we used structured illumination microscopy (SIM) to determine whether $Dsg1_{\Delta 7N}$-GFP, $Dsg1_{\Delta 7C}$-GFP, and $Dsg1_{G552R}$-GFP formed

desmosomes with normal characteristics (Figure 4.6A). We assessed both desmosome quantity and length and only quantified those desmosomes that fit our definition: mirrored DP railroad tracks sandwiching Dsg1-GFP. While "true" desmosomes were identified in all cell lines, we found that significantly fewer desmosomes formed per border in all of the variants analyzed here (Figure 4.6B). Similarly, desmosomes were also significantly shorter than those formed in cells expressing $Dsg1_{WT}$-GFP (Figure 4.6C). These results corroborate findings from the Triton X-100 solubility assay, further suggesting that these $Dsg1_{TMD}$-GFP variants are less capable of assembling desmosomes and implying that Dsg1 TMD length is important for supporting desmosome assembly, possibly through initial raft association.

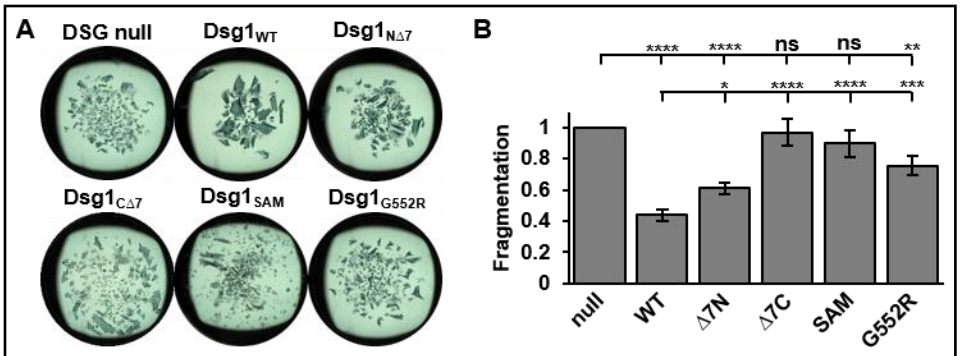

Figure 4.7: Short $Dsg1_{TMD}$ variants form weaker desmosomes than $Dsg1_{WT}$. A) Images show monolayer fragmentation of DSG-null cells and DSG-null cells expressing $Dsg1_{WT}$-GFP, $Dsg1_{\Delta 7N}$-GFP, $Dsg1_{\Delta 7C}$-GFP, $Dsg1_{SAM}$-GFP, or $Dsg1_{G552R}$-GFP. B) Quantification of A. $Dsg1_{TMD}$ variants were compared to DSG-null cells to assess degree of desmosome function rescue and to DSG-null cells expressing $Dsg1_{WT}$-GFP. Error bars show mean +/- SEM (n=6, each replicate includes 4 monolayers). *p < 0.05, **p < 0.01, ***p < 0.001, ****p < 0.0001

The reduced raft association of the $Dsg1_{TMD}$-GFP variants and PG, reduced cytoskeletal attachments, and reduced desmosome quantity and length, all suggest that desmosome function will be limited in these cell lines. We used a dispase cell dissociation assay to test desmosome function. In this assay, the enzyme dispase is used to lift confluent cell monolayers off their substrate. The monolayers are subjected to mechanical stress on an orbital shaker resulting in fragmentation dependent on desmosome strength (Figure 2.4) (119). We compared the

fragmentation of $Dsg1_{TMD}$-GFP variant cell monolayers to both DSG-null cell monolayers which fragment readily and to $Dsg1_{WT}$-GFP cell monolayers in which desmosome function is rescued. With these comparisons, we were able to determine which $Dsg1_{TMD}$-GFP variants could rescue desmosome function in the DSG-null cells and whether any of the $Dsg1_{TMD}$-GFP variants could rescue as well as $Dsg1_{WT}$-GFP. We found that neither $Dsg1_{\Delta 7C}$-GFP nor $Dsg1_{SAM}$-GFP could rescue desmosome function compared to DSG-null cells. In contrast, $Dsg1_{\Delta 7N}$-GFP and $Dsg1_{G552R}$-GFP were able to partly rescue desmosome function, but neither could do so as well as $Dsg1_{WT}$-GFP (Figure 4.7A, B).

Altogether, this characterization of $Dsg1_{TMD}$-GFP variants addressing the importance of Dsg1 TMD length suggest that TMD length is involved in raft association of Dsg1. Furthermore, the combined reduction in raft association with reduced desmosome assembly and function suggests an important role for Dsg1 raft association in these mechanisms. Intriguingly, truncation or introduction of an arginine residue seems to have a greater impact when applied to the C-terminal end of the TMD versus the N-terminal end. The exact relevance of this is interesting but unclear. However, further characterization of the remaining $Dsg1_{TMD}$-GFP variants and the physical properties that each addresses may shed some light on this observation.

4.2.4 TMD palmitoylation does not contribute to Dsg1 raft association or desmosome assembly.

Palmitoylation occurs at cysteine residues adjacent to the cytoplasmic side of TMDs (153). We created a $Dsg1_{TMD}$-GFP variant that cannot be palmitoylated by replacing the normal cysteines with alanines. In contrast, $Dsg1_{WT}$-GFP will be palmitoylated in its normal fashion. Characterization of cells expressing the $Dsg1_{AADA}$-GFP variant will address how palmitoylation may contribute to raft association of Dsg1 and subsequent desmosome assembly and function.

Utilizing the sucrose gradient fractionation assay described above, we found that there is a slight but insignificant decrease in DRM segregation between $Dsg1_{AADA}$-GFP and $Dsg1_{WT}$-GFP (Figure 4.8A, B), suggesting that $Dsg1_{AADA}$-GFP remains capable of associating with rafts. We also assessed the segregation of DSC2 and PG with DRMs and found small but insignificant decreases in segregation of DSC2 and PG (Figure 4.8C-F) in cells expressing $Dsg1_{AADA}$-GFP compared to $Dsg1_{WT}$-GFP. Therefore, loss of palmitoylation does not appear to substantially affect raft association of Dsg1.

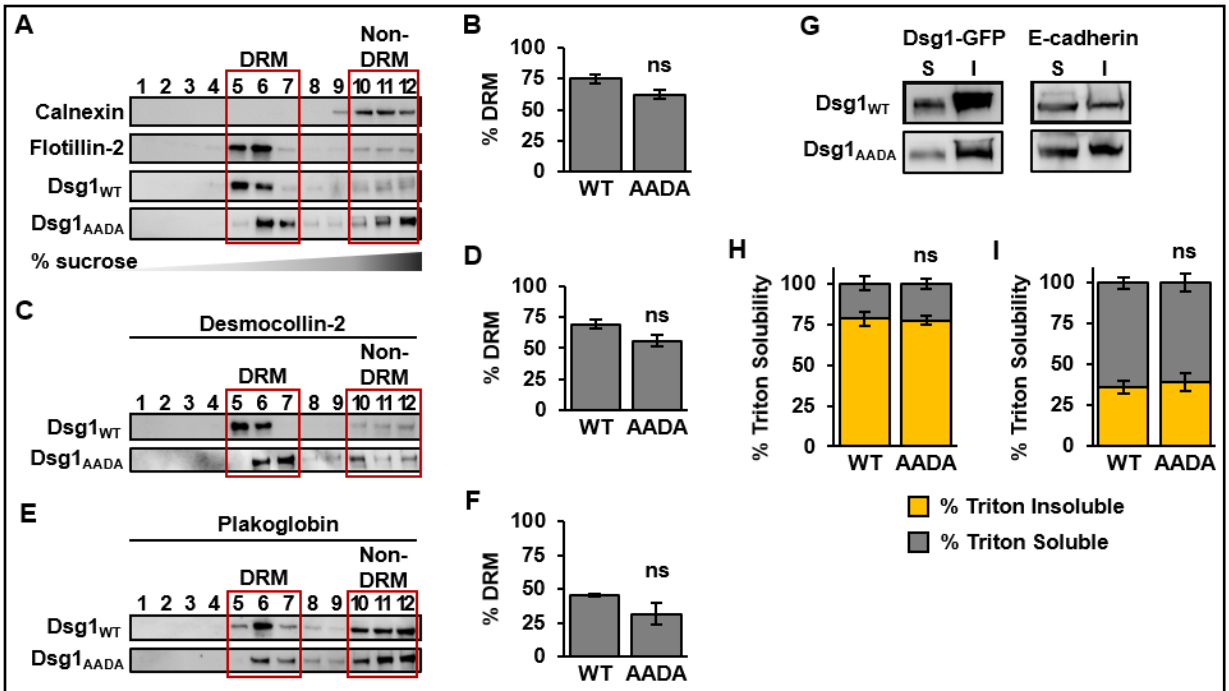

Figure 4.8: Palmitoylation is not required for Dsg1 raft association. A) Western blots show segregation of $Dsg1_{TMD}$-GFP between DRM and non-DRM fractions. Calnexin = non-DRM marker. Flotillin-2 = DRM marker. Remaining blots show Dsg1-GFP in DSG-null cells expressing $Dsg1_{WT}$-GFP or $Dsg1_{AADA}$-GFP. B) Quantification of A. C) Western blots show segregation of DSC2. D) Quantification of C. E) Western blots show segregation of PG. F) Quantification of E. G) Western blots show distribution of Triton X-100 soluble versus insoluble Dsg1-GFP or E-cadherin in DSG-null cells expressing $Dsg1_{WT}$-GFP or $Dsg1_{AADA}$-GFP. H) Quantification of Dsg1-GFP blots in G. I) Quantification of E-cadherin blots in G. Error bars = mean +/- SEM (n=4). *$p < 0.05$

Considering the minor effects on raft partitioning observed in sucrose gradient fractionations, we considered whether there might be any impact on cytoskeletal attachment and desmosome assembly using the Triton X-100 solubility assay described above. We observed no

differences in the solubility of Dsg1$_{AADA}$-GFP in Triton X-100 (Figure 4.8G, H). We also found that no global differences in Triton X-100 solubility exist between the two cell lines, as solubility of E-cadherin was also unchanged (Figure 4.8G, I). Therefore, cells expressing Dsg1$_{AADA}$-GFP appear to assemble desmosomes with normal cytoskeletal attachment as well as those expressing Dsg1$_{WT}$-GFP.

Having already seen by immunofluorescence and widefield microscopy (Figure 4.4) that Dsg1$_{AADA}$-GFP localizes to cell borders with DP, we used SIM to verify that Dsg1$_{AADA}$-GFP formed desmosomes with normal characteristics (Figure 4.9A). Again quantifying desmosome quantity and length, we found that Dsg1$_{AADA}$-GFP formed as many desmosomes per border as Dsg1$_{WT}$-GFP (Figure 4.9B), but those desmosomes were slightly shorter on average (Figure 4.9C). This suggests that palmitoylation may not be involved in desmosome assembly but may play a role in regulation of desmosome size or desmosome maintenance independent of raft association.

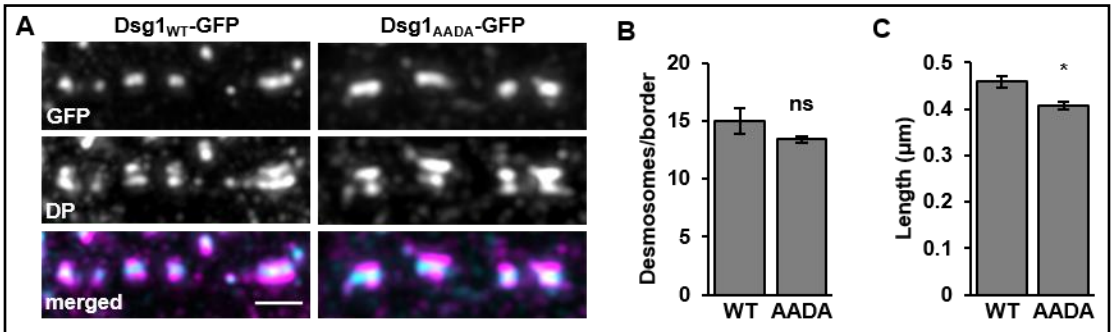

Figure 4.9: Unpalmitoylated Dsg1 forms small desmosomes. A) SIM images show resolved desmosomes in DSG-null cells expressing Dsg1$_{WT}$-GFP or Dsg1$_{AADA}$. Magenta = DP. Cyan = Dsg1-GFP. Scale bar = 1 µm. B) Quantification of desmosome number per border. C) Quantification of desmosome length. Error bars = mean +/- SEM (n=3, 10 images per replicate). *p < 0.05

While Dsg1$_{AADA}$-GFP has only minor effects on Dsg1 raft association and desmosome characteristics, it remains to be seen whether Dsg1$_{AADA}$-GFP affects desmosome function. Again comparing fragmentation of Dsg1$_{AADA}$-GFP cell monolayers to both DSG-null cell monolayers and Dsg1$_{WT}$-GFP cell monolayers using the dispase cell dissociation assay, we found that expression of Dsg1$_{AADA}$-GFP rescued desmosome function relative to the DSG-null cells, but it

did not rescue as fully as Dsg1$_{WT}$-GFP (Figure 4.10A, B). While this may indicate that loss of palmitoylation has some effect on Dsg1 function, this effect does not appear to be directly related to raft partitioning.

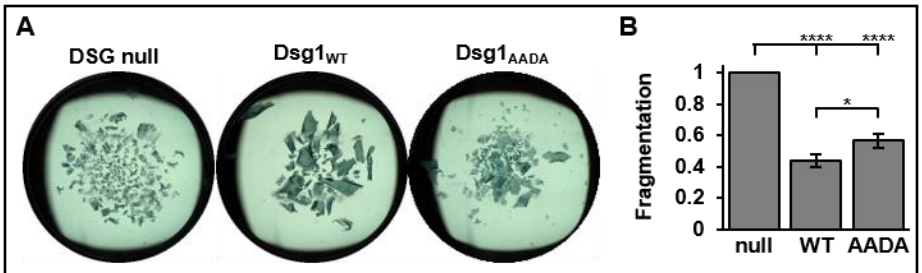

Figure 4.10: Dsg1 palmitoylation is required for strong desmosomes. A) Images show monolayer fragmentation of DSG-null cells and DSG-null cells expressing Dsg1$_{WT}$-GFP or Dsg1$_{AADA}$-GFP. B) Quantification of A. Dsg1$_{TMD}$ variants were compared to DSG-null cells to assess degree of desmosome function rescue and to DSG-null cells expressing Dsg1$_{WT}$-GFP. Error bars show mean +/- SEM (n=6, each replicate includes 4 monolayers). *p < 0.05, ****p < 0.0001

Altogether, this characterization of Dsg1$_{TMD}$-GFP variants addressing the importance of palmitoylation suggests that this posttranslational modification is not involved in raft association of Dsg1. However, the shorter desmosomes observed in SIM images coupled with the reduced ability to rescue desmosome function in DSG-null cells compared to those expressing Dsg1$_{WT}$-GFP suggest that palmitoylation plays an important role in desmosome dynamics.

4.2.5 Altering Dsg1$_{TMD}$ surface area reduces raft association, desmosome assembly, and function

TMD surface area refers to the cumulative area of the TMD residue side chains that physically interact with lipids (65). TMDs which are largely composed of “bulky” residues like leucine have greater exposed surface areas than those composed of residues with smaller side chains, such as alanine. Single-pass transmembrane proteins containing TMDs with smaller surface areas are more likely to associate with rafts than those with larger surface areas as the smaller surface area will be more energetically favored in the ordered lipid and cholesterol-

enriched environment of raft domains. In the Dsg1 TMD, we have altered the exposed surface area in two ways, both with the intent of increasing or decreasing exposed surface area. First, we substituted residues for alanines to reduce surface area or for leucines to increase surface area. Second, we created $Dsg1_{TMD}$ chimeras in which the TMD was replaced with the raft associating LAT TMD (66) or the non-raft associating E-cadherin TMD (50). Importantly, surface area has previously been shown to be important for raft association of LAT (65). Similarly, the many leucines in the E-cadherin TMD create a bulkier TMD than seen in Dsg1. If exposed surface area of the Dsg1 TMD is important for raft association and desmosome assembly and function, then the $Dsg1_{TMD}$-GFP variants with reduced surface area ($Dsg1_{Ala}$-GFP and $Dsg1_{LAT}$-GFP) should behave similarly to $Dsg1_{WT}$-GFP while those with increased surface area ($Dsg1_{Leu}$-GFP and $Dsg1_{Ecad}$-GFP) should have reduced raft association which may further impact desmosome assembly and function as seen with those $Dsg1_{TMD}$-GFP variants addressing TMD length.

As with the other TMD property categories being characterized here, we used sucrose gradient fractionations to assess the ability of each $Dsg1_{TMD}$-GFP variant to segregate with DRMs. DRM segregation was significantly reduced for all the $Dsg1_{TMD}$-GFP variants in this category (Figure 4.11A, B), despite our expectation that reducing the TMD surface area would not affect this characteristic of Dsg1 behavior. We also found reduced DRM segregation of DSC2 (Figure 4.11C, D) and PG (Figure 4.11E, F), suggesting that the TMD alterations in these variants impacts raft association of Dsg1 as well as other desmosomal proteins.

Due to the extensive reduction in raft association of Dsg1 as well as other desmosomal proteins in cells expressing these $Dsg1_{TMD}$-GFP variants, we asked whether cytoskeletal attachment and desmosome assembly was affected in these cell lines, again using the Triton X-100 solubility assay. We observed significantly increased Triton X-100 solubility for all these

TMD variants, suggesting reduced cytoskeletal attachment and desmosome formation (Figure 4.11G, H). There was no global impact on Triton X-100 solubility as E-cadherin had normal solubility levels across these cell lines (Figure 4.11G, I).

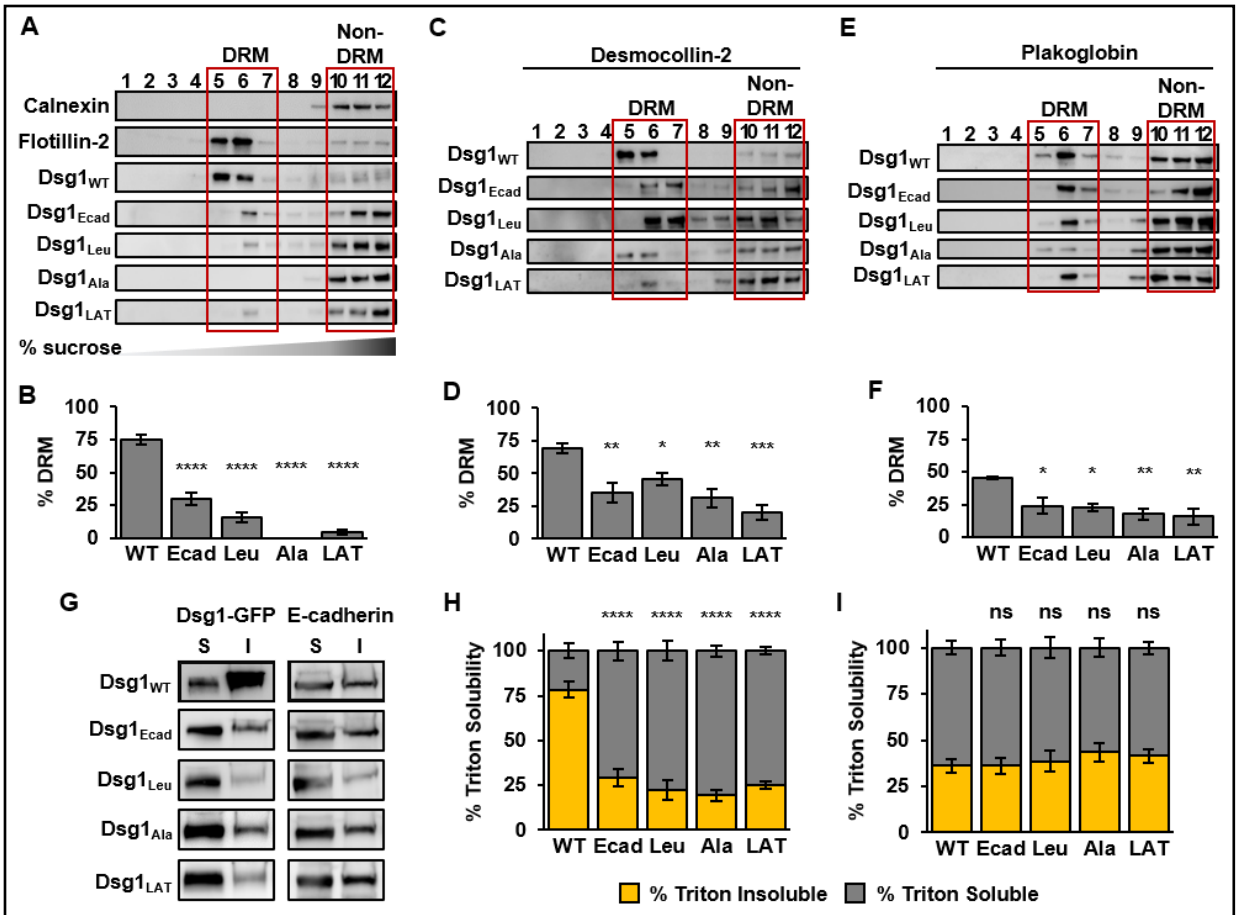

Figure 4.11: TMD exposed surface area guides Dsg1 raft association. A) Western blots show segregation of $Dsg1_{TMD}$-GFP between DRM and non-DRM fractions. Calnexin = non-DRM marker. Flotillin-2 = DRM marker. Remaining blots show Dsg1-GFP in DSG-null cells expressing $Dsg1_{WT}$-GFP, $Dsg1_{Ecad}$-GFP, $Dsg1_{Leu}$-GFP, $Dsg1_{Ala}$-GFP, or $Dsg1_{LAT}$-GFP. B) Quantification of A. C) Western blots show segregation of DSC2. D) Quantification of C. E) Western blots show segregation of PG. F) Quantification of E. G) Western blots show distribution of Triton X-100 soluble versus insoluble Dsg1-GFP or E-cadherin in DSG-null cells expressing $Dsg1_{WT}$-GFP, $Dsg1_{Ecad}$-GFP, $Dsg1_{Leu}$-GFP, $Dsg1_{Ala}$-GFP, or $Dsg1_{LAT}$-GFP. H) Quantification of Dsg1-GFP blots in G. I) Quantification of E-cadherin blots in G. Error bars = mean +/- SEM (n=4). *p < 0.05, **p < 0.01, ***p < 0.001, ****p < 0.0001

Some of these results thus far may not be surprising considering localization results obtained by widefield immunofluorescence microscopy. In Figure 4.4, $Dsg1_{Ala}$-GFP was found to have substantial localization issues and $Dsg1_{LAT}$-GFP localized to cell borders but appeared diffuse through the membrane, in contrast to other cell lines in which the expressed $Dsg1_{TMD}$-GFP variant

formed discrete DP-positive puncta at cell borders. Only $Dsg1_{Ecad}$-GFP and $Dsg1_{Leu}$-GFP colocalized with DP into discrete cell border puncta. Results from our sucrose gradient fractionations and Triton X-100 solubility assays suggest that desmosomes may have difficulty forming in these cell lines. By SIM, we were able to identify classical, mirrored DP railroad track formation in all cell lines (Figure 4.12A), however, quantification revealed significantly fewer desmosomes per border in all cell lines (Figure 4.12B). Though fewer desmosomes formed overall, the length of these desmosomes was not significantly different from $Dsg1_{WT}$-GFP with the exception of $Dsg1_{Ala}$-GFP (Figure 4.12C). It should be noted that due to the trafficking issues of $Dsg1_{Ala}$-GFP, desmosomes are rarely observed in these cells.

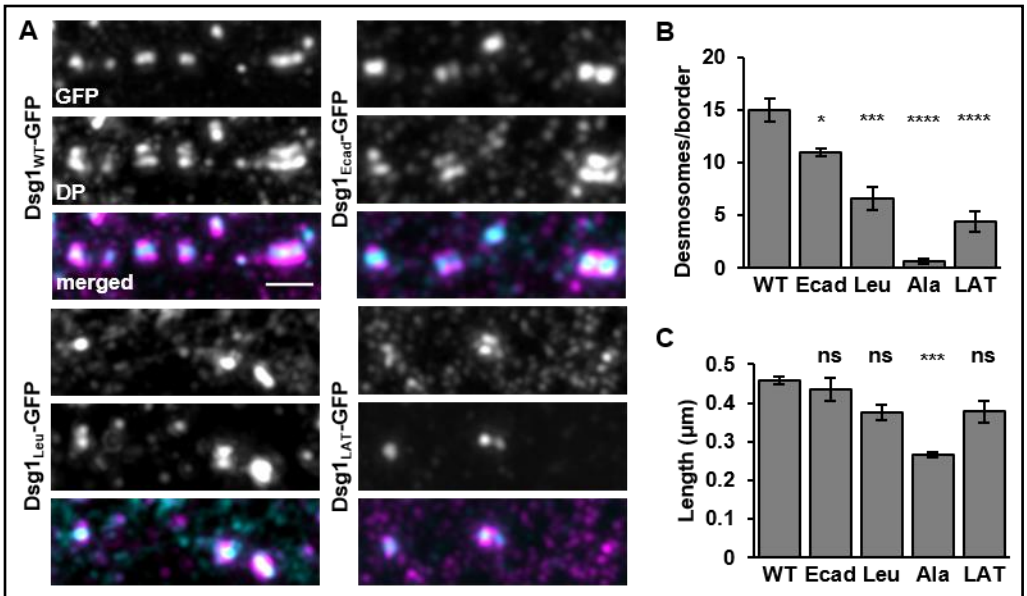

Figure 4.12: $Dsg1_{TMD}$ variants with altered surface area support the formation of fewer desmosomes. A) SIM images show resolved desmosomes in DSG-null cells expressing $Dsg1_{WT}$-GFP, $Dsg1_{Ecad}$-GFP, $Dsg1_{Leu}$-GFP, or $Dsg1_{LAT}$-GFP. Images for cells expressing $Dsg1_{Ala}$-GFP not shown. Magenta = DP. Cyan = Dsg1-GFP. Scale bar = 1 μm. B) Quantification of desmosome number per border. C) Quantification of desmosome length. Error bars = mean +/- SEM (n=3, 10 images per replicate). *$p < 0.05$, ***$p < 0.001$, ****$p < 0.0001$

The results from our previous assays suggested that cells expressing these $Dsg1_{TMD}$-GFP variants would be unlikely to rescue desmosome function in the DSG-null cells in a dispase cell

dissociation assay. As expected, none of these Dsg1$_{TMD}$-GFP variants were able to do so (Figure 4.13A, B).

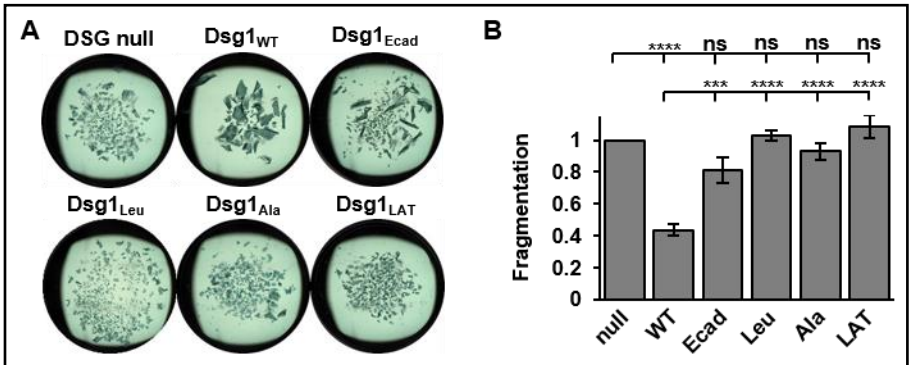

Figure 4.13: Dsg1$_{TMD}$ variants with altered surface areas form non-functional desmosomes. A) Images show monolayer fragmentation of DSG-null cells versus DSG-null cells expressing Dsg1$_{WT}$-GFP, Dsg1$_{Ecad}$-GFP, Dsg1$_{Leu}$-GFP, Dsg1$_{Ala}$-GFP, or Dsg1$_{LAT}$-GFP. B) Quantification of A. Dsg1$_{TMD}$ variants were compared to DSG-null cells to assess degree of desmosome function rescue and to DSG-null cells expressing Dsg1$_{WT}$-GFP. Error bars show mean +/- SEM (n=6, each replicate included 4 monolayers). ***p < 0.001, ****p < 0.0001

Altogether, this characterization of Dsg1$_{TMD}$-GFP variants suggest that exposed surface area of residue side chains is relevant to the raft associating mechanism of Dsg1. Furthermore, in line with the results from those variants that addressed TMD length, the combined reduction in raft association with reduced desmosome assembly and function continues to imply an important role for Dsg1 raft association in these desmosomal mechanisms. Intriguingly, we saw a loss in raft association, desmosome assembly and function from all variants addressing exposed surface area, including those that were expected to maintain raft association. The exact relevance of this is unclear. While this completes our analysis of the role of known TMD physical properties potentially involved in Dsg1 raft association, it remains to be seen whether a specific motif or residue(s) in the Dsg1 TMD might be involved in raft association.

4.2.6 Scrambling the Dsg1 TMD sequence reduces raft association but has differential effects on desmosome assembly and function.

The above sections characterize mutants which address the TMD physical properties of length, surface area, and palmitoylation on Dsg1 raft association. Among these, we have collected evidence for the involvement of TMD length and TMD surface area but not palmitoylation towards the ability of Dsg1 to associate with rafts and assemble into functional desmosomes. In the process of designing those $Dsg1_{TMD}$-GFP variants which address TMD length and TMD surface area, it was necessary to make extensive changes to the Dsg1 TMD sequence, i.e., stretches of residues were removed to shorten the length and TMDs from different proteins introduced to adjust surface area. Therefore, it is difficult to differentiate between the changes made to the Dsg1 TMD length or surface area versus overall changes made to the Dsg1 TMD sequence as the main driver of our results. Our approach thus far assumes that the overall hydrophobicity of the Dsg1 TMD or the TMD as a whole is more important for raft association than any individual part of the TMD sequence. Yet, cholesterol- or lipid-binding domains, or even TMD-TMD dimerization domains could be the main driver of Dsg1 raft association. There are no such identified motifs in the Dsg1 TMD to date, but this is the first study to specifically examine the TMD of a desmosomal cadherin. To address this possibility, our final two $Dsg1_{TMD}$-GFP variants were scrambled versions of the Dsg1 TMD, $Dsg1_{scr1}$-GFP and $Dsg1_{scr2}$-GFP. These were generated by running the amino acid sequence through a random sequence generator. Based on previous work performed on other raft-associating single-pass transmembrane proteins, we anticipated that scrambling the Dsg1 TMD sequence would not affect raft association of Dsg1.

By sucrose gradient fractionations, we found that both $Dsg1_{scr1}$-GFP and $Dsg1_{scr2}$-GFP showed significantly reduced DRM association relative to $Dsg1_{WT}$-GFP (Figure 4.14A, B). DRM association of DSC2 was not significantly affected by expression of $Dsg1_{scr1}$-GFP or $Dsg1_{scr2}$-GFP (Figure 4.14C, D), but DRM association of PG was significantly reduced in these cell lines

compared to expression of $Dsg1_{WT}$-GFP (Figure 4.14E, F). The drastic reduction in raft association of $Dsg1_{scr1}$-GFP and $Dsg1_{scr2}$-GFP suggests that we have disrupted some key quality of the Dsg1 TMD.

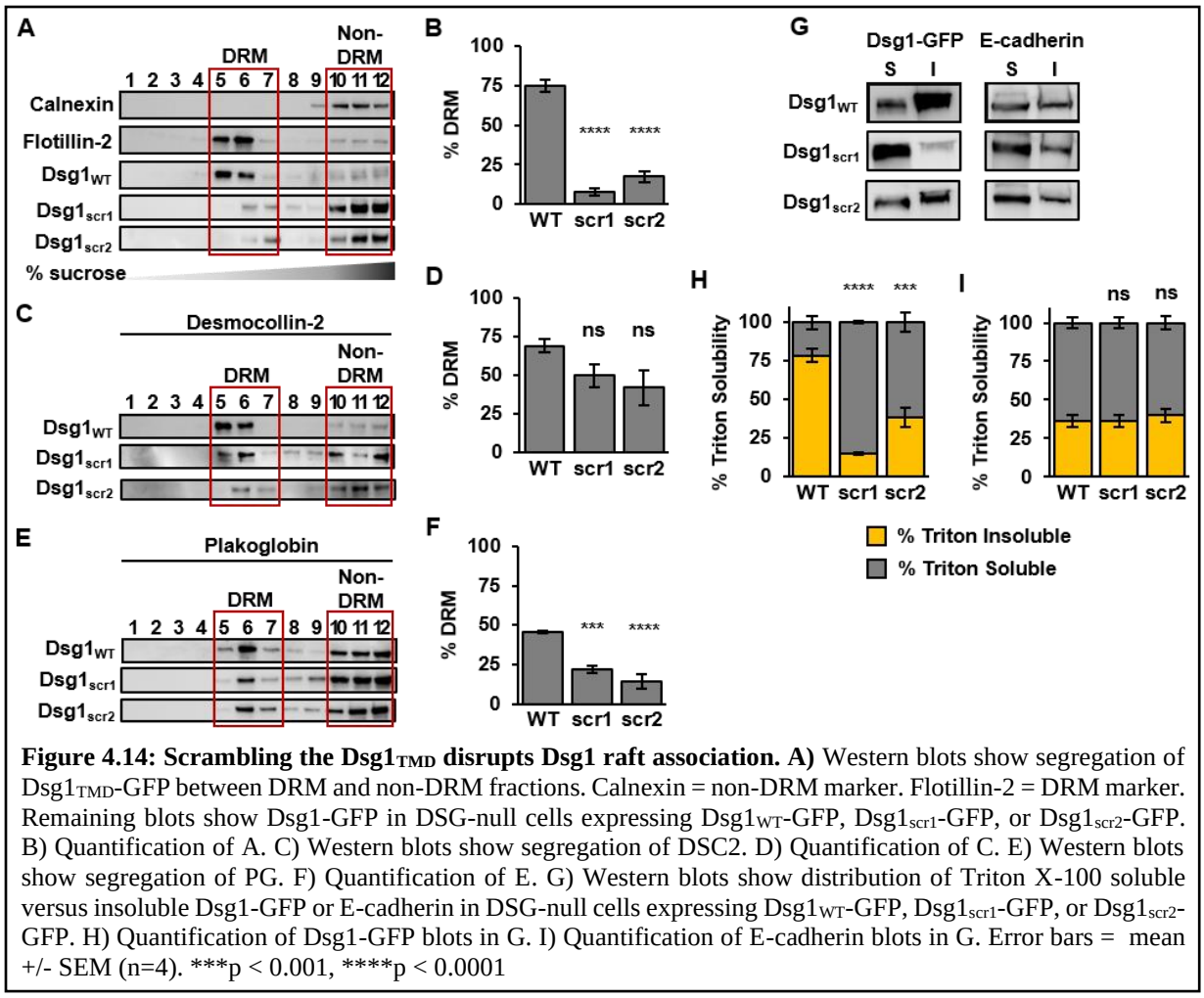

Figure 4.14: Scrambling the $Dsg1_{TMD}$ disrupts Dsg1 raft association. A) Western blots show segregation of $Dsg1_{TMD}$-GFP between DRM and non-DRM fractions. Calnexin = non-DRM marker. Flotillin-2 = DRM marker. Remaining blots show Dsg1-GFP in DSG-null cells expressing $Dsg1_{WT}$-GFP, $Dsg1_{scr1}$-GFP, or $Dsg1_{scr2}$-GFP. B) Quantification of A. C) Western blots show segregation of DSC2. D) Quantification of C. E) Western blots show segregation of PG. F) Quantification of E. G) Western blots show distribution of Triton X-100 soluble versus insoluble Dsg1-GFP or E-cadherin in DSG-null cells expressing $Dsg1_{WT}$-GFP, $Dsg1_{scr1}$-GFP, or $Dsg1_{scr2}$-GFP. H) Quantification of Dsg1-GFP blots in G. I) Quantification of E-cadherin blots in G. Error bars = mean +/- SEM (n=4). ***$p < 0.001$, ****$p < 0.0001$

Considering that reduced raft association of Dsg1 and PG could affect cytoskeletal attachment and desmosome assembly, we assessed the Triton X-100 solubility of each $Dsg1_{TMD}$-GFP and found that Triton X-100 solubility was increased for both $Dsg1_{scr1}$-GFP and $Dsg1_{scr2}$-GFP, with there being a greater effect on $Dsg1_{scr1}$-GFP (Figure 4.14G, H). The Triton X-100 solubility of E-cadherin was unaffected across these cell lines, suggesting that the change in Triton X-100 solubility is specific to Dsg1 and not a global affect (Figure 4.14G, I). Thus, scrambling the

Dsg1 TMD appears to affect cytoskeletal attachment and desmosome assembly in cells expressing these two Dsg1$_{TMD}$-GFP variants.

In Figure 4.4, we found that localization of Dsg1$_{scr2}$-GFP appeared at cell borders in discrete puncta that colocalized with DP. In contrast, Dsg1$_{scr1}$-GFP had some border localization with DP, but also displayed strong intracellular localization patterns. Using SIM, we were able to identify mirrored DP railroad tracks in both cell lines indicating desmosome formation (Figure 4.15A). In cells expressing Dsg1$_{scr2}$-GFP, desmosome quantity and length were not significantly different from those in Dsg1$_{WT}$-GFP-expressing cells, but cells expressing Dsg1$_{scr1}$-GFP had significantly fewer desmosomes per border and shorter desmosomes (Figure 4.15B, C). While this outcome for Dsg1$_{scr1}$-GFP is consistent with our previous results as well as observations made for many of the other Dsg1$_{TMD}$-GFP variants which had reduced raft association, finding apparently normal desmosomes from cells expressing Dsg1$_{scr2}$-GFP is surprising.

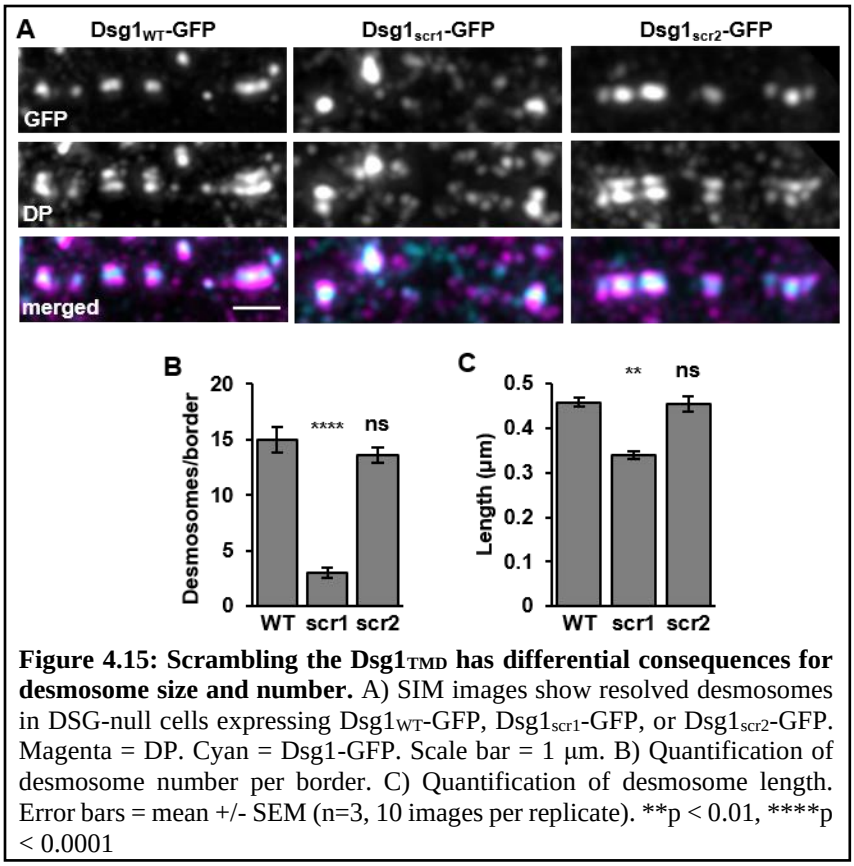

Figure 4.15: Scrambling the Dsg1$_{TMD}$ has differential consequences for desmosome size and number. A) SIM images show resolved desmosomes in DSG-null cells expressing Dsg1$_{WT}$-GFP, Dsg1$_{scr1}$-GFP, or Dsg1$_{scr2}$-GFP. Magenta = DP. Cyan = Dsg1-GFP. Scale bar = 1 µm. B) Quantification of desmosome number per border. C) Quantification of desmosome length. Error bars = mean +/- SEM (n=3, 10 images per replicate). **p < 0.01, ****p < 0.0001

Finally, we used the dispase cell dissociation assay to assess desmosome function in cells expressing $Dsg1_{scr1}$-GFP or $Dsg1_{scr2}$-GFP versus those expressing no desmogleins or $Dsg1_{WT}$-GFP (Figure 4.18A, B). Both $Dsg1_{scr1}$-GFP and $Dsg1_{scr2}$-GFP showed some degree of rescue in DSG-null cells. While neither could rescue as well as $Dsg1_{WT}$-GFP, $Dsg1_{scr2}$-GFP performed surprisingly well. These results continue to suggest that Dsg raft association is important for desmosome assembly and function. However, $Dsg1_{scr2}$-GFP suggests that the processes can be uncoupled. Furthermore, there may be an unidentified motif or specific residues which are required for raft association of DSG1.

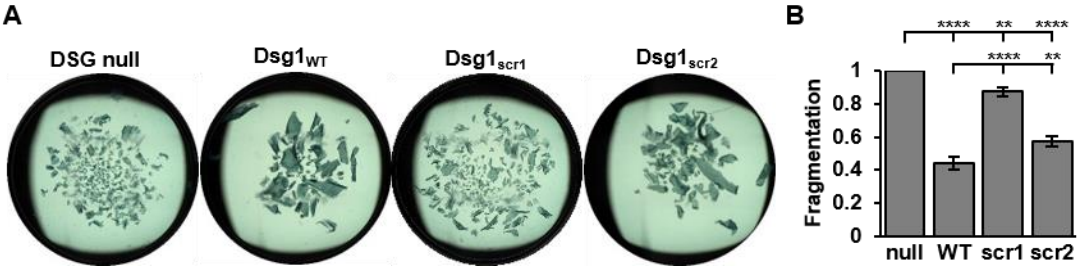

Figure 4.16: Scrambling the $Dsg1_{TMD}$ has differential consequences for desmosome strength. A) Images show monolayer fragmentation of DSG-null cells versus DSG-null cells expressing $Dsg1_{WT}$-GFP, $Dsg1_{scr1}$-GFP, or $Dsg1_{scr2}$-GFP. B) Quantification of A. $Dsg1_{TMD}$ variants were compared to DSG-null cells to assess degree of desmosome function rescue and to DSG-null cells expressing $Dsg1_{(WT)}$-GFP. Error bars show mean +/- SEM (n=6, each replicate included 4 monolayers). **p < 0.01, ****p < 0.0001

4.2.7 Dsg1 raft association predicts desmosome function

Based on our characterization of a panel of $Dsg1_{TMD}$-GFP variants, TMD length and TMD surface area but not palmitoylation are involved in the raft partitioning mechanism of Dsg1. However, the possibility that we disrupted an unidentified motif or residue(s) essential for raft association cannot be ruled out with the experiments performed here. That being said, several interesting patterns have emerged in our data. $Dsg1_{TMD}$-GFP variants which showed the least ability to segregate with DRMs in our sucrose gradient fractionation assay were also the least capable of rescuing desmosome function and vice-versa. We plotted this relationship and found a

strong correlation between DRM segregation and desmosome function (Figure 4.19A, Table 4.2). This suggests that, without Dsg1 raft association, functional desmosomes do not form.

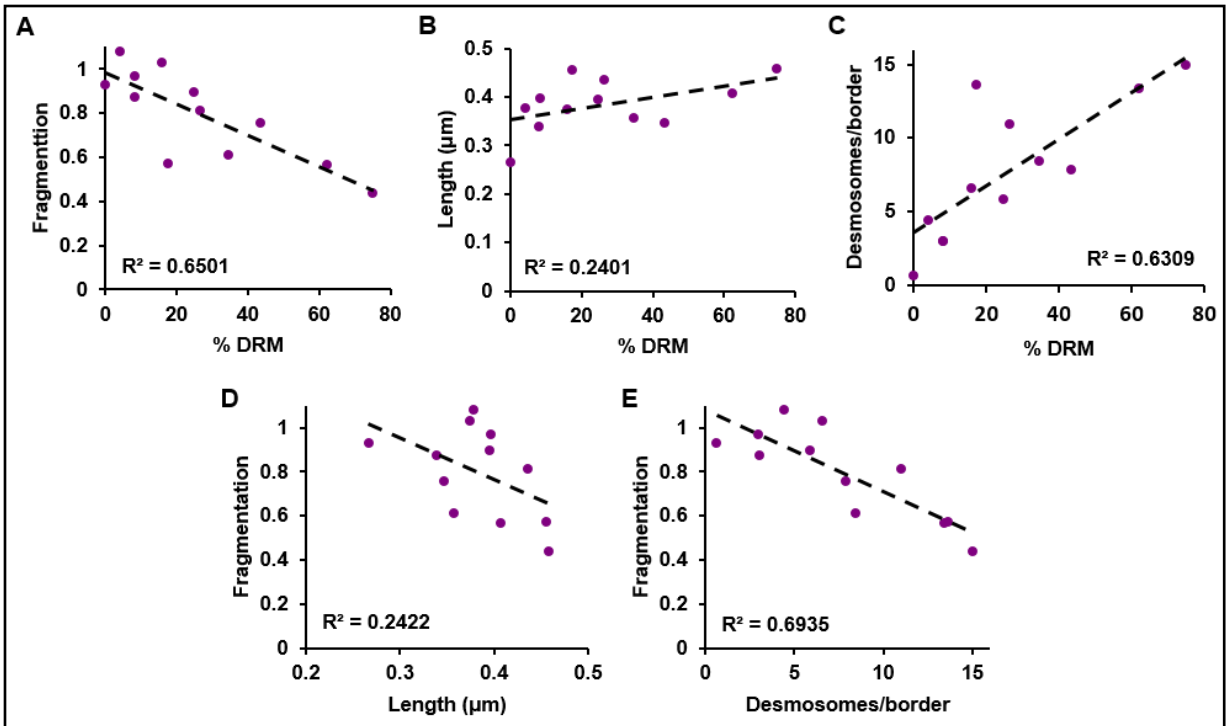

Figure 4.17: Dsg1 raft association predicts desmosome strength and quantity but not length. A) Correlation between raft association of each $Dsg1_{TMD}$-GFP variant and desmosome strength as assessed by sucrose gradient fractionations and dispase cell dissociation assays. B) Correlation between raft association of each $Dsg1_{TMD}$-GFP variant and desmosome length as assessed by sucrose gradient fractionations and SIM image analysis. C) Correlation between raft association of each $Dsg1_{TMD}$-GFP variant and desmosome number as assessed by sucrose gradient fractionations and SIM image analysis. D) Correlation between desmosome length and strength as assessed by SIM image analysis and dispase cell dissociation assay. E) Correlation between desmosome quantity and strength as assessed by SIM image analysis and dispase cell dissociation assay.

We further found that DRM association is strongly correlated with the number of desmosomes per border but not desmosome length (Figure 4.19B-C, Table 4.2). In return, the number of desmosomes per border but not desmosome length correlates with desmosome function (Figure 4.19D-E, Table 4.2). These correlations indicate that desmosome adhesion is dependent on desmosome quantity where a greater number of small desmosomes will be stronger than a few large desmosomes. Furthermore, this indicates that the raft association requirement may be an early step in desmosome assembly that promotes clustering of desmogleins and desmocollins.

Table 4.2: Collected results from sucrose gradient fractionations, SIM analysis, and dispase assays used for correlations in Figure 4.17.

	Fractionation	**SIM Analysis**		**Dispase Assay**
Variant	*% DRM*	*Length (μm)*	*Desmosomes/Border*	*Fragmentation*
Dsg1$_{WT}$	74.90	0.45	15.0	0.44
Dsg1$_{scr1}$	8.13	0.34	3.0	0.87
Dsg1$_{scr2}$	17.44	0.45	13.6	0.57
Dsg1$_{LAT}$	4.10	0.38	4.4	1.08
Dsg1$_{Ala}$	0.00	0.27	0.6	0.93
Dsg1$_{Δ7N}$	34.64	0.36	8.5	0.61
Dsg1$_{G552R}$	43.33	0.35	7.9	0.76
Dsg1$_{Δ7C}$	8.18	0.40	3.0	0.97
Dsg1$_{SAM}$	24.70	039	5.9	0.90
Dsg1$_{Ecad}$	26.50	0.43	11.0	0.81
Dsg1$_{Leu}$	15.82	0.37	6.6	1.03
Dsg1$_{AADA}$	62.16	0.41	13.4	0.57

4.3 DISCUSSION

We designed a panel of Dsg1$_{TMD}$-GFP variants to determine which Dsg1$_{TMD}$ physical properties contribute to Dsg1 raft association as a means to understand the relationship between Dsg1 raft association, desmosome assembly and function. We found reduced raft association in most Dsg1$_{TMD}$-GFP variants which usually coincided with reduced Dsg1 cytoskeletal attachment, desmosome quantity, length, and function. In particular, TMD length and exposed surface area had the greatest effect on raft association, desmosome assembly, and function. However, palmitoylation does not appear to play a dominant role in Dsg1 raft association. Most intriguingly, we identified one TMD variant, Dsg1$_{scr2}$-GFP, which showed reduced raft association with mostly normal desmosome assembly and function, suggesting that these processes can be uncoupled. Our results support a model whereby Dsg1 raft association, through TMD-centric properties, supports normal desmosome assembly and function. We propose a modified model of that discussed in Chapter 1 whereby raft association nucleates desmosomal cadherin clustering until a critical mass is reached at which point desmosome elongation is independent of raft association (Figure 4.18).

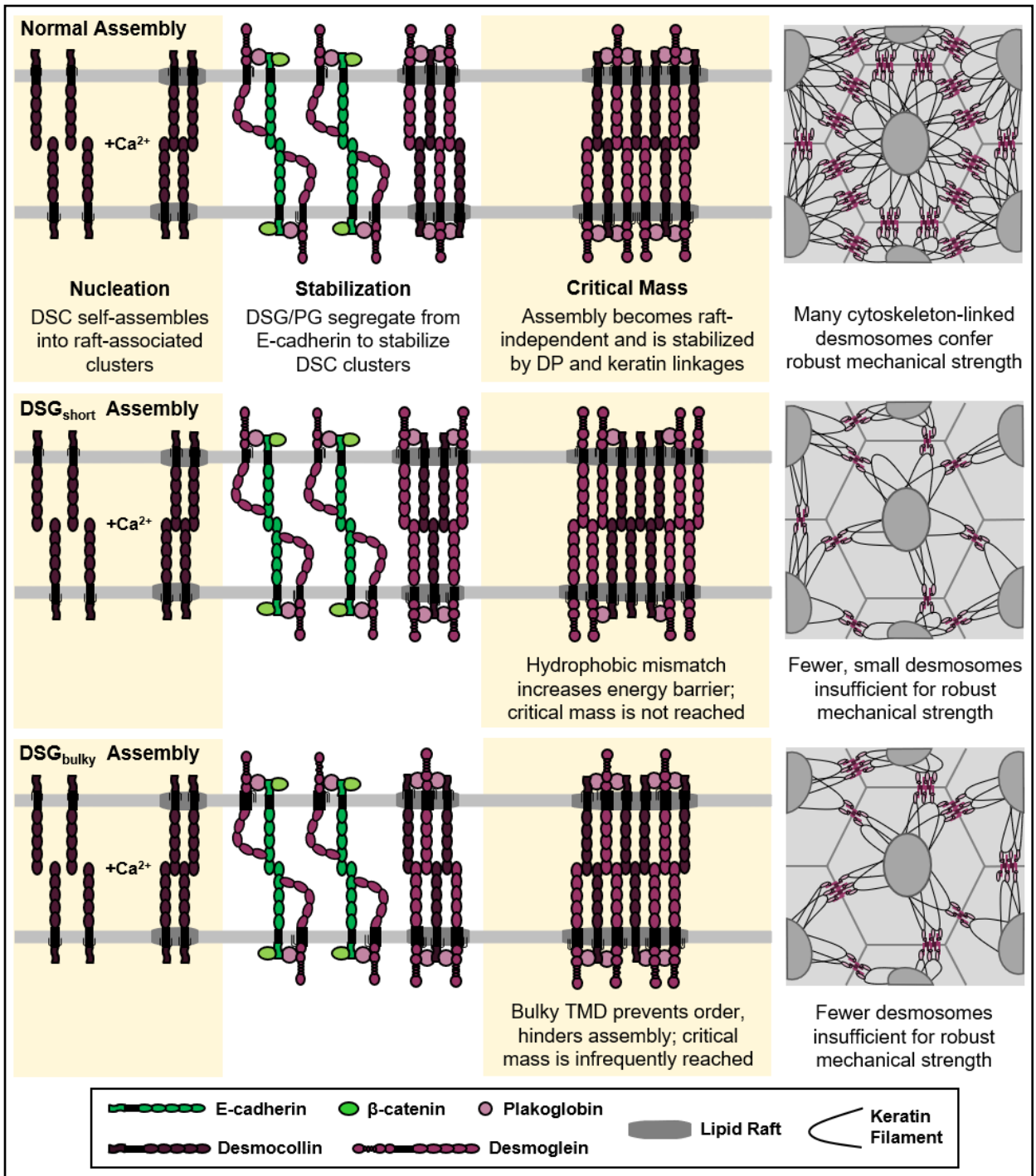

Figure 4.18: Raft-driven model of desmosome assembly. In normal assembly, raft-associated DSC clusters self-assemble. Protein-protein interactions between armadillo proteins (β-catenin, PG) promote segregation of DSG/PG complexes. DSG/PG complexes join DSC clusters, enhancing stability of nascent desmosomal clusters. Raft-dependent assembly continues until clusters reach a critical mass at which point growth becomes raft-independent. Linkage to keratin filament network through DP stabilizes desmosomal rafts. DSG_{short} obstructs assembly by introducing hydrophobic mismatch and increasing the energy barrier to raft association and desmosome assembly. DSG_{short} may gravitate towards cluster edges, preventing further growth and creating fewer, small desmosomes which are insufficient for normal function. DSG_{bulky} obstructs assembly by preventing order among lipids and proteins. Critical mass is difficult to reach; fewer desmosomes are insufficient for normal function.

4.3.1 Dsg1 TMD properties and raft association

Raft association is a continuum of probabilities that relies on energetically-favorable events. Prior to experimentation, we attempted to characterize the $Dsg1_{TMD}$ variants by calculating raft affinities from a formula that factors in the contributions of TMD length, exposed surface area, and palmitoylation to determine the energy required for raft partitioning of a TMD with unique properties (65). Such a reduced model may not capture the full picture for any single-pass transmembrane protein. The two truncated variants ($Dsg1_{\Delta 7N}$-GFP and $Dsg1_{\Delta 7C}$-GFP) were calculated to require much less energy for raft partitioning due to the model perceiving the truncation as a smaller surface area. If these are meant to be independent properties which individually contribute to raft partitioning, then the model may require revision. For example, single-pass transmembrane proteins which localize to the ER and Golgi apparatus have shorter TMDs and, in this model, smaller exposed surface areas, yet we would not expect these membrane proteins to associate with rafts. In contrast to these aberrant calculations, our sucrose gradient fractionations revealed more consistent results. Furthermore, these results, but not the raft affinity calculations, correlated with desmosome function (Figure 4.19), showing that the experimental data is a better indicator for the relationship between lipid rafts and desmosomes than the raft affinity calculation model.

Many, but not all, of the $Dsg1_{TMD}$-GFP variants behaved as predicted. Our predictions were based on the assumption that the altered physical property in each variant would be important for Dsg1 raft association. This appears to be the case for TMD length and surface area but not palmitoylation. Furthermore, the surprising behavior of our scrambled TMD variants make it difficult to determine whether a TMD physical property versus an unidentified motif is the true driver of Dsg1 raft association. TMD length, exposed surface area, and palmitoylation as drivers

of raft partitioning were identified based on the raft partitioning behavior of the protein LAT and further tested in additional raft associating and non-raft associating proteins (64-66). However, it remains possible that these TMD properties are not relevant to all raft associating single-pass transmembrane proteins, or that some single-pass transmembrane proteins only require a subset of these TMD properties to associate with rafts. Furthermore, there may be additional, unidentified TMD properties that can drive raft association, as the behavior of our scrambled TMD variants may suggest.

It is also necessary to consider the lipid environment in which the desmogleins exist and that the unique desmoglein TMD, which is conserved nearly in entirety across mammalian, avian, reptilian, and fish species ((154), see Figure 5.5, 5.6), must be equipped to drive clustering of desmosomal cadherins within the membrane. While proteins like LAT may require raft association to assemble with other proteins into a transient signaling complex, desmogleins assemble with desmocollins and intracellular adaptor proteins to form stable, massive, highly ordered, protein dense structures. Desmosomal cadherins make up a substantial portion of the lipid bilayer in these structures, potentially meaning that protein-protein interactions are more important than protein-lipid interactions in stable, fully-formed desmosomes.

4.3.1.1 TMD length

We expected the length of the Dsg1 TMD to play an important role in Dsg1 raft association based on our previous work with the disease-causing $Dsg1_{SAM}$ and $Dsg1_{PPK}$ mutants, both of which possess TMD-centric glycine-to-arginine substitutions. These mutants are characterized in Chapter 3, in which we discuss the likelihood that the arginine "snorkels" at the membrane:cytoplasm interface (143, 144), effectively shortening the Dsg1 TMD to 16 residues in $Dsg1_{SAM}$ and 11

residues in $Dsg1_{PPK}$. Based on these findings, the Dsg1 TMD variants were intended to address the contribution of length towards raft association by mimicking $Dsg1_{SAM}$. $Dsg1_{\Delta 7C}$ complements $Dsg1_{SAM}$ by removing the same number of residues "lost" in $Dsg1_{SAM}$. $Dsg1_{G552R}$ explores how an arginine might behave on the other end of the TMD. $Dsg1_{\Delta 7N}$ complements $Dsg1_{G552R}$. We found that none of these TMD variants associated with rafts at normal levels and this loss of raft association impacted downstream desmosomal processes. These outcomes are likely the result of hydrophobic mismatch between the length of the TMD and the width of the lipid bilayer. Accommodating the shorter stretch of hydrophobic residues would cause distortion of surrounding lipids which is not favorable for raft association or even for plasma membrane localization (64, 69).

Intriguingly, a C-terminal arginine or truncation appears to be more detrimental to Dsg1 raft association and downstream processes than an equivalent N-terminal arginine or truncation. There are several possibilities to explain this difference. The Dsg1 TMD boundaries have not been experimentally verified; we have relied on hydropathy plots to determine the edges. The C-terminal end is likely anchored and defined by palmitoylation. Truncation at this end may do more than introduce hydrophobic mismatch. In contrast, the N-terminal end is less defined and the sequence immediately adjacent to the TMD is poorly conserved across species. Adjacent residues, many of which are nonpolar, may help compensate for the loss in length. Alternatively, these differences, particularly if viewed alongside results from the scrambled Dsg1 TMDs, may suggest that a motif or residue, if present, is located near the C-terminal end of the TMD and was disrupted in $Dsg1_{\Delta 7C}$-GFP. If that is the case, then our findings from $Dsg1_{\Delta 7N}$-GFP may be solely indicative of the importance of TMD length while findings from $Dsg1_{\Delta 7C}$-GFP are telling us more. This may be further supported by results from $Dsg1_{G552R}$-GFP and $Dsg1_{SAM}$-GFP, where a snorkeling N-

terminal arginine ($Dsg1_{G552R}$-GFP) might only shorten the TMD whereas a snorkeling C-terminal arginine ($Dsg1_{SAM}$-GFP) could shorten the TMD and affect a motif. The potential nature of such a motif is further discussed in Chapter 5.

4.3.1.2 Palmitoylation

We observed no significant change in the raft association of $Dsg1_{AADA}$-GFP relative to $Dsg1_{WT}$-GFP. This was not surprising as similar findings have been reported for Dsg2 and Dsg3 (6, 76). While this previous work showed no relationship between palmitoylation of Dsg2 or Dsg3 and raft association, these experiments were carried out in A431 parental cells with endogenous DSGs. Therefore, it remained possible that endogenous wild type DSGs pulled the mutant non-palmitoylated DSGs into rafts. Our work suggests that this is unlikely to be the case as we expressed our $Dsg1_{AADA}$-GFP TMD variant in a DSG-null background. Nonetheless, our work and previous work indicate an important role for DSG palmitoylation. Despite apparently normal raft association, $Dsg1_{AADA}$-GFP could not support normal length desmosomes, nor could it rescue desmosomes in DSG-null cells as well as $Dsg1_{WT}$-GFP. Dsg2 palmitoylation has been shown to impact Dsg2 stability (76). Specifically, loss of palmitoylation increases turnover of non-desmosomal Dsg2 pools. We have not yet assessed protein turnover in our $Dsg1_{AADA}$-GFP-expressing cells, but a rapidly turning over pool of non-desmosomal Dsg1 may result in reduced availability of Dsg1 during and after desmosome assembly leading to smaller, possibly weaker desmosomes. The exact role of DSG palmitoylation in desmosome assembly and function remains a fascinating area and warrants further work to understand these mechanisms. In particular, the palmitoyl acyltransferase(s) responsible for palmitoylating DSGs remain unknown. This can be further extended to nearly all desmosomal proteins as all except DP have been shown to be palmitoylated (112). Such a route will be further explored in Chapter 5.

4.3.1.3 Exposed Surface Area

As with TMD length, we suspected a role for TMD exposed surface area in Dsg1 raft association based on modeling of $Dsg1_{SAM}$-GFP that predicted altered surface areas. Exposed surface area is an inherently difficult property to explore as it requires extensive modification to a native TMD. We anticipated that a $Dsg1_{TMD}$ variant with increased exposed surface area ($Dsg1_{Leu}$-GFP) would be less capable of associating with rafts while one with decreased surface area ($Dsg1_{Ala}$-GFP) would be similar to $Dsg1_{WT}$-GFP. In a similar vein, we anticipated that $Dsg1_{TMD}$ chimeras would behave based on the origin of the inserted TMD (raft associating LAT versus non-raft associating E-cadherin). These outcomes would reflect the concept that "narrow" TMDs are more amenable to raft association than "bulky" TMDs as they can more readily pack into the ordered lipid environment. Instead, we found that any substantial change to the $Dsg1_{TMD}$ surface area, whether increased or decreased, affected raft association. A caveat of this finding is that $Dsg1_{Ala}$-GFP was trapped in the ER where it may not have been normally incorporated into the lipid bilayer. Therefore, it is difficult to conclude whether decreased surface area is as detrimental as increased surface area to Dsg1 raft association. However, even $Dsg1_{LAT}$-GFP, which bears a similar surface area to $Dsg1_{WT}$-GFP, showed very little raft association. Furthermore, the variants with increased surface area fared better in sucrose gradient fractionations than those which were expected to be similar to $Dsg1_{WT}$-GFP. While this may be further evidence that a motif was disrupted in these variants as the scrambled $Dsg1_{TMD}$ variants suggest, there is another explanation specific to changes in exposed surface area.

Differing exposed surface areas of the various residue side chains create nooks and crannies important for lipid packing. As stated previously, the DSG TMDs are all remarkably well-conserved and would have similar surfaces to each other. Such surfaces may allow for packing

with lipids, cholesterol, and other desmosomal cadherins during assembly or within the mature desmosome but would be absent in most of the $Dsg1_{TMD}$ variants used here. The role of the Dsg1 TMD surface may even extend to localization and endocytic processes as TMD exposed surface area has also been shown to be involved in cell localization and endocytosis through asymmetrical surfaces (149, 155). Thin exoplasmic TMD surfaces coupled with bulky endoplasmic TMD surfaces are readily found in single-pass transmembrane proteins which localize to the plasma membrane and endocytic organelles. Such bulk distribution packs well into asymmetric lipid bilayers.

4.3.2 Dsg1 TMD sequence and raft association

As mentioned above, extensive changes to the Dsg1 TMD were often necessary to assess the contribution of certain TMD physical properties towards the raft associating nature of DSGs. While such changes were meant to assess TMD length or surface area, outcomes observed from those variants could also be attributed to the interruption of unknown motifs. Such motifs could be involved in protein-lipid, protein-cholesterol, or protein-protein interactions and potentially have important roles in DSG trafficking, function, or stability which translate into key parts of desmosomal processes. These possibilities will be discussed in more detail in Chapter 5.

Whether lipid or cholesterol binding sites or dimerization motifs exist in the Dsg1 TMD, and how these potential functional domains might contribute to raft association or other desmosomal processes is largely speculative, though the peculiar differences in the behavior of the $Dsg1_{scr1}$ versus $Dsg1_{scr2}$ TMD variants may suggest the obstruction of such a site. One important and potentially relevant difference between the design of the scrambled $Dsg1_{TMD}$ variants is the placement of proline residues. Two flanking proline residues exist in $Dsg1_{WT}$. These residues are

conserved among the DSGs but are absent in the DSCs and classical cadherins. These residues are also well-conserved across species (see Figure 5.1 and 5.2). Prolines are rare in the α-helices of soluble proteins as their inability to form stabilizing hydrogen bonds with other residue sidechains cause helix breakage (156). In contrast, prolines are fairly common in the TMDs of membrane proteins, particularly near the edges or in the center, where they can distort the TMD helix to promote lipid packing or introduce functionally important kinks or swivels (156-158). This can be accomplished through a GxxP motif which has increased flexibility due to a lack of hydrogen bonding between the glycine and proline (159). Furthermore, proline isomerization between the cis and trans forms has been shown to act as a molecular switch in a variety of voltage-gated ion channels and GPCRs, conferring structural changes that can activate or inactivate a protein or transmit signals (158). Whether and how the prolines in the DSG1 TMD could be functionally important has not been studied. However, random scrambling of the Dsg1 TMD to create $Dsg1_{scr1}$ resulted in one proline near an edge and one proline near the center of the TMD while the normal proline positioning was purposely maintained in $Dsg1_{scr2}$. It has been shown that substitution of prolines into various positions within a TMD is not energetically favorable. Therefore, it is not surprising that $Dsg1_{scr1}$ behaved so poorly compared to $Dsg1_{WT}$. The apparent uncoupling of Dsg1 raft association from desmosome assembly and function observed in cells expressing $Dsg1_{scr2}$ may suggest that appropriately placed proline residues are sufficient for desmosome assembly and function irrespective of raft association. While the mechanism behind this phenomenon is unclear, a Dsg1 mutant that does not require raft association in order to assemble functional desmosomes is a powerful tool for further desmosome studies. For our purposes here, the potential contributions from lipid or cholesterol binding vs TMD dimerization vs TMD prolines is impossible to sort out with these scrambled mutants but could more readily be addressed with different mutants specific

for each of these possibilities. Therefore, further work is required to understand whether each of these possibilities contribute towards DSG1 raft association or desmosome assembly and function. Such future directions are thoroughly discussed in Chapter 4.

4.3.3 The role of raft association in desmosome assembly and consequences for disease

While we sought to determine the mechanism of TMD-driven DSG1 raft association, our work here has also been useful in beginning to understand how DSG1 raft association translates to desmosome assembly and function. Characterizing our panel of $Dsg1_{TMD}$ variants provided a set of closely related Dsg1 species bearing unique properties with which we were able to observe previously unappreciated trends.

Though the $Dsg1_{TMD}$ variants remained capable of forming desmosomes, none of the variants equaled $Dsg1_{WT}$ in all desmosomal properties tested. This was most apparent in results from sucrose gradient fractionations, where nearly all variants showed significantly reduced DRM segregation. These disparities often translated into reduced desmosome quantity and strength but not size. This implies that raft association is necessary for the formation of functional desmosomes. Desmosomes observed in cells expressing the $Dsg1_{TMD}$ variants are likely formed from the fraction of each variant observed in DRMs. Since energetic favorability determines the likelihood of raft association, reduced raft association observed from nearly all $Dsg1_{TMD}$ variants implies that this event and any downstream processes, such as desmosome formation, became energetically unfavorable and less likely to occur. This suggests that raft association is a rate-limiting step that is most essential early in assembly when desmosomal cadherins first begin to cluster.

However, raft association does not seem to regulate desmosome size, which was only sometimes reduced in cells expressing certain variants. The reduced ability of cells expressing

short $Dsg1_{TMD}$ variants to form full-length desmosomes is likely a result of hydrophobic mismatch. Though palmitoylation is not necessary for DSG raft association, smaller than average desmosomes formed by cells expressing $Dsg1_{AADA}$ may indicate an effect on protein packing within the plane of the bilayers. Cells expressing those variants with altered exposed surface area formed normal-sized desmosomes on average, despite severely reduced raft association. This suggests that, once clustering of desmosomal cadherins and intracellular adaptor proteins reaches a critical mass, increases in length can occur independently of raft association.

Lastly, the correlation between raft association and desmosome function is likely indirect and mediated by the initiation of desmosome assembly through raft-mediated clustering of desmosomal cadherins and other desmosomal proteins. Ultimately, the robustness of desmosome-mediated cell-cell adhesion relies on the presence of many desmosomes along each border and can be disrupted if only a few desmosomes form, even if those desmosomes are of a normal length. Such a mechanism could be readily disrupted in disease states. For example, research with the disease-causing $DSG1_{SAM}$, which is a heterozygous mutation and expressed alongside $DSG1_{WT}$ in the patient, suggests that this mutant acts dominant negatively, but the mechanism itself remains elusive. The inability of $Dsg1_{SAM}$ to associate with rafts may be dominant negative in and of itself by preventing that initial stage of raft-mediated desmosomal cadherin clustering. This hypothesis can be tested by dual expression of $Dsg1_{WT}$ alongside $Dsg1_{SAM}$ in the DSG-null cells.

4.3.4 A newer model of raft-driven segregation of adherens junctions and desmosomes during junction assembly

In Chapter 1, we proposed a model whereby raft association drives segregation of junctional complexes during assembly, focusing on the segregation of adherens junctions and

desmosomes (Figure 1.4). As discussed in Chapter 1, the early stages of adherens junction and desmosome assembly involve transient dimerization of E-cadherin and Dsg2 followed by clustering between Dsg2 and independently formed Dsc2 dimers (107). Intracellularly, PG-binding to Dsg prevents β-catenin-binding (106). We proposed that this sequence of interactions is further promoted by raft association. However, the details of this proposed raft-mediated segregation mechanism model remain murky. Here, we found that DSC2 raft association was largely unaffected by reduced $Dsg1_{TMD}$ raft association. This suggests that DSC2 associates with rafts independently of desmogleins. The Dsc2 dimerization that occurs early in desmosome assembly may involve raft association which is furthered by the inclusion of Dsg2 and promoted by the correct binding of PG over β-catenin. The raft associating mechanism of desmocollins remains unexplored but will be discussed further in Chapter 5.

4.3.5 Conclusions

By creating a panel of $Dsg1_{TMD}$ variants, we have used a critical, but previously overlooked portion of the Dsg1 protein to further our understanding of the relationship between lipid raft membrane microdomains and desmosome assembly and function. The raft associating mechanism of desmosomal proteins that simultaneously promotes segregation from nascent adherens junctions and furthers junction assembly is slowly becoming clearer. However, this work has also raised many new questions to be addressed with future work. In Chapter 5, we will discuss some of these avenues and propose new hypotheses and experiments to be pursued.

4.4 Materials and Methods

Generation of mutants and lentivirus

Cloning of plasmids expressing $Dsg1_{WT}$-GFP and $Dsg1_{SAM}$-GFP was previously described (6). Short sequences bearing a $Dsg1_{TMD}$ sequence variant flanked by appropriate restriction sites were obtained from Invitrogen's Gene Art Strings and inserted into the plasmid expressing $Dsg1_{WT}$-GFP using existing restriction sites. Sequencing was performed through Genewiz to verify clones. This was done for $Dsg1_{scr2}$-GFP, $Dsg1_{LAT}$-GFP, $Dsg1_{G552R}$-GFP, $Dsg1_{Ecad}$-GFP, $Dsg1_{\Delta 7N}$-GFP. The plasmids expressing $Dsg1_{Leu}$-GFP, $Dsg1_{scr1}$-GFP, $Dsg1_{AADA}$-GFP, $Dsg1_{\Delta 7C}$-GFP $Dsg1_{Ala}$-GFP were ordered through Genscript. Lentivirus for $Dsg1_{WT}$-GFP and $Dsg1_{SAM}$-GFP was purchased from Cyagen VectorBuilder. Lentivirus for all remaining plasmids was made by transfection into HEK-293T cells together with necessary lentiviral regulatory genes. Lentivirus was collected from culture supernatants 48-72 h after transfection and concentrated by high-speed centrifugation.

Structural predictions and raft affinity calculations

TMD sequences were analyzed using the Robetta structure prediction server (136). Raft affinities were calculated using the following formula:

$$\Delta G_{raft} = \Delta\gamma_{TMD,Lo\text{-}Ld}(ASA) + n_{palm}(\Delta G_{palm}) - 2B_{LP}(d_{TMD} - 0.5(d_{Lo}+d_{LD})) \quad (65)$$

Cell line generation, culture, and reagents

A431 cells were cultured in DMEM (Corning 10-013-CV) with 10% fetal bovine serum (Hyclone SH30071.03) and 1X antibiotic-antimycotic solution (Corning 30-004-CI). DSG-null cells were stably infected with lentiviruses expressing murine $Dsg1a_{TMD}$-GFP constructs. Blasticidin (5μg/ml) was used to select for infected cells. No clonal isolation was performed. Cell lines

expressing Dsg1$_{TMD}$-GFP variants were subjected to fluorescence-activated cell sorting with equivalent gating to obtain populations with roughly equal Dsg1-GFP expression levels.

Immunofluorescence

Cells were cultured to 70% confluence on glass coverslips and fixed in 3.7% paraformaldehyde (PFA) in PBS+ on ice for 10 min. Cells were blocked and permeabilized in PBS+ containing 0.1% Triton X-100 and 3% BSA for 10 min. Saponin was used in place of Triton for intracellular organelle colocalization studies. Primary and secondary antibodies (listed below) were diluted into blocking solution (PBS+ containing 3% BSA and 0.05% Triton X-100). Cells were rinsed using PBS+ containing 0.05% Triton X-100. Cells were mounted to glass microscope slides using Prolong Gold mounting medium (ThermoFisher Scientific).

Antibodies

Antibodies used were as follows: rabbit anti-calnexin (Enzo Life Sciences ADI-SPA-860); mouse anti-flotillin-2 (BD Trans Lab610383); rabbit anti-GFP (Life A11122); mouse anti-GFP (Abcam ab1218); rabbit anti-DP (Bethyl A303-356A); mouse anti-PG (BD Trans Lab 610253); mouse anti-Dsc2/3 (Life Technologies 326200); mouse anti-E-cadherin (BD Trans Lab 610182); mouse anti-GM130 (BD TransLab 610822); rabbit anti-VAPB (invitrogen PA5-53023); mouse anti-β-actin (Sigma A5451). Secondary antibodies conjugated to Alexa Fluors were purchased from Invitrogen. Horseradish peroxidase-conjugated secondary antibodies were purchased from BioRad.

Image acquisition

Widefield microscopy was performed using a Nikon Ti-E inverted microscope (100x/1.49 NA oil immersion objective) equipped with a motorized stage and a Hamamatsu C11440-22CU digital camera. Images were deconvolved using Microvolution (124) in ImageJ. SIM was performed

using a Nikon N-SIM system on an Eclipse Ti-E microscope system equipped with a 100x/1.49 NA oil immersion objective, 488- and 561-nm solid-state lasers in three-dimensional SIM mode. Images were captured using an EM charge-couple device camera (DU-897; Andor Technology) and reconstructed using NIS-Elements software with the N-SIM module (version 5.02; Nikon). All microscopy was performed at room temperature. Widefield microscopy and SIM results are representative of three independent replicates with 10 cells per condition.

Triton solubility assay

Cells were cultured until confluent in six-well tissue culture plates. Cells were washed twice with ice-cold PBS+. The Triton-soluble pool was isolated by incubating cells with Triton lysis buffer (1% Triton X-100, 10 mM Tris, pH7.5, 140 mM NaCl, 5 mM EDTA, 2 mM EGTA, with protease inhibitor [Roche 11836170001]) for 10 min on ice. Lysate was then centrifuged at 13,200xg for 10 min at 4°C to pellet the Triton-insoluble fraction. The Triton-soluble supernatant was collected and mixed 1:1 with 2x Laemmli sample buffer containing 5% β-mercaptoethanol. The Triton-insoluble pellet was resuspended in 2x Laemmli sample buffer (Bio-Rad 161-0737) containing 5% β-mercaptoethanol. All samples were heated to 95°C for 10 min and vortexed half-way through, prior to being run on a gel for western blotting.

Isolation of DRM

DRMs were isolated as described previously (118). Briefly, cells were cultured in 10-cm^2 dishes and washed with PBS+. Cells were collected by scraping in TNE buffer supplemented with protease inhibitors (Roche 11836153001) and pelleted by centrifugation at 0.4xg at 4°C for 5 min (5415R; Eppendorf). Cells were resuspended in TNE buffer and homogenized using a 25-gauge needle. TNE buffer containing 1% Triton X-100 was added and cells were incubated on ice for 30 min. Four hundred-twenty microliters of detergent extract were mixed with 840µl of 56% sucrose

in TNE and placed at the bottom of a centrifuge tube. Volumes (1.9µl) of 35 and 5% sucrose were layered on top of the sample. Following an 18-hr centrifugation at 4°C (44,000 rpm, SW55 rotor, Beckman Opima LE-80 K Ultracentrifuge), 420-µl fractions (1-11, remaining volume combined to make up fraction 12) were removed from top to bottom of the gradient and stored at -20°C until processed for western blot analysis. Flotillin-2 and calnexin were used as raft and non-raft markers, respectively.

Dispase-based fragmentation assay

Cells were cultured until confluent in 24-well tissue culture plates and treated with 1 U/ml dispase (Corning) for 15 min at 37°C. Cell sheets released from the plate were rinsed with PBS+, transferred to 1.5 ml Eppendorf tubes in 500µl PBS+, and then subjected to mechanical stress on an orbital shaker on its highest setting for 45 sec. Fragments were transferred to a fresh 24-well plate, fixed with 1% PFA, and stained with methylene blue (Sigma). Plates were imaged on an Elispot scanner (Cellular Technologies, Ltd) and fragments counted with ImageJ.

Statistics

Error bars represent standard error of the mean. Significance was determined using one-way ANOVA followed by Dunnett's post-hoc and p-values have been indicated. Statistical analysis of immunofluorescence results was conducted on at least 3 independent experiments with 10 images per condition per replicate. For all experiments involving western blotting, statistical analysis was conducted on results from four independent experiments. Statistical analysis of dispase assays was conducted on results from seven independent experiments.

4.5 ACKNOWLEDGEMENTS

The author would like to thank Dr. Daniel Conway for generating the DSG-null A431 cells which made this work possible as well as Dr. Ilya Levental for calculating the raft affinities of the $Dsg1_{TMD}$ variants. Work in the Kowalczyk lab is supported by grants R01AR050501 and R01AR048266 from the National Institutes of Health. SEZ was supported by a training grant from the National Institutes of Health T32GM008367. This research project was also supported in part by the Emory University Integrated Cellular Imaging Microscopy Core, the Emory Flow Cytometry Core (EFCC), and the Emory Integrated Genomics Core (EIGC).

CHAPTER 5

Future Directions and Conclusions

ABSTRACT

We created a desmoglein (DSG)-null cell model, established a role for the DSG1 transmembrane domain (TMD) in raft association, desmosome assembly and function, and began dissecting the DSG1 raft association mechanism. While we attained new insights into the desmosome assembly process and the role that raft association plays, we also uncovered new questions and identified related areas in which knowledge is severely lacking. Here, we delve into those areas, assessing the current state of knowledge in relation to DSGs, raft association, and desmosomal processes and suggesting experiments to address the gaps. Addressing these gaps will continue to utilize the DSG-null cells as well as those expressing the $Dsg1_{TMD}$-GFP variants, but we also look to the use of null systems to study other desmosomal proteins. We consider areas such as palmitoylation in desmosomal processes, conserved TMD-centric proline residues, important motifs that may contribute to protein-lipid or protein-protein interactions, raft associating mechanisms of desmocollins, and raft association in segregation of adherens junctions and desmosomes. We conclude by discussing the desmosome as a stable platform whose function extends beyond cell-cell adhesion.

5.1 INTRODUCTION

We generated a desmoglein (DSG)-null cell model system and used it to dissect the relationship between raft association of DSG1 and desmosome assembly and function. In doing so, we identified that length and exposed surface area but not palmitoylation of the $Dsg1_{TMD}$ are necessary for raft association. However, we were unable to rule out whether the $Dsg1_{TMD}$ sequence contains an important residue or motif necessary for raft association as others have ruled out for different raft associated proteins, such as LAT (65). Instead, this lack of clarity has uncovered new avenues to explore. In this chapter, we will explore new questions that this work has revealed and thoughts on how to address these questions in future work.

5.2 Null model systems for studying desmosomal dynamics

In Chapter 2, we generated a DSG-null A431 cell line which exhibited mislocalization of desmosomal proteins and lacked functional desmosomes. We went on to use this cell line to explore differing pathomechanisms of two disease-causing $DSG1_{TMD}$ mutants and to characterize a panel of $Dsg1_{TMD}$ variants, all aimed at establishing a role for the $DSG1_{TMD}$ in desmosomal processes and understanding the nature of that role. However, DSG-null cells are infinitely useful for experiments involving any of the DSGs. Having used this cell line to establish a panel of cell lines expressing $Dsg1_{TMD}$-GFP variants, we can continue experimentation with some of these lines to better understand desmosomal processes. Some of these possibilities will be discussed below. We can also make additional $Dsg1_{TMD}$ variants to fully resolve the TMD-mediated raft associating mechanism of Dsg1 and establish whether a similar mechanism applies to the other DSGs. By switching out the GFP tag for another marker, these variants could also be mixed and matched within a cell population to explore interactions.

5.2.1 Identifying roles for the DSG intracellular domains

Moving beyond the $Dsg1_{TMD}$, the intracellular domains of DSGs, including the intracellular anchor (IA), intracellular cadherin segment (ICS), intracellular proline-rich linker (IPL), repeating unit domains (RUD), and desmoglein terminal domain (DTD) (see Figure 3.1, 5.1) remain largely uncharacterized. The ICS contains the plakoglobin (PG)-binding site (22, 23, 106) while the IPL, RUD, and DTD domains, which are unique to DSGs, have been shown to be disordered and capable of binding various desmosomal protein partners (160). In Dsg2, the unique cytoplasmic tail contributes to strong cell-cell adhesion by stabilizing surface pools and preventing internalization (25).

Expression of truncated or domain deleted Dsg1 species in our DSG-null cells can help reveal the roles of these unique regions in desmosomal processes. Such endeavors have already begun as we have created a small series of truncations by removing everything but the IA which deletes the PG-binding region ($Dsg1_{IA}$), introducing a disease-causing nonsense mutation which truncates the intracellular domain in the IPL at G795 ($Dsg1_{G795*}$), or removing the DTD ($Dsg1_{\Delta DTD}$) (Figure 5.1).

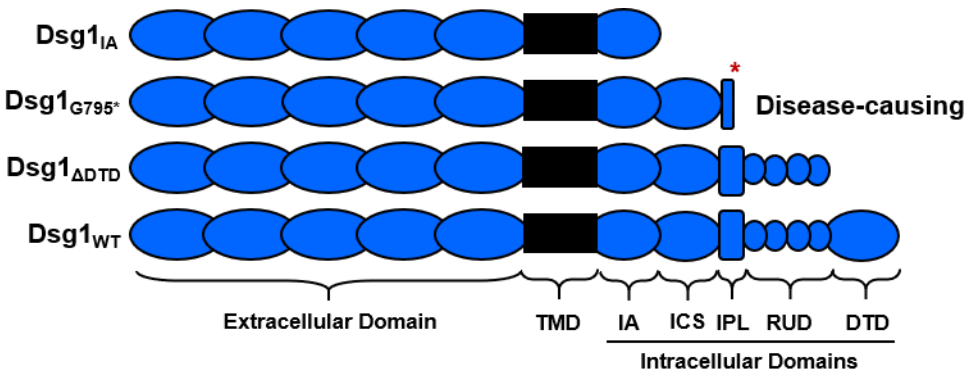

Figure 5.1: Dsg1 truncations to define intracellular domain functions. Schematics of truncated Dsg1 constructs compared to $Dsg1_{WT}$. Blue = extracellular and intracellular domains. Black = TMD. IA = intracellular anchor. ICS = intracellular cadherin segment. IPL = intracellular proline-rich linker. RUD = repeating unit domain. DTD = desmoglein terminal domain. $Dsg1_{IA}$ removes all intracellular domains except IA. $Dsg1_{G795*}$ is a homozygous SAM syndrome-causing nonsense mutation that introduces a premature stop codon at residue 795 (red asterisk), retaining IA and ICS. $Dsg1_{\Delta DTD}$ removes the DTD.

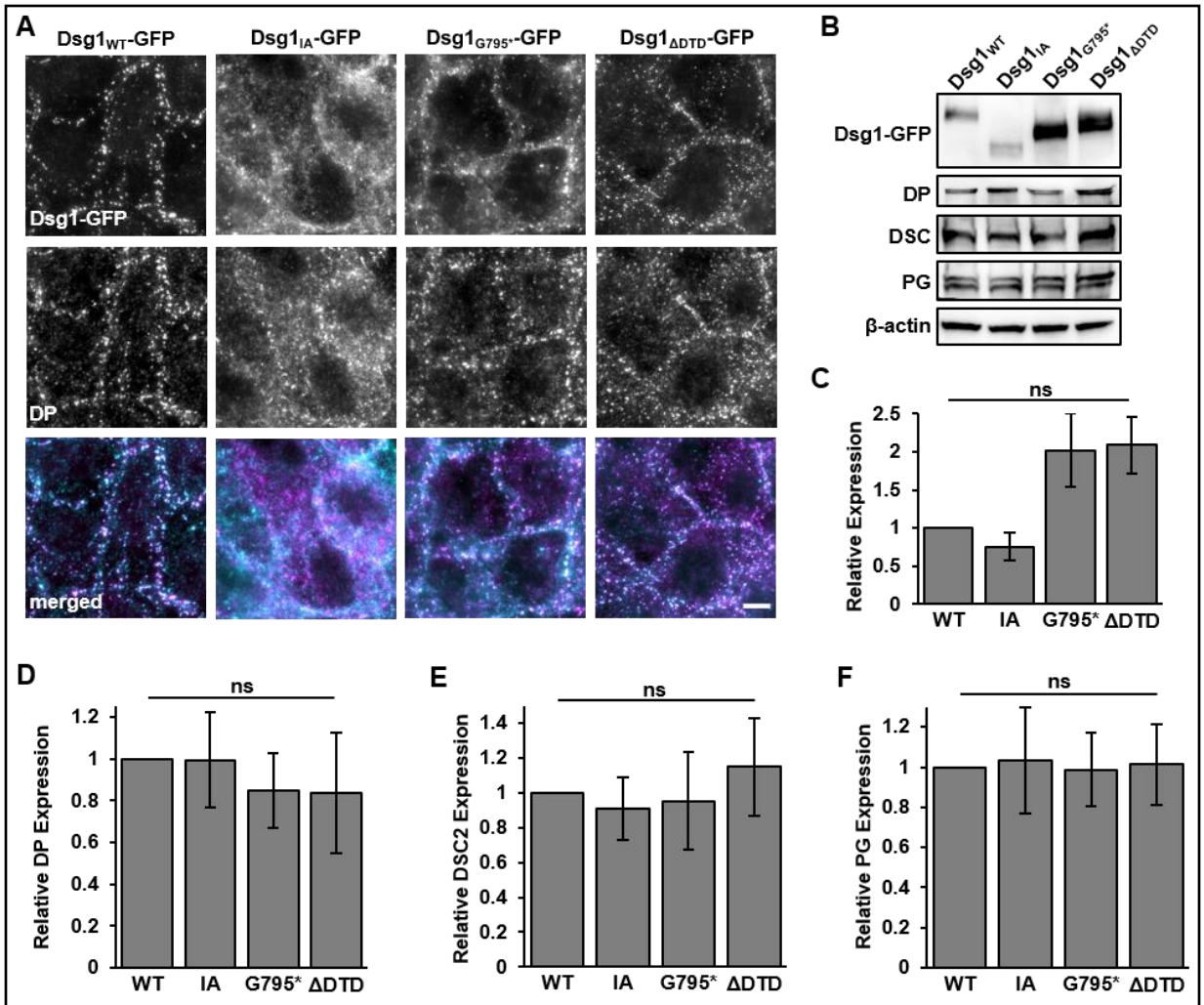

Figure 5.2: Truncated Dsg1-GFP variants localize to the plasma membrane and do not alter expression of desmosomal proteins. A) Widefield immunofluorescence images stained for Dsg1-GFP and DP show membrane localization of Dsg1 truncations and colocalization with DP in cells expressing $Dsg1_{WT}$-GFP or the Dsg1-GFP truncations. Scale bar = 10 μm. B) Western blots of whole cell lysates show slight but insignificant elevation of $Dsg1_{G795*}$-GFP and $Dsg1_{\Delta DTD}$-GFP expression relative to $Dsg1_{WT}$-GFP while $Dsg1_{IA}$-GFP has similar levels. C). Quantification of Dsg1-GFP blots in B. D) Quantification of DP blots in B. E) Quantification of DSC2 blots in B. F) Quantification of PG blots in B. Error bars show mean +/- SEM (n = 4).

Characterization of DSG-null cells stably expressing these truncated Dsg1-GFP constructs is underway. Immunofluorescence experiments have shown that all three truncated Dsg1-GFP constructs maintain membrane localization, however, only $Dsg1_{\Delta DTD}$-GFP forms discrete, DP-positive puncta along cell borders (Figure 5.2A). $Dsg1_{IA}$-GFP is diffuse, and $Dsg1_{G795*}$-GFP appears to act as a hybrid, forming some discrete, DP-positive puncta but also appearing more diffuse than $Dsg1_{WT}$-GFP or $Dsg1_{\Delta DTD}$-GFP. Western blots of whole cell lysates showed that Dsg1

$Dsg1_{G795*}$-GFP and $Dsg1_{\Delta DTD}$-GFP levels are elevated relative to $Dsg1_{WT}$-GFP though not significantly (Figure 5.2B, C), but the levels of the other desmosomal proteins, including DP, DSC2, and PG do not differ from cells expressing $Dsg1_{WT}$-GFP (Figure 5.2B, D-F).

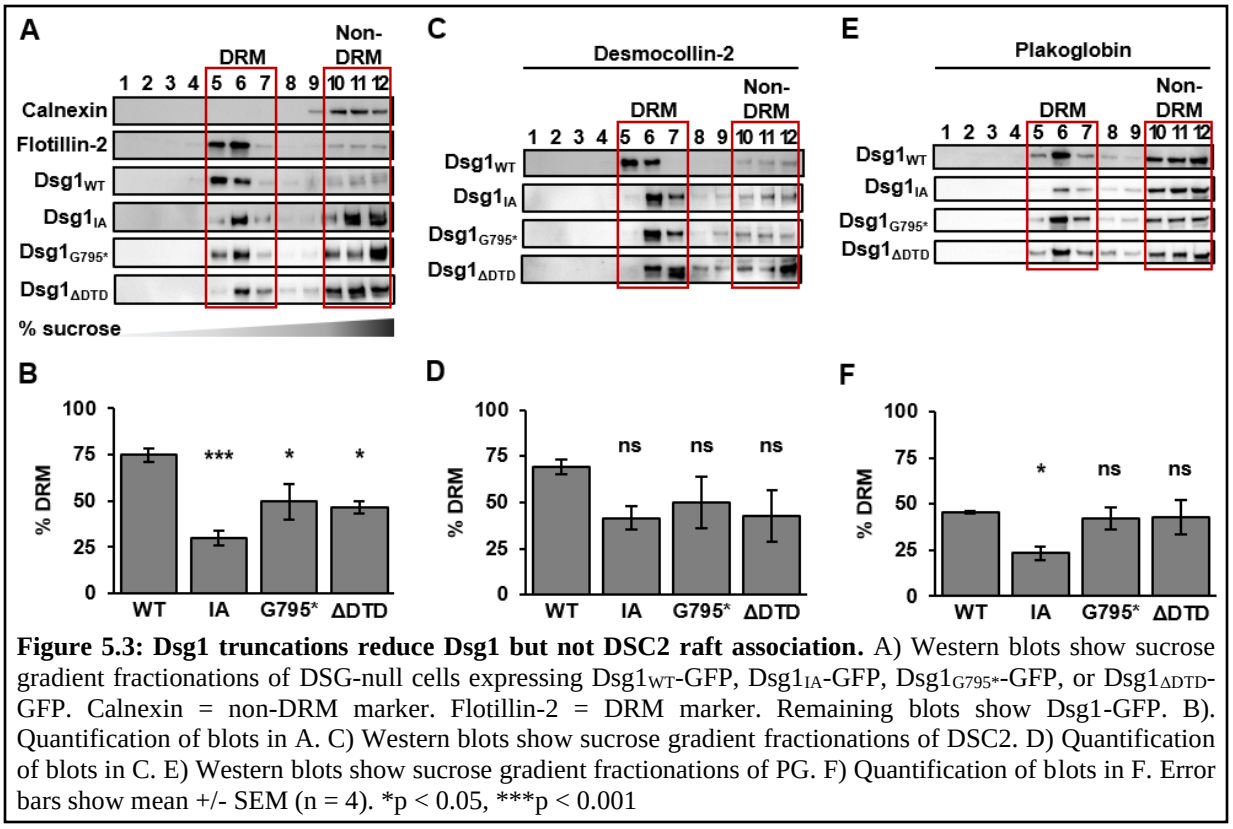

Figure 5.3: Dsg1 truncations reduce Dsg1 but not DSC2 raft association. A) Western blots show sucrose gradient fractionations of DSG-null cells expressing $Dsg1_{WT}$-GFP, $Dsg1_{IA}$-GFP, $Dsg1_{G795*}$-GFP, or $Dsg1_{\Delta DTD}$-GFP. Calnexin = non-DRM marker. Flotillin-2 = DRM marker. Remaining blots show Dsg1-GFP. B). Quantification of blots in A. C) Western blots show sucrose gradient fractionations of DSC2. D) Quantification of blots in C. E) Western blots show sucrose gradient fractionations of PG. F) Quantification of blots in F. Error bars show mean +/- SEM (n = 4). *$p < 0.05$, ***$p < 0.001$

By sucrose gradient fractionations, we found reduced DRM segregation of the truncated Dsg1-GFP constructs with the greatest effect in the DSG-null cells expressing $Dsg1_{IA}$-GFP (Figure 5.3A, B). Based on the diffuse nature of $Dsg1_{IA}$-GFP that we observed by immunofluorescence, this is unsurprising. In contrast, DRM segregation of DSC2 was unaffected by the expression of truncated Dsg1-GFP constructs (Figure 5.3C, D), and DRM segregation of PG was only affected in DSG-cells expressing $Dsg1_{IA}$-GFP (Figure 5.3E, F). This decrease in DRM segregation of PG is likely due to the inability of $Dsg1_{IA}$-GFP to bind PG. Just as PG requires Dsg1 for raft association as we observed in Chapter 3 and Chapter 4, it appears that Dsg1 also requires PG or other interactions with desmosomal proteins to maintain raft association. Furthermore, if the cytoplasmic

tail is necessary for surface stability as in Dsg2 (25), then reduced raft association may be the result of reduced surface stability and increased endocytic rates.

Dispase cell dissociation assays have also been performed with these cell lines to determine if truncated Dsg1-GFP constructs are able to form functional desmosomes (Figure 5.4). $Dsg1_{IA}$-GFP was not able to rescue desmosome function in the DSG-null cells while DSG-null cells expressing $Dsg1_{G795*}$-GFP and $Dsg1_{\Delta DTD}$-GFP formed weak desmosomes. The inability to form strong desmosomes has been observed in similar truncated Dsg2 constructs (25), indicating that the DSG intracellular domains are structurally and functionally important.

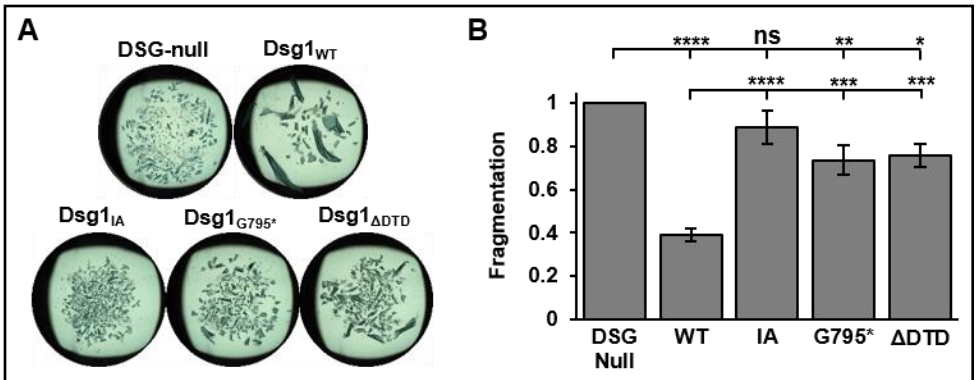

Figure 5.4: Truncated Dsg1-GFP variants do not form functional desmosomes. A) Images depicting monolayer fragmentation of DSG-null cells versus DSG-null cells expressing $Dsg1_{WT}$-GFP, $Dsg1_{IA}$-GFP, $Dsg1_{G795*}$-GFP, or $Dsg1_{\Delta DTD}$-GFP. B) Quantification of images in A. Error bars show mean +/- SEM (n = 6, each replicate includes 4 monolayers). *$p < 0.05$, **$p < 0.01$, ***$p < 0.001$, ****$p < 0.0001$

This characterization is incomplete. In particular, super-resolution microscopy techniques such as the structured illumination microscopy (SIM) experiments performed in Chapter 3 and Chapter 4 will be important to identify any differences in quantity or length of desmosomes forming in DSG-null cells expressing these truncated Dsg1-GFP constructs. Additionally, moving beyond steady-state experiments will be necessary. As the intracellular region of Dsg2 has been linked to surface stabilization and inhibition of endocytosis, this will involve endocytosis assays, assessing cell surface levels, and fluorescence recovery after photobleaching (FRAP) experiments. Depending on the outcomes of such endeavors, additional experiments can be planned to further

understand the roles of these intracellular domains and additional truncations or single-domain deletions can be generated and expressed in the DSG-null cells as necessary.

5.2.2 Null model systems beyond desmogleins

A431 cells can also be used to create other null cells. For example, we already have desmocollin (DSC)-null A431 cells which can be characterized and eventually used to understand desmocollins, as well as a dual knockout of DSG and DSC. Additionally, we have acquired a classical cadherin null A431 cell line which can be used to understand the dependency of desmosome assembly on adherens junction components as well as understand the segregation mechanism. Lastly, our work has raised questions regarding the involvement of PG and PKPs in promoting and/or maintaining raft association of the desmosomal cadherins. Null model systems for these proteins can also be created to further study their contributions. Therefore, the DSG-null model system we created for this work will continue to be used for other efforts and the experimental paradigm remains useful to study other desmosomal proteins and processes.

5.3 Further exploration of desmosomal dynamics with Dsg1$_{TMD}$ variants

Desmosomal processes are dynamic, yet the experiments performed here were done at steady state. These steady state experiments were sufficient for understanding the raft associating capabilities of the Dsg1$_{TMD}$ variants and how that translates to stable desmosome formation and function. However, some of our results suggest that most of the Dsg1$_{TMD}$-GFP variants negatively impact desmosome assembly and steady state experiments will not be sufficient to understand these effects. For example, we observed that desmosomes form from each Dsg1$_{TMD}$ variant, but the number of desmosomes forming varied widely and correlated with the level of raft association of each variant. This could indicate that an early stage of desmosome assembly requires raft

association or that desmosomes form normally but readily disassemble without raft association. Furthermore, the observation of desmosome formation from non-raft associating $Dsg1_{TMD}$-GFP variants drives more questions. Do these desmosomes form from the proportion of raft-associating $Dsg1_{TMD}$-GFP observed in sucrose gradient fractionations? Does this proportion of raft-associating $Dsg1_{TMD}$-GFP overcome an energy barrier to form desmosomes? Or are interactions between the extracellular or intracellular domains forcing non-raft associating $Dsg1_{TMD}$ variants into desmosomes? If the former possibility occurs, then the desmosomes observed by SIM are likely reduced in number because desmosome formation becomes a rarer event, i.e., an increased energy barrier decreases the rate of desmosome formation. However, if the latter possibility occurs, it is more likely that the desmosomes observed by SIM are the result of normal rates of formation but increased disassembly rates. Therefore, disturbing the system by applying calcium switches or altering cholesterol levels with methyl-β-cyclodextrin in a subset of the cell lines expressing the $Dsg1_{TMD}$-GFP variants would provide more information and help answer these and other questions. Additionally, determining trafficking rates as well as the surface levels and stability of some of these variants will also provide important information that is currently lacking from our datasets.

5.4 Identifying the role of transmembrane prolines in desmogleins

The $Dsg1_{scr1}$ and $Dsg1_{scr2}$ TMD variants were designed to address the possibility that a motif or specific residue(s) is necessary for raft association, but these two variants behaved in surprising ways (see Figures 4.14-4.16). The loss of raft association and desmosome assembly and function observed in cells expressing $Dsg1_{scr1}$-GFP suggested that a specific residue or motif in the TMD sequence may be important rather than or in addition to one of the physical properties of

TMDs. However, cells expressing $Dsg1_{scr2}$-GFP formed apparently normal desmosomes which rescued the DSG-null cells nearly as well as $Dsg1_{WT}$-GFP despite experiencing reduced raft association. Importantly, the positioning of two proline residues near the edge of the Dsg1 TMD was maintained in $Dsg1_{scr2}$ but not in $Dsg1_{scr1}$. Furthermore, the process of designing many of the other Dsg1 TMD variants caused one or both proline residues to be lost. Therefore, the apparent uncoupling of Dsg1 raft association from desmosome assembly and function revealed by $Dsg1_{scr2}$ may expose an important functional role for prolines in the DSG TMD.

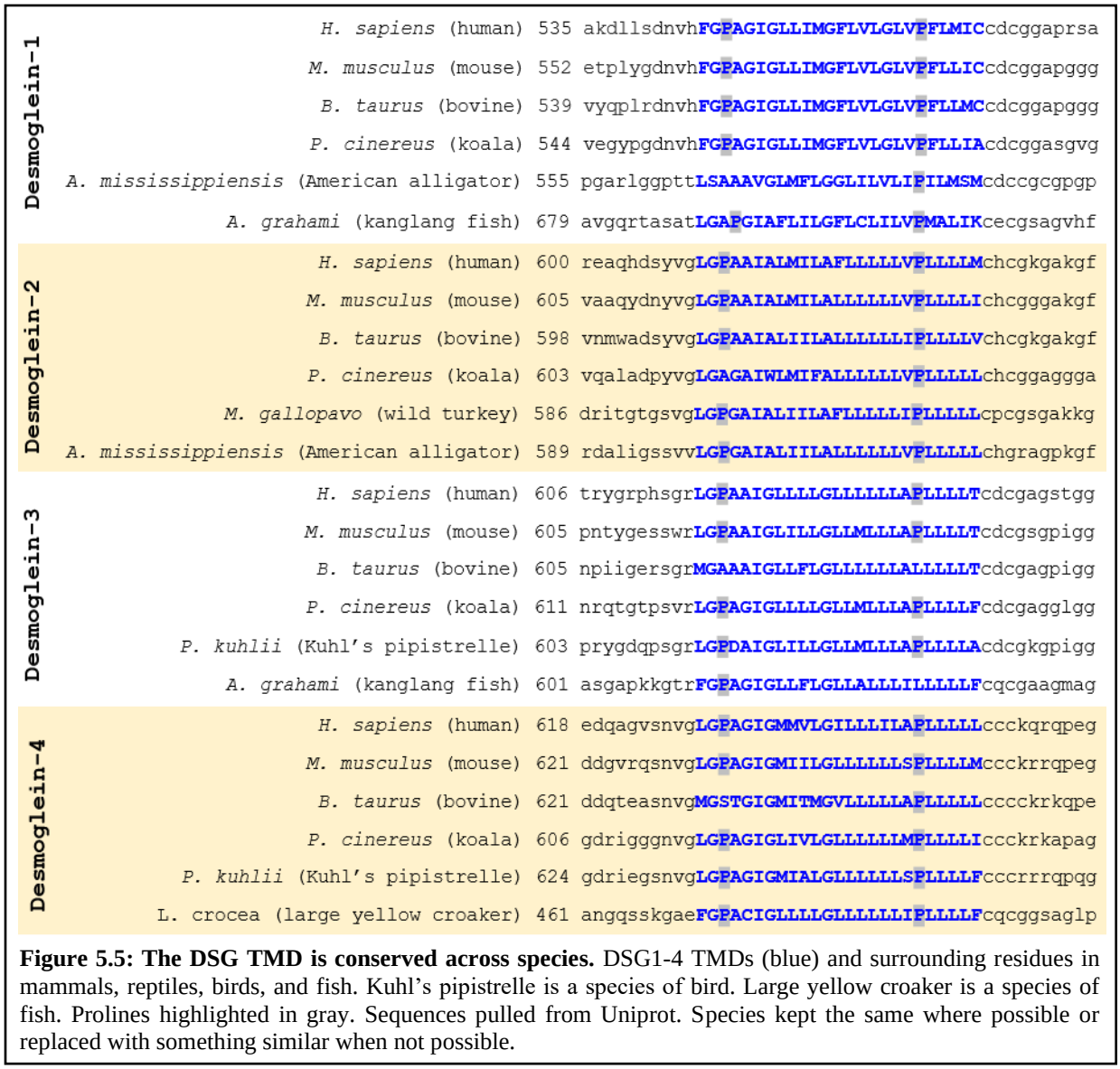

Figure 5.5: The DSG TMD is conserved across species. DSG1-4 TMDs (blue) and surrounding residues in mammals, reptiles, birds, and fish. Kuhl's pipistrelle is a species of bird. Large yellow croaker is a species of fish. Prolines highlighted in gray. Sequences pulled from Uniprot. Species kept the same where possible or replaced with something similar when not possible.

Proline residues in the DSG1 TMD are conserved both between DSG1-DSG4 and among numerous species going back to reptiles, birds, and fishes where desmosomal cadherins first emerge (154) (Figure 5.5). Proline residues are widely known as "helix-breakers" and are rare in α-helices of soluble proteins (161). The unique, cyclical structure of proline prevents the formation of hydrogen bonds necessary for stable α-helices (156). In contrast, prolines are surprisingly common in the TMD α-helices of membrane proteins where they are mostly found in the middle of the TMD or near the edges (158, 162, 163). In these locations, proline can provide improved flexibility which can benefit lipid packing or act as a molecular switch through cis-trans isomerization causing important structural changes for signal transmittance or protein activation (158). Substituted prolines in a membrane protein are generally unfavorable (164). Therefore, it is not surprising that we observed drastic changes in Dsg1 function when the prolines were rearranged in $Dsg1_{scr1}$.

We can address the possible role of these prolines in the Dsg1 TMD by creating additional $Dsg1_{TMD}$ variants. These variants would involve mutating one or both prolines within the context of the wildtype Dsg1 TMD, stably expressing these new variants in our DSG-null cells, and using the same set of experiments shown in Chapter 4 to determine the effect that these prolines might have on raft association versus desmosome assembly and function. While this will address whether the prolines are necessary for these processes, we can also ask if these prolines are sufficient for desmosome assembly and function by placing them in their normal positions in the context of one of our variants, such as $Dsg1_{Leu}$.

Should experimentation with these new $Dsg1_{TMD}$ variants show that the proline(s) alone has an important role, we can pursue additional avenues to determine that role and how it contributes to desmosome assembly and function. This role will likely fall into one of two possible

categories: flexibility to promote lipid or protein packing in the plane of the desmosomal bilayers or a cis-trans isomerization to activate a molecular switch (158).

We can readily anticipate how either of these scenarios might fit into what is already known about desmosome dynamics. Due to the protein density of desmosomes along the membrane plane, the desmosomal cadherin TMDs must be able to pack closely with each other, cholesterol, and other lipids, including palmitoyl groups. However, the C-terminal ends of the DSG TMDs are bulkier than the N-terminal ends. Additional flexibility, particularly around the C-terminal end of the TMD where the proline is more highly conserved, could help with packing. We can begin to explore an association between proline placement and lipid packing through molecular dynamics simulations and move into cell models by using lipid probes that can reveal membrane distortion or lipid packing.

Proline isomerization can act as a molecular timer (165). If the prolines undergo cis-trans isomerization, this could serve as a switch that regulates desmosome dynamics. For example, the prolines could be in one conformation during trafficking, but isomerization to the other conformation would be a necessary step during desmosome assembly that occurs at the plasma membrane. In relation to this possibility, cis-trans isomerization could modulate binding partner sets (165). Though the trans isomer is more common than the cis isomer (166, 167), the presence of adjacent aromatic residues such as the phenylalanine next to the C-terminal proline in DSG1 (Figure 5.5) promote maintenance of the cis conformation (168, 169), and may be involved in conformational regulation. Unfortunately, there are no methods for directly detecting cis- versus trans-proline in cellular contexts at this time. Therefore, any work in this direction would have to be indirect such as linking the activity of a peptidyl-prolyl isomerase (PPIase) to desmosome dynamics.

Cis-trans prolyl isomerization can happen spontaneously but slowly (170), making PPIases necessary for any processes that require rapid isomerization. Cells could be treated with drugs targeting each of the three families of PPIases (171, 172) to determine if this causes desmosomal defects, either during steady state or with calcium switches. Observing desmosomal defects from one drug treatment but not another could also help narrow down the possibilities since the three families of PPIases including FK506-binding proteins (FKBPs), cyclophilins, and parvulins each have a number of members (173, 174). Interestingly, FKBP3 and FKBP4, PPIA, and PPIB were identified in an unpublished BioID screen using the biotin ligase, BirA, fused to the C-terminal end of Dsg2 or Dsg3 in A431 cells (Conway, unpublished). Another BioID screen using BirA fused to DP in mouse keratinocytes also identified PPIA (175). These possibilities are all expressed in human skin, HaCaT, and A431 cells and have potentially appropriate subcellular localization (176, 177) making them good candidates to consider for knockdown studies to determine if these proteins might be involved in desmosome dynamics.

5.5 Considering the possible role of motifs in the desmoglein TMD

TMDs are not inert protein segments existing solely to join extracellular and intracellular protein domains. Instead, TMDs actively interact with their environment, whether that be adjacent lipids or other proteins. These interactions can further dictate subcellular localization, protein activation or inactivation, and signal transmittance among other processes (178). Even TMD shape can determine localization or endocytic rates (149, 155). Raft association of single-pass transmembrane proteins is directly reliant on how a protein's TMD associates with the lipid bilayer with the goal of avoiding hydrophobic mismatch and reducing energy expenditure. While this has been linked to several TMD physical properties as discussed at length throughout this dissertation,

it remains possible that TMD-lipid, TMD-cholesterol, or TMD-TMD interactions can also play a role in the raft associating mechanism of some proteins. Based on our results with the $Dsg1_{TMD}$ variants, TMD physical properties such as length and exposed surface area may be important, but other unidentified factors may also be involved in the raft associating mechanism of DSGs. As the desmosome is a unique protein structure that partly exists in the plane of the lipid bilayer, it stands to reason that such factors may play important roles in desmosomal processes.

Important motifs involved in lipid-binding, TMD-TMD interactions, or other membrane dynamics would be expected to be conserved across species. To identify well-conserved residues in the TMDs of DSG1-DSG4, we collected sequences from various species using Uniprot (179) and then plotted the frequency of each TMD residue in its respective position with Weblogo (180, 181) (Figure 5.6). This revealed that most residues in the DSG1 and DSG3 TMDs are remarkably well conserved. The C-terminal ends of the DSG2 and DSG4 TMDs are also conserved while the N-terminal ends of these two DSGs have more variation. While this level of conservation is interesting, determining whether particular motifs might exist becomes difficult. Such conservation could make a good argument for the importance of TMD physical properties over motifs but comparing conserved elements among the DSG TMDs may also offer some insight. For example, the position of the two prolines discussed above is conserved between the four desmoglein TMDs. Additionally, two stretches of leucines dominate the C-terminal end of the DSG2, DSG3, and DSG4 TMDs. Though these stretches of leucines are not fully present in the DSG1 TMD, L14, L16, L18, and L22 are conserved between all four desmoglein TMDs while L8 is conserved among DSG1-DSG3. Lastly, G2 is conserved in all the desmoglein TMDs, G5 is conserved in DSG1 and DSG4, and G7 and G12 are conserved in DSG1, DSG3, and DSG4. Some of these observations are relevant to known binding motifs, discussed next.

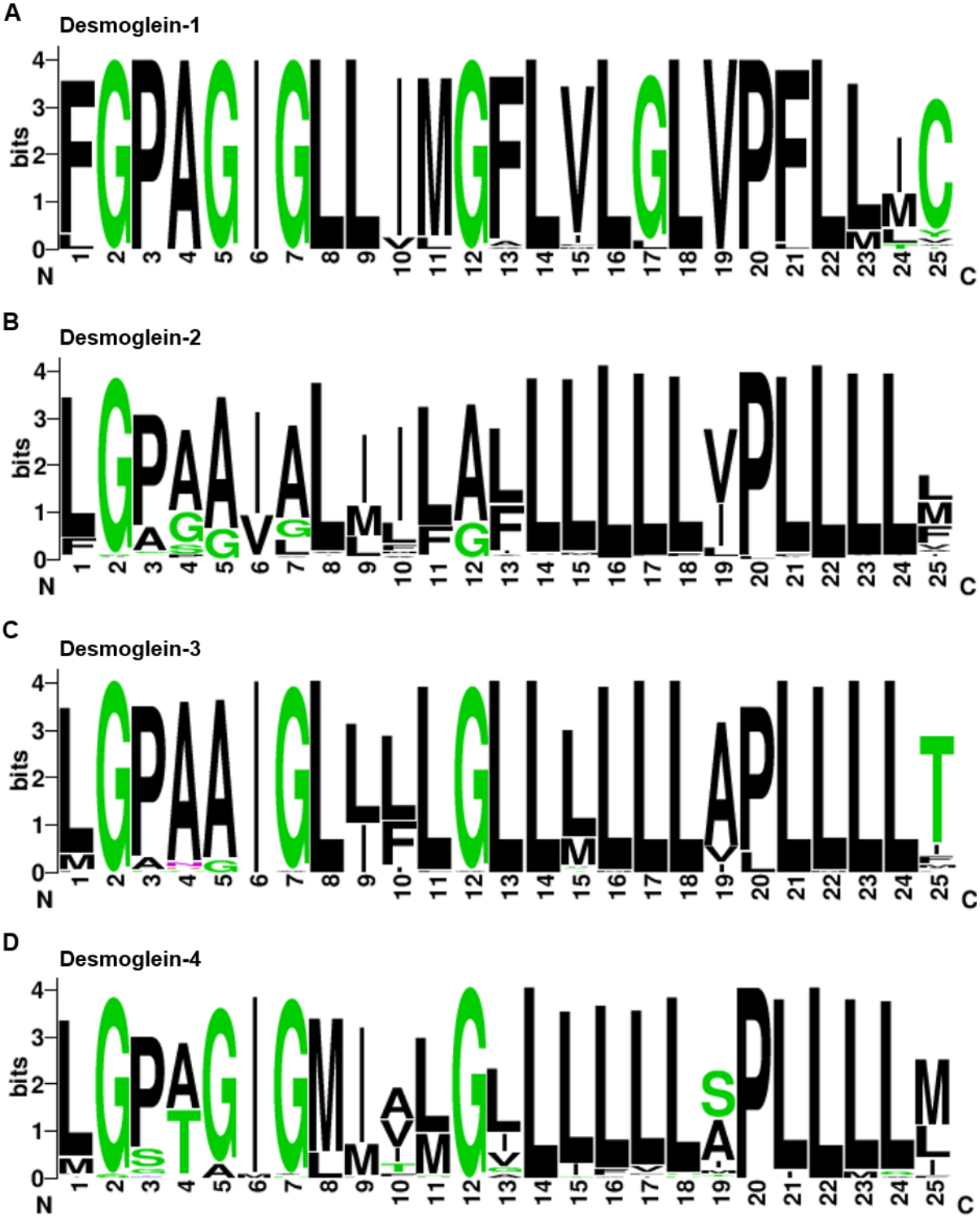

Figure 5.6: Residue conservation across DSG TMDs. A) DSG1 TMD across 96 species. B) DSG2 TMD across 151 species. C) DSG3 TMD across 61 species. D) DSG4 TMD across 65 species. Sequences were collected from Uniprot, and plots were created at https://weblogo.berkeley.edu/logo.cgi.

5.5.1 Lipid-binding Motifs

As raft-associating proteins, DSGs must associate with lipid bilayer regions that are enriched for sphingolipids and cholesterol. It is unknown if DSGs directly bind either of these lipid raft denizens, but sphingolipid- and cholesterol-binding motifs have been identified in the TMDs of other membrane proteins.

The sphingolipid binding domain (I/L/T/V)xx(I/L/T/V)(I/L/T/V)xx(I/L/T/V)(F/W/Y) which starts 13 (+/-3) residues from the N-terminal end of a TMD has been found in numerous membrane proteins and verified in a subset (182, 183). The DSG1, DSG2 and DSG3 TMDs have sequences that vaguely work with this motif, however, an aromatic residue at the C-terminal end tends to be absent. The DSC sequences are difficult to assess for the presence of this motif due to the uncertainty surrounding the C-terminal end of these TMDs, though some mildly well-conserved phenylalanines exist in potentially relevant positions. Even without an aromatic residue, the rigidity of the branched chain residues present in other positions may allow for interactions between a sphingolipid or other lipid. Due to the sphingolipid enrichment within lipid rafts, it may be pertinent to test the desmosomal cadherin TMDs for sphingolipid-binding even without the clear presence of an appropriate motif. If any of the desmosomal cadherins were shown to bind sphingolipids, mutational analysis could be performed to determine which residues are involved and non-sphingolipid binding mutants could be expressed ibn our DSG-null cells to discover functional consequences.

5.5.2 Cholesterol-binding motifs

TMDs bind cholesterol through the cholesterol recognition amino acid consensus (CRAC) motif and its mirror consensus, CARC, which follow the pattern (L/V)x_{1-5}(Y/F/W)x_{1-5}(K/R) and (R/K)x_{1-5}(Y/F/W)x_{1-5}(L/V); one or both of these can appear in a TMD (184). Such a motif does

not appear to exist in DSGs which tend to lack positively charged residues on either end as well as appropriately placed aromatic residues (Figure 5.5). A GxxxG motif more commonly associated with TMD oligomerization (see below) has also been reported to be involved in cholesterol binding (185). GxxxxG is present in the DSGs, but this does not appear to be a relevant motif. Therefore, it seems unlikely that DSGs directly bind cholesterol unless through an unidentified motif. In contrast, positively-charged residues such as lysine and arginine are common on either end of the DSC TMDs, a conserved tryptophan starts these TMDs, and a conserved leucine follows within five positions (Figure 5.7, see Figures 5.8, 5.9). DSC1 may have mirror-imaged CRAC and CARC domains, though the aromatic residue on the C-terminal end is not fully conserved. It would be very interesting if DSGs were able to bind sphingolipids while DSCs could bind cholesterol. This could be an important mechanism related to both raft association and clustering of the desmosomal cadherins.

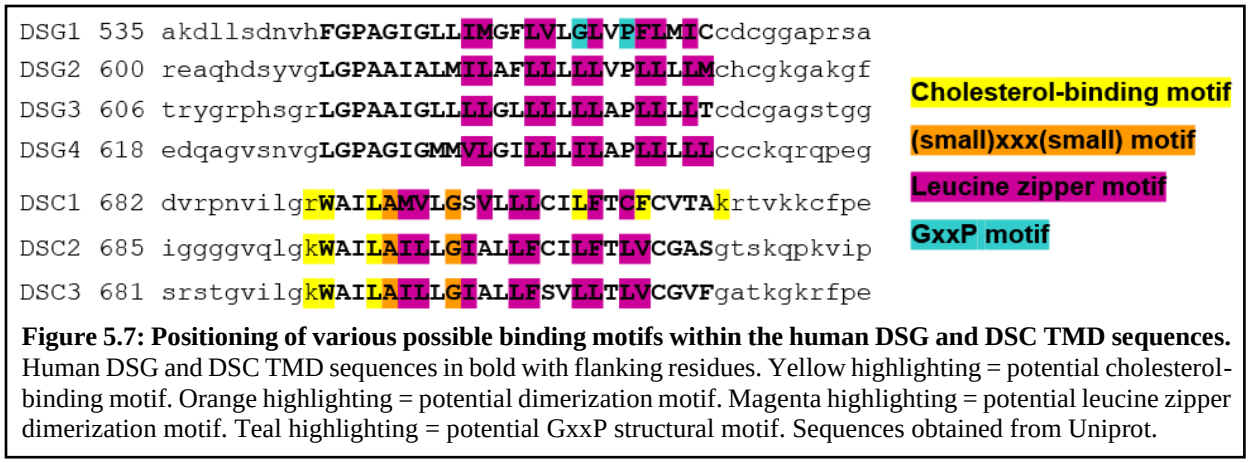

Figure 5.7: Positioning of various possible binding motifs within the human DSG and DSC TMD sequences. Human DSG and DSC TMD sequences in bold with flanking residues. Yellow highlighting = potential cholesterol-binding motif. Orange highlighting = potential dimerization motif. Magenta highlighting = potential leucine zipper dimerization motif. Teal highlighting = potential GxxP structural motif. Sequences obtained from Uniprot.

5.5.3 TMD-TMD Dimerization

TMD-TMD dimerization has been shown to promote the assembly of large protein complexes via noncovalent interactions within the plane of the membrane for various purposes including signaling and cell-cell adhesion (186-188). Several motifs that allow for dimerization have been identified, including GxxxG, QxxS, and leucine zipper-like motifs (178, 189-192).

GxxxG has been identified in a number of membrane proteins (140, 188, 189). While several conserved glycines exist in the DSG TMDs as mentioned above, none have the appropriate distribution to fulfill the well-documented GxxxG dimerization motif. However, the (small)xxx(small) motif, where small equates to glycine, alanine, or serine, is also well documented. But even the distribution of these residues does not fit into this motif. Instead, the DSCs have AxxxG at position 5-9, and these residues are well conserved (Figure 5.7, see Figures 5.8, 5.9). However, such motifs are abundant in TMDs and do not always promote dimerization (189). QxxS, sometimes defined as polar(xx)polar can also mediate TMD dimerization (191, 192). Such a motif is absent in desmoglein TMDs, but mutation to PxxS has been shown to maintain dimerization (193). While such a motif is also absent from desmoglein TMDs, this showed that a proline located along the interaction interface could promote dimerization. It is not clear to what extent this phenomenon occurs and more work would be required to determine if either of the prolines in the desmoglein TMDs are along an interaction interface, assuming that there is an interaction interface for dimerization. On the other hand, proline can also disrupt dimerization interfaces as has been shown in E-cadherin (187). As introduced prolines have been shown to be detrimental (164), this observation may not be relevant. Of the known TMD-TMD dimerization motifs, the leucine zipper-like motif may be the best candidate. This motif follows the heptad pattern *abcdefg* where leucine is commonly in the *ga..de.ga..de.ga* positions and works by creating "knobs and holes" that readily pack together (190, 194). Additionally, isoleucine, valine, methionine, and phenylalanine can also be present in these positions. Between the abundant leucines found in all the DSG TMDs and these other residues, a leucine zipper motif may be present (Figure 5.7). Furthermore, E-cadherin TMD-TMD dimerization has been shown to occur via a leucine zipper-like motif and have functional significance for adhesion (72).

A variety of bacterial-based assays have been developed to test TMD-TMD dimerization, such as ToxCAT and AraTM (195, 196). In AraTM, GFP expression is coupled to TMD-TMD dimerization events through the AraC promoter. We have used this assay to produce preliminary data that $Dsg1_{WT}$ dimerizes (not shown). Whether this dimerization occurs through a leucine zipper-like motif as in E-cadherin or one of the other motifs discussed has yet to be seen. A mutational analysis would help determine which residues are necessary for dimerization. As it is unknown whether TMD-TMD dimerization is also involved in raft association of DSG1, using our $Dsg1_{TMD}$ variants in this assay may help reveal this possibility.

5.5.4 Structural TMD motifs

Apart from lipid-binding or TMD-TMD dimerization, motifs can also be involved in structural aspects of a TMD. For example, a GxxP motif has been shown to promote helix flexibility and bending due to a lack of stabilizing hydrogen bonds (158, 159). While this motif can be found in the DSG1 TMD, it is not present in the TMDs of the other desmogleins (Figure 5.7). If significant, it would likely be involved in a DSG1-specific function that does not apply to the other desmogleins.

5.6 Understanding the contribution of palmitoylation towards desmosomal processes

Here we found that palmitoylation of the Dsg1 TMD is not required for raft association of Dsg1. However, we found slight decreases in desmosome length, and the palmitoylation mutant did not rescue desmosome function in DSG-null cells as well as $Dsg1_{WT}$. This suggests that palmitoylation may play an important role in desmosome dynamics. Future work should focus on determining the role of palmitoylation in desmosome dynamics as well as identifying the palmitoyl acyltransferase responsible for palmitoylating Dsg1. One possibility is that the long, saturated

hydrocarbon chain of palmitoyl groups promotes packing among the desmosomal proteins at the membrane and may help maintain the structure as a raft. Therefore, without this maintenance, desmosomes remain small and may experience increased turnover rates. A Dsg2 palmitoylation mutant has been shown to have increased turnover rates compared to wildtype Dsg2 (76). Increased turnover of $Dsg1_{AADA}$ would be expected to have consequences for desmosomal turnover and affect desmosome length and strength. We can perform protein turnover assays to determine if overall protein stability is affected as well as endocytosis assays to see if turnover at the surface is affected by loss of palmitoylation. Additionally, we can perform fluorescence recovery after photobleaching analyses to see if desmosomal versus non-desmosomal surface $Dsg1_{AADA}$-GFP shows different behavior compared to $Dsg1_{WT}$-GFP or if desmosomal dynamics differ between cells expressing each construct. A Dsg2 palmitoylation mutant was also found to form desmosomes more slowly than wildtype Dsg2 following a calcium switch (76). As our work was done entirely with cells at steady state, disrupting the system further with calcium switches would also help to offer some insight into the role of palmitoylation in desmosomal processes.

These experiments would help establish a role for palmitoylation in desmosome dynamics, but it will also be important to determine how desmosomal proteins, including DSGs, are palmitoylated. Palmitoylation is carried out by palmitoyl acyltransferases (PAT), of which there are 23 in humans (79). Possible candidates include ZDHHC13 (81, 82, 197, 198), ZDHHC21 (80), and DHHC5 (199). Of these, ZDHHC13 and ZDHHC21 are implicated in epidermal differentiation and integrity, though no studies have specifically linked these with desmosomes. DHHC5 has been shown to palmitoylate DSG2 in HeLa cells (199). DHHC5 has also appeared in an unpublished BioID screen using BirA-tagged DSG2 but not DSG3 expressed in A431 cells (Conway, unpublished) and a BioID screen using BirA-tagged DP in mouse primary keratinocytes

(175). As PATs are promiscuous (79), it remains possible that DSG2 can be palmitoylated by other DHHC enzymes, and it remains to be seen which PATs palmitoylate the other desmosomal proteins. To determine which PATs might be good candidates to consider, we collected localization and expression level information about the PATs in A431 and HaCaT cell lines and skin tissue from the Human Protein Atlas (Table 5.1). Though information regarding protein level expression in A431s or HaCaTs was often missing, this revealed that DHHC3, DHHC5, DHHC9, DHHC20 may be good candidates with several others also being possibilities if they are expressed at the protein level. siRNA knockdown studies could be used alongside acyl biotin exchange to determine if loss of PAT expression of one or more of these candidates leads to loss of DSG or desmosomal protein palmitoylation. Should this identify a particular PAT, further experiments could be performed to assess how this PAT might be involved in regulating desmosome dynamics.

Table 5.1: Localization and expression of PATs in cultured cells commonly used in desmosomal studies and skin. Information collected from the Human Protein Atlas (176, 177).

DHHC isoform	**Localization**	**A431**		**HaCaT**		**Skin***	
		RNA	*Protein*	*RNA*	*Protein*	*RNA*	*Protein*
DHHC1	Cytosol	+	+	+	+	+	-
DHHC2	Plasma membrane	-	NA	-	NA	+	medium
DHHC3†	Golgi body	+	+	+	NA	+	medium
DHHC4	NA	+	NA	+	NA	+	-
DHHC5†	Plasma membrane, Nucleus	+	+	+	NA	+	medium
DHHC6	NA	-	NA	-	NA	+	-
DHHC7	Golgi body	+	NA	+	NA	+	-
DHHC8	Cytosol, Nucleus	+	+	+	NA	+	-
DHHC9†	ER, Golgi body, cytosol	+	+	+	+	+	low
DHHC11	Mitochondria	low	NA	+	NA	+	medium
DHHC11b	Mitochondria	-	-	+	-	+	medium
DHHC12	Nucleus, Keratin Filaments	+	NA	+	NA	+	medium
DHHC13	Vesicles, Golgi body	+	+	+	NA	+	-
DHHC14	Nucleoli, Mitochondria	-	NA	-	NA	+	-
DHHC15	Nucleus, Cytosol	-	-	-	-	+	-
DHHC16	Nucleus, Cytosol	+	+	+	NA	+	-
DHHC17	Golgi body, Vesicles	+	NA	+	NA	+	-
DHHC18	Microtubules	+	+	+	NA	+	-

DHHC19	NA	-	-	-	-	basal	NA
DHHC20†	Vesicles, plasma membrane	+	+	+	NA	+	low
DHHC21	Golgi body, Cytosol	+	NA	+	NA	+	medium
DHHC22	Plasma membrane	-	-	-	-	NA	NA
DHHC23	Nucleus	+	+	+	NA	+	NA
DHHC24	Vesicles, Cytosol	+	NA	+	NA	+	low

*Levels in basal and suprabasal keratinocytes. Many DHHC are expressed in other skin cell types. †DHHCs whose expression levels and localization make them potential candidates for desmosomal palmitoylators. Of these, DHHC5 has been identified in BioID screens involving desmosomal proteins.

5.7 The raft associating mechanism of desmocollins

Little is known about DSCs. Both DSCs and DSGs are required for strong desmosomal adhesion (18, 19). Mutations in DSC2 have been linked with heart disorders such as arrhythmogenic right ventricular cardiomyopathy/dysplasia (200). Loss of DSC1 causes epidermal fragility, abnormal differentiation, and barrier defects in mice (41) while loss of DSC3 in mice causes skin blistering (43). Mechanistically, DSC2 requires glycosylation to be transported to the plasma membrane (201), and its transport along microtubules occurs independently of DSG2 (202). At the membrane, DSC3 but not DSC2 heterophilically binds E-cadherin in the absence of calcium (203), but DSC2 forms calcium-dependent homodimers (108). DSC2 is palmitoylated but the cysteine residue(s) involved have not been identified (112). Lastly, DSC2 has been shown to associate with rafts ((49), this work), but the raft-associating mechanism remains unknown. We anticipate that this mechanism is fairly similar to that of the DSGs.

A similar study to the one conducted here could be performed wherein one designs and expresses a series of DSC_{TMD} variants in a DSC-null background, such as the uncharacterized DSC-null A431 cells mentioned above. In our work here, we rarely observed reduced raft association of DSC2 when Dsg1 raft association was reduced. This suggests that the ability of DSCs to associate with rafts is independent of DSGs and is in line with previous work that shows

early clustering of Dsc2 during desmosome assembly (108) while Dsg2 initially interacts with E-cadherin before clustering with Dsc2 (107), although the role of raft association was not addressed in those studies. In the context of DSC-null cells or DSG-null cells expressing a DSC_{TMD} variant, it would be very interesting to see whether DSG2 raft association occurs independently of DSC.

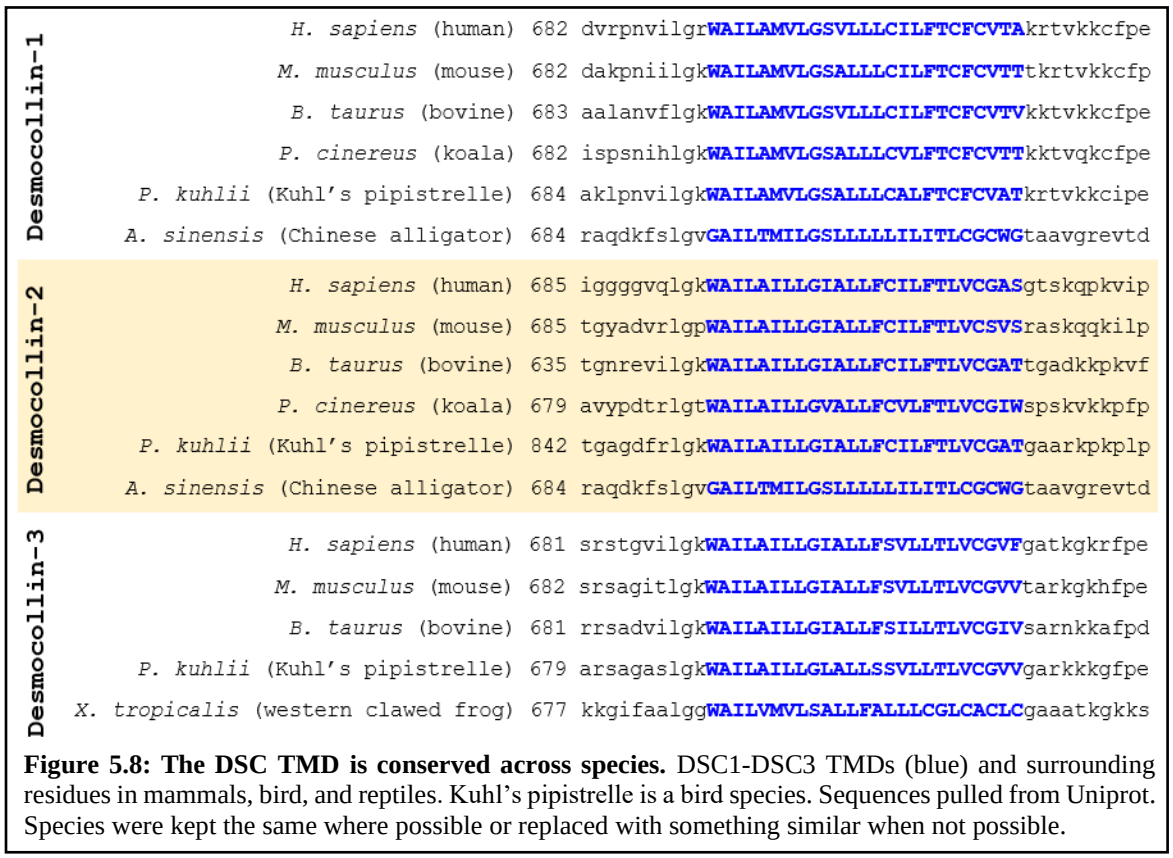

Figure 5.8: The DSC TMD is conserved across species. DSC1-DSC3 TMDs (blue) and surrounding residues in mammals, bird, and reptiles. Kuhl's pipistrelle is a bird species. Sequences pulled from Uniprot. Species were kept the same where possible or replaced with something similar when not possible.

Additionally, should further study into the DSG TMD reveal a possible motif or specific residues that drives raft association of DSGs, such a motif or residue may also be found in DSCs. Like DSG, the DSC TMD is also well-conserved among mammals, reptiles, and birds, and the TMDs of DSC1, DSC2, and DSC3 are similar to each other (Figure 5.8). As with the DSG TMD sequences, we collected a series of DSC TMD sequences from Uniprot (179) and plotted the frequency of residues in each position using Weblogo (180, 181). We found strong residue conservation at many positions with greater conservation in the N-terminal half of the TMD versus the C-terminal half (Figure 5.9). The residue dichotomy towards the C-terminal end is mostly due

to the inclusion of birds and reptiles. Doing this analysis with only mammalian species results in nearly full agreement among these residues (indicated by red asterisk in Figure 5.9). In mammals, C22 is a probable candidate for palmitoylation as it is conserved across DSC1-3 while the exact positioning of this cysteine is more variable in non-mammalian species. As we observed among the DSG TMDs, high levels of conservation within each TMD make assessing residues of importance difficult, however, comparing TMDs to each other brings several positions into focus. For example, L4, L8, L12, L13, and L17 are conserved across DSC1-3 while L7 and L20 are also well-conserved in DSC2 and DSC3. Many of the conserved residues are consistent with the potential motifs mapped in Figure 5.7 and make for additional interesting avenues to explore.

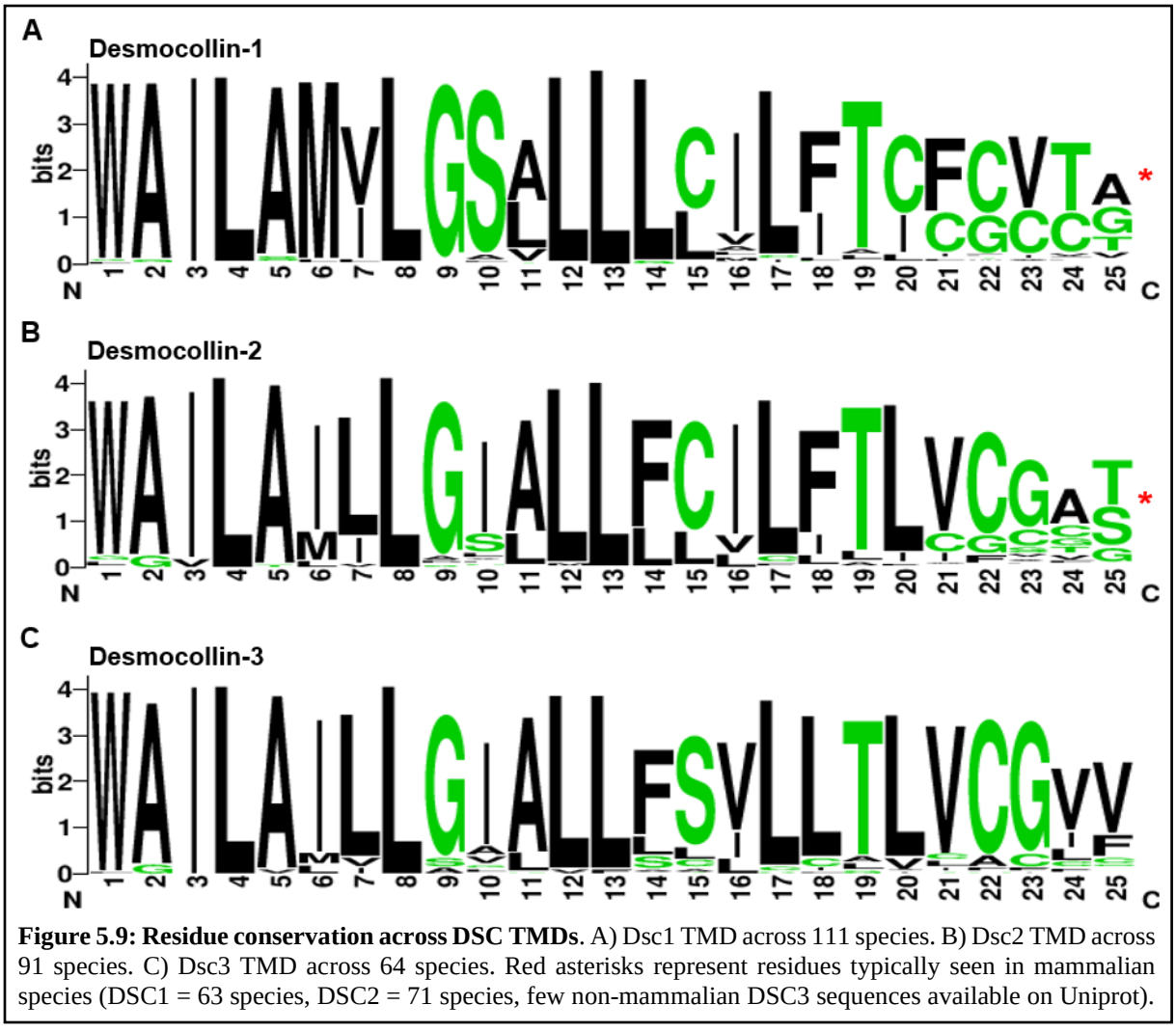

Figure 5.9: Residue conservation across DSC TMDs. A) Dsc1 TMD across 111 species. B) Dsc2 TMD across 91 species. C) Dsc3 TMD across 64 species. Red asterisks represent residues typically seen in mammalian species (DSC1 = 63 species, DSC2 = 71 species, few non-mammalian DSC3 sequences available on Uniprot).

5.8 The role of raft association in segregation of adherens junctions and desmosomes

The segregation of adherens junctions and desmosomes is driven, in part, by protein-protein interactions. As discussed in Chapter 1, PG and β-catenin can both bind E-cadherin and desmoglein, but binding of PG to desmoglein prevents binding of β-catenin, promoting the exclusion of adherens junction components (106). This mechanism alone is likely insufficient for complete segregation. Unlike desmosome components, adherens junction components do not associate with rafts and are unaffected by raft-disrupting agents (50, 204). Furthermore, adherens junction components are not palmitoylated while desmosome components, with the exception of DP, are palmitoylated (112). Though palmitoylation alone does not seem to be required for raft association of desmogleins ((6, 76), this work), unpalmitoylated PKP2 and PKP3 mutants lose raft association and prevent desmosome assembly (112). Furthermore, inhibiting palmitoylation with 2-bromopalmitate inhibits desmosome assembly without disrupting adherens junctions (112). Palmitoylation may aid in junction segregation by allowing for the differentiation of classical cadherins from desmosomal cadherins and for the clustering of palmitoylated components together and away from non-palmitoylated proteins. In that vein, PKPs have been shown to be important for clustering of desmosomal cadherins to increase size and stability of desmosomes (83, 86, 89, 90). Thus, PG and PKP work together; while PG initiates segregation by protein-protein interactions, PKP stabilizes growing desmosomal cadherin oligomers through both protein and lipid interactions. The desmosomal cadherin oligomers are likely raft-associated at this stage but require palmitoylated PKP-mediated stabilization to assemble larger complexes. This raft association is then an additional mechanism meant to further exclude adherens junction components.

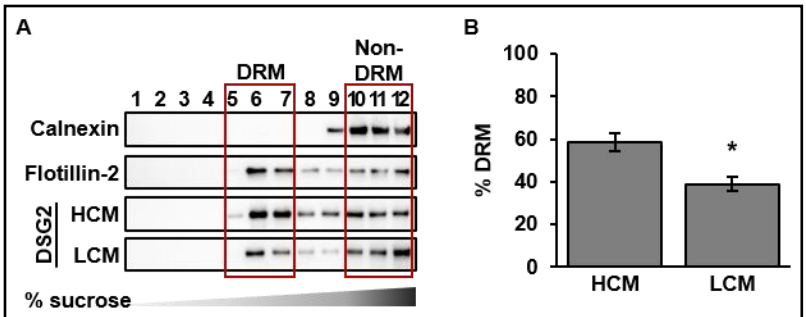

Figure 5.10: DSG2 raft association is calcium dependent. A) Western blots of sucrose gradient fractionations show DRM segregation of DSG2 in A431s in high (HCM) versus low calcium media (LCM). Calnexin = non-DRM marker. Flotillin-2 = DRM marker. B) Quantification of blots in A. Error bars show standard deviation (n = 2). *p < 0.05

These ideas can be tested in several ways. Overexpression of PKP1 has been shown to induce the calcium-independent, hyperadhesive state in keratinocytes and even to induce desmosomal protein clustering in low calcium conditions (89). Identifying other conditions under which PKP1 overexpression can induce desmosome formation would further show the ability of PKP to cluster desmosomal components. For example, PKP1 overexpression in the DSG-null cells may allow for clustering of endogenous DSC2 and even relocalization of DP to cell-cell borders. If the desmosomal cadherins need PKP1 for stabilization, their clustering may be too transient to study in the early stages of desmosome assembly. However, the raft-associating state of desmogleins varies by conditions. Dsg2 and Dsg3 exhibit reduced raft association under low calcium conditions ((50), Figure 5.10). Therefore, sucrose gradient fractionations following overexpression of PKP1 in low calcium conditions would show increases in raft association of desmogleins if PKP1 is able to cluster in these conditions. This could also be done in the DSG-null cells that express some of the $Dsg1_{TMD}$-GFP variants to see if clustering by overexpressed PKP1 can overcome or bypass the raft association energy barrier. Alternatively, PKP1 overexpression in classical cadherin-null cells may be able to bypass the need for adherens junction components. In contrast, PG overexpression cannot induce desmosome formation on its own in

classical cadherin-null A431D cells (205), suggesting that clustering is not the role of PG. If PKP1 is capable of clustering desmosomal cadherins under these various conditions, further testing with PKP1 mutants that lack desmosomal protein binding domains or the palmitoylated cysteine would help determine how PKP functions to cluster desmosomal cadherins.

To then understand the role of palmitoylation in these processes, it will be imperative to determine how and when desmosomal proteins are palmitoylated. Determining how palmitoylation occurs has been discussed above but knowledge of where and when is also unknown. Are desmosomal proteins palmitoylated in both low and normal calcium conditions or only when calcium is present? Does palmitoylation occur at the plasma membrane or during trafficking? Do conditions for palmitoylation vary between membrane versus cytoplasmic desmosomal proteins? Different PATs inhabit different cellular compartments (79), so determining which PAT(s) palmitoylate each desmosomal protein would give some insight into location. Comparing palmitoylation levels during low versus normal calcium conditions may also reveal additional mechanisms for palmitoylation of desmosomal proteins. For example, if palmitoylation occurs during trafficking, regardless of calcium levels, then it is likely important for driving membrane localization as is the case for some proteins (206). However, if palmitoylation occurs in response to increased calcium levels, then it may be part of a mechanism that stabilizes desmosomal proteins at the cell surface. Pursuing these various directions will help reveal the segregation mechanism between adherens junctions and desmosomes.

5.8.1 Raft association as a driver of junction segregation

It is possible that similar principles apply to tight junction assembly. Tight junction components are also raft associated (5) and also require adherens junctions to drive assembly (207, 208). Like the desmogleins and desmocollins, the claudins are palmitoylated (209-211).

Furthermore, there are overlapping protein-protein interactions between tight junction and adherens junction components (212, 213). In simple polarized epithelial cells, such as those lining the intestines, mature junctions are arranged along the basolateral sides of adjacent cells such that tight junctions are most apical followed by adherens junctions and then desmosomes. An attractive model is that E-cadherin associates with tight junction and desmosomal components to initiate the formation of the apical junctional complex, but that this process is followed by the recruitment of raft lipids and cholesterol into tight junction and desmosome domains to drive the segregation of the proteins into distinct membrane domains. In this manner, differential raft association would be a key driver of the overall organization of the apical junctional complex.

5.9 Desmosomes assemble and mediate robust cell-cell adhesion through a hierarchy of molecular interactions

The work here is another small stepping stone in our endeavor to understand desmosomal processes and brings into focus the hierarchy of molecular interactions required to generate robust cell-cell adhesion in tissues. We can add new information to the orchestrated series of interactions through which desmosomes assemble and think of these interactions as occurring in a hierarchy (Figure 5.12). At the earliest stage in desmosome assembly, classical and desmosomal cadherins cluster with cadherins in the opposing cell and with those in the proximal membrane plane (19, 107, 108). Weak adhesion is mediated by individual trans strand-swap dimers between the EC1 and EC2 domains (17, 18). Cytoplasmic, membrane-localized armadillo proteins, including β-catenin and PG, stabilize nascent cadherin clusters through direct protein-protein interactions (22, 23, 106, 214-217). In the next stage, exclusionary binding among the cadherins and armadillo proteins as well as protein-lipid interactions drive segregation of DSG-PG complexes away from

classical cadherin-β-catenin complexes and towards raft-associated DSC clusters (106, 107). Clusters grow laterally, bringing together more desmosomal cadherins and armadillo proteins,

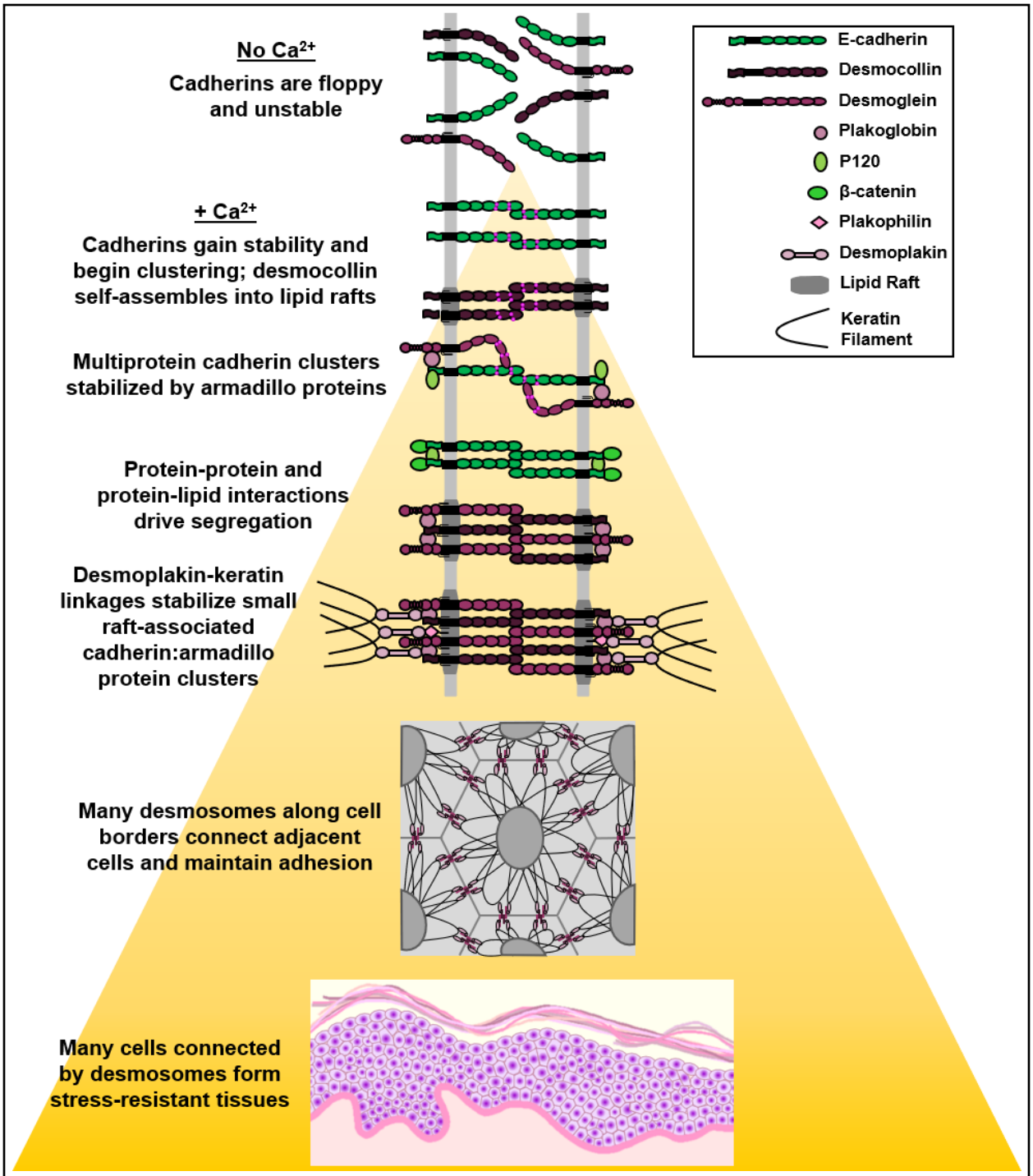

Figure 5.11: Strength in numbers: hierarchy of desmosomal interactions. Interactions within assembling desmosomes build on each other to stabilize the growing complex and create a platform for further growth. Affinity between individual desmosomal cadherin transdimers multiplied by hundreds of clustered dimers within desmosomes generate an adhesive interface. Desmosomes along cell borders maintain adhesion between adjacent cells within tissues and promote mechanical stress-resistance and tissue integrity.

including PG and PKP. In the last stage of desmosome assembly, DP connects keratin to stabilize desmosomal clusters (122, 218). Adhesion in a single desmosome is mediated by individual strand swap dimers between hundreds of desmosomal cadherins on each side of the cell border. Many desmosomes along a single cell-cell border interlock adjacent cells. When such borders are multiplied among the many cells in a tissue, the robust adhesive strength of the desmosomes confers stress-resistance to these tissues. With the integrity of tissues being dependent on this hierarchy of interactions, mutations in the genes encoding the desmosomal proteins can follow numerous pathomechanisms to cause disease.

5.10 Beyond cell-cell adhesion: the desmosome as a stable molecular platform

By definition, lipid rafts are transient membrane events, yet desmosomal structures are highly stable membrane domains. A stable structure is necessary for maintaining strong adhesion but could also create a cellular locale around which other, non-adhesive mechanisms are conducted. In this way, the desmosome is both a cell junction that mediates adhesion and a molecular platform on which many cellular processes depend. This then raises the question of whether the raftiness of the desmosome is a requirement for it to also be a molecular platform. A proteomics study on the inner dense and outer dense desmosomal plaques uncovered numerous proteins with varying functions from cytoskeletal regulators to signaling and RNA-binding proteins whose localization and even function may be dependent on their association with mature desmosomes (175). The dependence of these proteins on normal desmosome dynamics was verified for a subset of hits, including tyrosine phosphatases Ptpn13 and Shp2, the microtubule-associated protein gephyrin, and the exocyst complex component ExoC4 among others, by assessing localization changes under DP knockdown conditions; these proteins were mislocalized

in the absence of DP expression. This finding raises a number of questions. Do these proteins require localization in the vicinity of the desmosome to function? Alternatively, does localization in the vicinity of the desmosome prevent their activity? In the absence of desmosomes, such as in DP-knockdown or DSG-null conditions, would these proteins lose or gain function? To what extent do non-adhesion proteins like these depend on the desmosome as a raft? Are these proteins capable of associating with rafts themselves? Sucrose gradient fractionations could be used to determine if these proteins segregate with DRM fractions and whether such segregation might be lost in the absence of desmosomes. Should this be the case even for a subset of these molecules, would they also localize to "non-raft" desmosomes, such as those formed from $Dsg1_{scr2}$-GFP? Such considerations may have consequences for the way we think about the SAM syndrome-causing $DSG1_{TMD}$ mutant and other disease-causing mutations in the genes encoding the desmosomal proteins.

5.11 Final Thoughts and Conclusions

Desmosomes represent an important intercellular junction that also offers unique properties for the broader study of raft-like membrane domains. Desmosomes are mesoscale domains that can be identified by both super-resolution optical imaging as well as electron microscopy. At the same time, desmosomal proteins have been identified as verified lipid raft targeting molecules. Desmosomes can also be identified within tissues and isolated from tissue homogenates, making these structures ideal for analysis of raft targeting properties of desmosomal proteins using both imaging and biochemical approaches. Ongoing studies to understand how raft association of desmosomal components impacts the ability of desmosomal proteins to cluster and mediate adhesion will be critical in defining how raft association contributes to the densely packed and

strongly adhesive nature of the desmosomal junction. Similarly, although keratin linkages are essential for strong desmosomal adhesion (219-221) we do not yet know how these linkages influence raft association, or alternatively, how raft association of desmosomal proteins influences keratin filament organization.

Desmosomes are both morphologically and functionally distinct from adherens junctions. One key difference is that desmosomes are tightly packed and can achieve a calcium-independent, hyperadhesive state (222-224). This state is characterized by the appearance of an electron-dense midline in electron microscopy images and stronger adhesion (223). Though the predominant state in tissues, the hyperadhesive state is reversible; desmosomes can return to a state of calcium-dependence for the purpose of wound healing or tissue remodeling (223). Hyperadhesion is regulated by phosphorylation of DP by PKCα (225, 226). PKC inhibition can even initiate desmosome assembly in the absence of adherens junctions or calcium (227, 228). Recent work has shown that PKC inhibition limits desmosomal plaque protein diffusion out of the desmosome, thereby conferring hyperadhesion and calcium independence (229). Lastly, desmosomal cadherins have recently been shown by fluorescence polarization to arrange into highly ordered configurations (230) that presumably contribute to desmosomal cadherin clustering and adhesion, but we do not yet know how raft association impacts desmosomal cadherin organization within desmosomes.

In addition to the assembly of the desmosomal membrane domain, it is important to consider that the relationship between lipid rafts and desmosomes may extend beyond desmosome dynamics and adhesive functions. Lipid rafts have been shown to impact the processes of proliferation, migration, apoptosis, and differentiation in keratinocytes (231-235). Desmosomal components have also been shown to play a role in each of these processes. The signaling

molecules p38 mitogen-activated protein kinase, Akt, ERK1/2, and EGFR have been found to be abnormally activated when lipid rafts are disrupted in keratinocytes by methyl-β-cyclodextrin (mβCD) treatment (93, 232, 235, 236). Similarly, many of the knockout mouse models described in Chapter 1 have revealed that desmosomal components are involved in regulating important signaling pathways, including the Wnt (44), EGFR, PI3-kinase/AKT, and NF-κB signaling pathways (29). Future studies will be needed to understand how the integration of desmosomal cadherin adhesion and signaling is achieved and how the association of signaling molecules and desmosomal components with raft domains impacts this adhesion and signaling network.

Reference List

1. Farquhar MG, Palade GE. Junctional complexes in various epithelia. J Cell Biol. 1963;17:375-412. Epub 1963/05/01. doi: 10.1083/jcb.17.2.375. PubMed PMID: 13944428; PMCID: PMC2106201.

2. Sezgin E, Levental I, Mayor S, Eggeling C. The mystery of membrane organization: composition, regulation and roles of lipid rafts. Nat Rev Mol Cell Biol. 2017;18(6):361-74. Epub 2017/03/31. doi: 10.1038/nrm.2017.16. PubMed PMID: 28356571; PMCID: PMC5500228.

3. Suzuki T, Zhang J, Miyazawa S, Liu Q, Farzan MR, Yao WD. Association of membrane rafts and postsynaptic density: proteomics, biochemical, and ultrastructural analyses. J Neurochem. 2011;119(1):64-77. Epub 2011/07/30. doi: 10.1111/j.1471-4159.2011.07404.x. PubMed PMID: 21797867; PMCID: PMC3184177.

4. Field KA, Holowka D, Baird B. Fc epsilon RI-mediated recruitment of p53_56lyn to detergent-resistant membrane domains accompanies cellular signaling. Proc Natl Acad Sci USA. 1995;92:9201-5. doi: 10.1073/pnas.92.20.9201.

5. Nusrat A, Parkos CA, Verkade P, Foley CS, Liang TW, Innis-Whitehouse W, Eastburn KK, Madara JL. Tight junctions are membrane microdomains. Journal of Cell Science. 2000;113:1771-81.

6. Lewis JD, Caldara AL, Zimmer SE, Stahley SN, Seybold A, Strong NL, Frangakis AS, Levental I, Wahl JK, 3rd, Mattheyses AL, Sasaki T, Nakabayashi K, Hata K, Matsubara Y, Ishida-Yamamoto A, Amagai M, Kubo A, Kowalczyk AP. The desmosome is a mesoscale lipid raft-like membrane domain. Mol Biol Cell. 2019;30(12):1390-405. Epub 2019/04/04. doi: 10.1091/mbc.E18-10-0649. PubMed PMID: 30943110; PMCID: PMC6724694.

7. Fiedler K, Kobayashi T, Kurzchalia TV, Simons K. Glycosphingolipid-enriched, detergent insoluble complexes in protein sorting in epithelial cells. Biochemistry. 1993;32:6365-73. doi: 10.1021/bi00076a009.

8. Scheiffele P, Rietveld A, Wilk T, Simons K. Influenza viruses select ordered lipid domains during budding from the plasma membrane. The Journal of Biological Chemistry. 1999;274(4):2038-44. doi: 10.1074/jbc.274.4.2038.

9. Head BP, Patel HH, Insel PA. Interaction of membrane/lipid rafts with the cytoskeleton: impact on signaling and function: membrane/lipid rafts, mediators of cytoskeletal arrangement and cell signaling. Biochim Biophys Acta. 2014;1838(2):532-45. Epub 2013/08/01. doi: 10.1016/j.bbamem.2013.07.018. PubMed PMID: 23899502; PMCID: PMC3867519.

10. Tsukita S, Furuse M, Itoh M. Multifunctional strands in tight junctions. Nature Reviews. 2001;2:285-93.

11. Umeda K, Ikenouchi J, Katahira-Tayama S, Furuse K, Sasaki H, Nakayama M, Matsui T, Tsukita S, Furuse M, Tsukita S. ZO-1 and ZO-2 independently determine where claudins are

polymerized in tight-junction strand formation. Cell. 2006;126(4):741-54. Epub 2006/08/23. doi: 10.1016/j.cell.2006.06.043. PubMed PMID: 16923393.

12. Garcia MA, Nelson WJ, Chavez N. Cell-Cell Junctions Organize Structural and Signaling Networks. Cold Spring Harb Perspect Biol. 2018;10(4). Epub 2017/06/11. doi: 10.1101/cshperspect.a029181. PubMed PMID: 28600395; PMCID: PMC5773398.

13. Goodenough DA. Connexins, connexons, and intercellular communication. Annu Rev Biochem. 1996;65(475-502). doi: 10.1146/annurev.bi.65.070196.002355.

14. Buckley CD, Tan J, Anderson KL, Hanein D, Volkmann N, Weis WI, Nelson WJ, Dunn AR. Cell adhesion. The minimal cadherin-catenin complex binds to actin filaments under force. Science. 2014;346(6209):1254211. Epub 2014/11/02. doi: 10.1126/science.1254211. PubMed PMID: 25359979; PMCID: PMC4364042.

15. Kowalczyk AP, Green KJ. Structure, function, and regulation of desmosomes. Prog Mol Biol Transl Sci. 2013;116:95-118. Epub 2013/03/14. doi: 10.1016/B978-0-12-394311-8.00005-4. PubMed PMID: 23481192; PMCID: PMC4336551.

16. Getsios S, Amargo EV, Dusek RL, Ishii K, Sheu L, Godsel LM, Green KJ. Coordinated expression of desmoglein 1 and desmocollin 1 regulates intercellular adhesion. Differentiation. 2004;72:419-33.

17. Nie Z, Merritt A, Rouhi-Parkouhi M, Tabernero L, Garrod D. Membrane-impermeable cross-linking provides evidence for homophilic, isoform-specific binding of desmosomal cadherins in epithelial cells. J Biol Chem. 2011;286(3):2143-54. Epub 2010/11/26. doi: 10.1074/jbc.M110.192245. PubMed PMID: 21098030; PMCID: PMC3023511.

18. Harrison OJ, Brasch J, Lasso G, Katsamba PS, Ahlsen G, Honig B, Shapiro L. Structural basis of adhesive binding by desmocollins and desmogleins. Proc Natl Acad Sci U S A. 2016;113(26):7160-5. Epub 2016/06/15. doi: 10.1073/pnas.1606272113. PubMed PMID: 27298358; PMCID: PMC4932976.

19. Chitaev NA, Troyanovsky SM. Direct Ca2+-dependent heterophilic interaction between desmosomal cadherins, desmoglein and desmocollin, contributes to cell-cell adhesion. The Journal of Cell Biology. 1997;138(1):193-201.

20. Schafer S, Koch PJ, Frank WW. Identification of the ubiquitous human desmoglein, Dsg2, and the expression catalogue of the dsg subfamily of desmosomal cadherins. Experimental Cell Research. 1994;211:391-9.

21. Troyanovsky SM, Troyanovsky RB, Eshkind LG, Leube RE, Franke WW. Identification of amino acid sequence motifs in desmocollin, a desmosomal glycoprotein, that are required for plakoglobin binding and plaque formation. Proc Natl Acad Sci U S A. 1994;91:10790-4.

22. Troyanovsky SM, Troyanovsky RB, Eshkind LG, Krutovskikh VA, Leube RE, Franke WW. Identification of the plakoglobin-binding domain in desmoglein and its role in plaque

assembly and intermediate filament anchorage. J Cell Biol. 1994;127(1):151-60. Epub 1994/10/01. doi: 10.1083/jcb.127.1.151. PubMed PMID: 7929560; PMCID: PMC2120186.

23. Mathur M, Goodwin L, Cowin P. Interactions of the cytoplasmic domain of the desmosomal cadherin Dsg1 with plakoglobin. The Journal of Biological Chemistry. 1994;269(19):14075-80.

24. Nilles LA, Parry DAD, Powers EE, Angst BD, Wagner RM, Green KJ. Structural analysis and expression of human desmoglein: a cadherin-like component of the desmosome. Journal of Cell Science. 1991;99:809-21.

25. Chen J, Nekrasova OE, Patel DM, Klessner JL, Godsel LM, Koetsier JL, Amargo EV, Desai BV, Green KJ. The C-terminal unique region of desmoglein 2 inhibits its internalization via tail-tail interactions. J Cell Biol. 2012;199(4):699-711. Epub 2012/11/07. doi: 10.1083/jcb.201202105. PubMed PMID: 23128240; PMCID: PMC3494854.

26. Rutman AJ, Buxton RS, Burdett IDJ. Visualisation by electron microscopy of the unique part of the cytoplasmic domain of desmoglein, a cadherin-like protein of the desmosome type of cell junction. FEBS Letters. 1994;353:194-6.

27. Samuelov L, Sarig O, Harmon RM, Rapaport D, Ishida-Yamamoto A, Isakov O, Koetsier JL, Gat A, Goldberg I, Bergman R, Spiegel R, Eytan O, Geller S, Peleg S, Shomron N, Goh CSM, Wilson NJ, Smith FJD, Pohler E, Simpson MA, McLean WHI, Irvine AD, Horowitz M, McGrath JA, Green KJ, Sprecher E. Desmoglein 1 deficiency results in severe dermatitis, multiple allergies and metabolic wasting. Nat Genet. 2013;45(10):1244-8. Epub 2013/08/27. doi: 10.1038/ng.2739. PubMed PMID: 23974871; PMCID: PMC3791825.

28. Elsholz F, Harteneck C, Muller W, Friedland K. Calcium--a central regulator of keratinocyte differentiation in health and disease. Eur J Dermatol. 2014;24(6):650-61. Epub 2014/12/17. doi: 10.1684/ejd.2014.2452. PubMed PMID: 25514792.

29. Brennan D, Hu Y, Joubeh S, Choi YW, Whitaker-Menezes D, O'Brien T, Uitto J, Rodeck U, Mahoney MG. Suprabasal Dsg2 expression in transgenic mouse skin confers a hyperproliferative and apoptosis-resistant phenotype to keratinocytes. J Cell Sci. 2007;120(Pt 5):758-71. Epub 2007/02/08. doi: 10.1242/jcs.03392. PubMed PMID: 17284515.

30. Delva E, Tucker DK, Kowalczyk AP. The desmosome. Cold Spring Harb Perspect Biol. 2009;1(2):a002543. Epub 2010/01/13. doi: 10.1101/cshperspect.a002543. PubMed PMID: 20066089; PMCID: PMC2742091.

31. Getsios S, Simpson CL, Kojima S, Harmon R, Sheu LJ, Dusek RL, Cornwell M, Green KJ. Desmoglein 1-dependent suppression of EGFR signaling promotes epidermal differentiation and morphogenesis. J Cell Biol. 2009;185(7):1243-58. Epub 2009/06/24. doi: 10.1083/jcb.200809044. PubMed PMID: 19546243; PMCID: PMC2712955.

32. Harmon RM, Simpson CL, Johnson JL, Koetsier JL, Dubash AD, Najor NA, Sarig O, Sprecher E, Green KJ. Desmoglein-1/Erbin interaction suppresses ERK activation to support

epidermal differentiation. J Clin Invest. 2013;123(4):1556-70. Epub 2013/03/26. doi: 10.1172/JCI65220. PubMed PMID: 23524970; PMCID: PMC3613912.

33. Franke WW, Borrmann CM, Grund C, Pieperhoff S. The area composita of adhering junctions connecting heart muscle cells of vertebrates. I. Molecular definition in intercalated disks of cardiomyocytes by immunoelectron microscopy of desmosomal proteins. Eur J Cell Biol. 2006;85(2):69-82. Epub 2006/01/13. doi: 10.1016/j.ejcb.2005.11.003. PubMed PMID: 16406610.

34. Vermij SH, Abriel H, van Veen TA. Refining the molecular organization of the cardiac intercalated disc. Cardiovasc Res. 2017;113(3):259-75. Epub 2017/01/11. doi: 10.1093/cvr/cvw259. PubMed PMID: 28069669.

35. Ohno S. The genetic background of arrhythmogenic right ventricular cardiomyopathy. J Arrhythm. 2016;32(5):398-403. Epub 2016/10/21. doi: 10.1016/j.joa.2016.01.006. PubMed PMID: 27761164; PMCID: PMC5063271.

36. Stahley SN, Kowalczyk AP. Desmosomes in acquired disease. Cell Tissue Res. 2015;360(3):439-56. Epub 2015/03/22. doi: 10.1007/s00441-015-2155-2. PubMed PMID: 25795143; PMCID: PMC4456195.

37. Kugelmann D, Radeva MY, Spindler V, Waschke J. Desmoglein 1 Deficiency Causes Lethal Skin Blistering. J Invest Dermatol. 2019;139(7):1596-9 e2. Epub 2019/01/21. doi: 10.1016/j.jid.2019.01.002. PubMed PMID: 30660666.

38. Eshkind L, Tian Q, Schmidt A, Franke WW, Windoffer R, Leube RE. Loss of desmoglein 2 suggests essential functions for early embryonic development and proliferation of embryonal stem cells. Eur J Cell Biol. 2002;81(11):592-8. Epub 2002/12/24. doi: 10.1078/0171-9335-00278. PubMed PMID: 12494996.

39. Koch PJ, Mahoney MG, Ishikawa H, Pulkkinen L, Uitto J, Shultz L, Murphy GF, Whitaker-Menezes D, Stanley JR. Targeted disruption of the Pemphigus Vulgaris antigen (desmoglein 3) gene in mice causes loss of keratinocyte cell adhesion with a phenotype similar to Pemphigus Vulgaris. The Journal of Cell Biology. 1997;137(5):1091-102. doi: 10.1083/jcb.137.5.1091.

40. Merritt AJ, Berika MY, Zhai W, Kirk SE, Ji B, Hardman MJ, Garrod DR. Suprabasal desmoglein 3 expression in the epidermis of transgenic mice results in hyperproliferation and abnormal differentiation. Mol Cell Biol. 2002;22(16):5846-58. Epub 2002/07/26. doi: 10.1128/mcb.22.16.5846-5858.2002. PubMed PMID: 12138195; PMCID: PMC133994.

41. Chidgey M, Brakebusch C, Gustafsson E, Cruchley A, Hail C, Kirk S, Merritt A, North A, Tselepis C, Hewitt J, Byrne C, Fassler R, Garrod D. Mice lacking desmocollin 1 show epidermal fragility accompanied by barrier defects and abnormal differentiation. J Cell Biol. 2001;155(5):821-32. Epub 2001/11/21. doi: 10.1083/jcb.200105009. PubMed PMID: 11714727; PMCID: PMC2150874.

42. Den Z, Cheng X, Merched-Sauvage M, Koch PJ. Desmocollin 3 is required for pre-implantation development of the mouse embryo. J Cell Sci. 2006;119(Pt 3):482-9. Epub 2006/01/19. doi: 10.1242/jcs.02769. PubMed PMID: 16418220.

43. Chen J, Den Z, Koch PJ. Loss of desmocollin 3 in mice leads to epidermal blistering. J Cell Sci. 2008;121(Pt 17):2844-9. Epub 2008/08/07. doi: 10.1242/jcs.031518. PubMed PMID: 18682494; PMCID: PMC2659849.

44. Hardman MJ, Liu K, Avilion AA, Merritt A, Brennan K, Garrod DR, Byrne C. Desmosomal cadherin misexpression alters beta-catenin stability and epidermal differentiation. Mol Cell Biol. 2005;25(3):969-78. Epub 2005/01/20. doi: 10.1128/MCB.25.3.969-978.2005. PubMed PMID: 15657425; PMCID: PMC544013.

45. Bierkamp C, McLaughlin KJ, Schwarz H, Huber O, Kemler R. Embryonic heart and skin defects in mice lacking plakoglobin. Developmental Biology. 1996;180:780-5. doi: 10.1006/dbio.1996.0346.

46. Rietscher K, Wolf A, Hause G, Rother A, Keil R, Magin TM, Glass M, Niessen CM, Hatzfeld M. Growth Retardation, Loss of Desmosomal Adhesion, and Impaired Tight Junction Function Identify a Unique Role of Plakophilin 1 In Vivo. J Invest Dermatol. 2016;136(7):1471-8. Epub 2016/04/02. doi: 10.1016/j.jid.2016.03.021. PubMed PMID: 27033150.

47. Gallicano GI, Kouklis P, Bauer C, Yin M, Vasioukhin V, Degenstein L, Fuchs E. Desmoplakin is required early in development for assembly of desmosomes and cytoskeletal linkage. The Journal of Cell Biology. 1998;143(7):2009-22. doi: 10.1083/jcb.143.7.2009.

48. Vasioukhin V, Bowers E, Bauer C, Degenstein L, Fuchs E. Desmoplakin is essential in epidermal sheet formation. Nature Cell Biology. 2001;3:1076-85. doi: 10.1038/ncb1201-1076.

49. Resnik N, Sepcic K, Plemenitas A, Windoffer R, Leube R, Veranic P. Desmosome assembly and cell-cell adhesion are membrane raft-dependent processes. J Biol Chem. 2011;286(2):1499-507. Epub 2010/11/13. doi: 10.1074/jbc.M110.189464. PubMed PMID: 21071449; PMCID: PMC3020758.

50. Stahley SN, Saito M, Faundez V, Koval M, Mattheyses AL, Kowalczyk AP. Desmosome assembly and disassembly are membrane raft-dependent. PLoS One. 2014;9(1):e87809. Epub 2014/02/06. doi: 10.1371/journal.pone.0087809. PubMed PMID: 24498201; PMCID: PMC3907498.

51. Vielmuth F, Waschke J, Spindler V. Loss of Desmoglein Binding Is Not Sufficient for Keratinocyte Dissociation in Pemphigus. J Invest Dermatol. 2015;135(12):3068-77. Epub 2015/08/20. doi: 10.1038/jid.2015.324. PubMed PMID: 26288352.

52. Skerrow CJ, Matoltsy AG. Chemical characterization of isolated epidermal desmosomes. Journal of Cell Biology. 1974;63:524-30.

53. Drochmans P, Freudenstein C, Wanson J-C, Laurent L, Keenan TW, Stadler J, Leloup R, Franke WW. Structure and biochemical composition of desmosomes and tonofilaments isolated from calf muzzle epidermis. Journal of Cell Biology. 1978;79:427-43.

54. Nava P, Laukoetter MG, Hopkins AM, Laur O, Gerner-Smidt K, Green KJ, Parkos CA, Nusrat A. Desmoglein-2: a novel regulator of apoptosis in the intestinal epithelium. Mol Biol Cell. 2007;18(11):4565-78. Epub 2007/09/07. doi: 10.1091/mbc.e07-05-0426. PubMed PMID: 17804817; PMCID: PMC2043542.

55. Resnik N, de Luca GMR, Sepcic K, Romih R, Manders E, Veranic P. Depletion of the cellular cholesterol content reduces the dynamics of desmosomal cadherins and interferes with desmosomal strength. Histochem Cell Biol. 2019. Epub 2019/06/11. doi: 10.1007/s00418-019-01797-1. PubMed PMID: 31179519.

56. Vollner F, Ali J, Kurrle N, Exner Y, Eming R, Hertl M, Banning A, Tikkanen R. Loss of flotillin expression results in weakened desmosomal adhesion and Pemphigus vulgaris-like localisation of desmoglein-3 in human keratinocytes. Sci Rep. 2016;6:28820. Epub 2016/06/28. doi: 10.1038/srep28820. PubMed PMID: 27346727; PMCID: PMC4922016.

57. Lewis BA, Engelman DM. Lipid bilayer thickness varies linearly with acyl chain length in fluid phosphatidylcholine vesicles. Journal of Molecular Biology. 1983;166:211-7.

58. Nezil FA, Bloom M. Combined influence of cholesterol and synthetic amphiphillic peptides upon bilayer thickness in model membranes. Biophys J. 1992;61:1176-83.

59. Kucerka N, Perlmutter JD, Pan J, Tristram-Nagle S, Katsaras J, Sachs JN. The effect of cholesterol on short- and long-chain monounsaturated lipid bilayers as determined by molecular dynamics simulations and X-ray scattering. Biophys J. 2008;95(6):2792-805. Epub 2008/06/03. doi: 10.1529/biophysj.107.122465. PubMed PMID: 18515383; PMCID: PMC2527263.

60. Niemela PS, Ollila S, Hyvönen MT, Karttunen M, Vattulainen I. Assessing the Nature of Lipid Raft Membranes. PLoS Computational Biology. 2005;preprint(2007). doi: 10.1371/journal.pcbi.0030034.eor.

61. Molugu TR, Brown MF. Cholesterol-induced suppression of membrane elastic fluctuations at the atomistic level. Chem Phys Lipids. 2016;199:39-51. Epub 2016/05/08. doi: 10.1016/j.chemphyslip.2016.05.001. PubMed PMID: 27154600; PMCID: PMC5310939.

62. Hedger G, Sansom MSP. Lipid interaction sites on channels, transporters and receptors: Recent insights from molecular dynamics simulations. Biochim Biophys Acta. 2016;1858(10):2390-400. Epub 2016/03/08. doi: 10.1016/j.bbamem.2016.02.037. PubMed PMID: 26946244; PMCID: PMC5589069.

63. Hulce JJ, Cognetta AB, Niphakis MJ, Tully SE, Cravatt BF. Proteome-wide mapping of cholesterol-interacting proteins in mammalian cells. Nat Methods. 2013;10(3):259-64. Epub 2013/02/12. doi: 10.1038/nmeth.2368. PubMed PMID: 23396283; PMCID: PMC3601559.

64. Diaz-Rohrer BB, Levental KR, Simons K, Levental I. Membrane raft association is a determinant of plasma membrane localization. Proc Natl Acad Sci U S A. 2014;111(23):8500-5. doi: 10.1073/pnas.1404582111. PubMed PMID: 24912166; PMCID: PMC4060687.

65. Lorent JH, Diaz-Rohrer B, Lin X, Spring K, Gorfe AA, Levental KR, Levental I. Structural determinants and functional consequences of protein affinity for membrane rafts. Nat Commun. 2017;8(1):1219. Epub 2017/11/02. doi: 10.1038/s41467-017-01328-3. PubMed PMID: 29089556; PMCID: PMC5663905.

66. Levental I, Lingwood D, Grzybek M, Coskun U, Simons K. Palmitoylation regulates raft affinity for the majority of integral raft proteins. Proc Natl Acad Sci U S A. 2010;107(51):22050-4. Epub 2010/12/07. doi: 10.1073/pnas.1016184107. PubMed PMID: 21131568; PMCID: PMC3009825.

67. Bretscher MS, Munro S. Cholesterol and the Golgi apparatus. Science. 1993;261:1280-1. doi: 10.1126/science.8362242.

68. Sharpe HJ, Stevens TJ, Munro S. A comprehensive comparison of transmembrane domains reveals organelle-specific properties. Cell. 2010;142(1):158-69. Epub 2010/07/07. doi: 10.1016/j.cell.2010.05.037. PubMed PMID: 20603021; PMCID: PMC2928124.

69. Mouritsen OG, Bloom M. Mattress model of lipid-protein interactions in membranes. Biophys J. 1984;46:141-53.

70. Lin Q, London E. Altering hydrophobic sequence lengths shows that hydrophobic mismatch controls affinity for ordered lipid domains (rafts) in the multitransmembrane strand protein perfringolysin O. J Biol Chem. 2013;288(2):1340-52. Epub 2012/11/15. doi: 10.1074/jbc.M112.415596. PubMed PMID: 23150664; PMCID: PMC3543017.

71. Yuan Z, Zhang F, Davis MJ, Boden M, Teasdale RD. Predicting the solvent accessibility of transmembrane residues from protein sequence. Journal of Proteome Research. 2006;5(5):1063-70. doi: 10.1021/pr050397b.

72. Xu L, Hu T-T, Luo S-Z. Leucine Zipper Motif Drives the Transmembrane Domain Dimerization of E-cadherin. International Journal of Peptide Research and Therapeutics. 2013;20(1):95-102. doi: 10.1007/s10989-013-9371-y.

73. Blaskovic S, Blanc M, van der Goot FG. What does S-palmitoylation do to membrane proteins? FEBS Journal. 2013;280(12):2766-74. doi: 10.1111/febs.12263.

74. Rocks O, Peyker A, Kahm M, Verveer PJ, Koerner C, Lumbierres M, Kuhlmann J, Waldmann H, Wittinghofer A, Bastiaens PIH. An acylation cycle regulates localization and activity of palmitoylated Ras forms. Science. 2005;307:1746-52. doi: 10.1594/PANGAEA.58229.

75. El-Husseini AE-D, Schnell E, Dakoji S, Sweeney N, Zhou Q, Prange O, Gauthier-Campbell C, Aguilera-Moreno A, Nicoll RA, Bredt DS. Synaptic strength regulated by palmitate cycling on PSD-95. Cell. 2002;108:849-63.

76. Roberts BJ, Svoboda RA, Overmiller AM, Lewis JD, Kowalczyk AP, Mahoney MG, Johnson KR, Wahl JK, 3rd. Palmitoylation of Desmoglein 2 Is a Regulator of Assembly Dynamics and Protein Turnover. J Biol Chem. 2016;291(48):24857-65. Epub 2016/10/21. doi: 10.1074/jbc.M116.739458. PubMed PMID: 27703000; PMCID: PMC5122758.

77. Fukata M, Fukata Y, Adesnik H, Nicoll RA, Bredt DS. Identification of PSD-95 palmitoylating enzymes. Neuron. 2004;44(6):987-96. Epub 2004/12/18. doi: 10.1016/j.neuron.2004.12.005. PubMed PMID: 15603741.

78. Ohno Y, Kihara A, Sano T, Igarashi Y. Intracellular localization and tissue-specific distribution of human and yeast DHHC cysteine-rich domain-containing proteins. Biochim Biophys Acta. 2006;1761(4):474-83. Epub 2006/05/02. doi: 10.1016/j.bbalip.2006.03.010. PubMed PMID: 16647879.

79. Philippe JM, Jenkins PM. Spatial organization of palmitoyl acyl transferases governs substrate localization and function. Mol Membr Biol. 2019;35(1):60-75. Epub 2020/01/24. doi: 10.1080/09687688.2019.1710274. PubMed PMID: 31969037; PMCID: PMC7031816.

80. Mill P, Lee AW, Fukata Y, Tsutsumi R, Fukata M, Keighren M, Porter RM, McKie L, Smyth I, Jackson IJ. Palmitoylation regulates epidermal homeostasis and hair follicle differentiation. PLoS Genet. 2009;5(11):e1000748. Epub 2009/12/04. doi: 10.1371/journal.pgen.1000748. PubMed PMID: 19956733; PMCID: PMC2776530.

81. Perez CJ, Mecklenburg L, Jaubert J, Martinez-Santamaria L, Iritani BM, Espejo A, Napoli E, Song G, Del Rio M, DiGiovanni J, Giulivi C, Bedford MT, Dent SYR, Wood RD, Kusewitt DF, Guenet JL, Conti CJ, Benavides F. Increased Susceptibility to Skin Carcinogenesis Associated with a Spontaneous Mouse Mutation in the Palmitoyl Transferase Zdhhc13 Gene. J Invest Dermatol. 2015;135(12):3133-43. Epub 2015/08/20. doi: 10.1038/jid.2015.314. PubMed PMID: 26288350; PMCID: PMC4898190.

82. Chen LY, Lin KR, Chen YJ, Chiang YJ, Ho KC, Shen LF, Song IW, Liu KM, Yang-Yen HF, Chen YJ, Chen YT, Liu FT, Yen JJY. Palmitoyl acyltransferase activity of ZDHHC13 regulates skin barrier development partly by controlling PADi3 and TGM1 protein stability. J Invest Dermatol. 2019. Epub 2019/11/02. doi: 10.1016/j.jid.2019.09.017. PubMed PMID: 31669413.

83. Bornslaeger EA, Godsel LM, Corcoran CM, Park JK, Hatzfeld M, Kowalczyk AP, Green KJ. Plakophilin-1 interferes with plakoglobin binding to desmoplakin, yet together with plakoglobin promotes clustering of desmosomal plaque complexes at cell-cell borders. Journal of Cell Science. 2001;114:727-38.

84. Sobolik-Delmaire T, Katafiasz D, Wahl JK, 3rd. Carboxyl terminus of Plakophilin-1 recruits it to plasma membrane, whereas amino terminus recruits desmoplakin and promotes desmosome assembly. J Biol Chem. 2006;281(25):16962-70. Epub 2006/04/25. doi: 10.1074/jbc.M600570200. PubMed PMID: 16632867.

85. Godsel LM, Hsieh SN, Amargo EV, Bass AE, Pascoe-McGillicuddy LT, Huen AC, Thorne ME, Gaudry CA, Park JK, Myung K, Goldman RD, Chew TL, Green KJ. Desmoplakin

assembly dynamics in four dimensions: multiple phases differentially regulated by intermediate filaments and actin. J Cell Biol. 2005;171(6):1045-59. Epub 2005/12/21. doi: 10.1083/jcb.200510038. PubMed PMID: 16365169; PMCID: PMC2171300.

86. Fuchs M, Foresti M, Radeva MY, Kugelmann D, Keil R, Hatzfeld M, Spindler V, Waschke J, Vielmuth F. Plakophilin 1 but not plakophilin 3 regulates desmoglein clustering. Cell Mol Life Sci. 2019. Epub 2019/04/06. doi: 10.1007/s00018-019-03083-8. PubMed PMID: 30949721.

87. McGrath JA, McMillan JR, Shemanko CS, Runswick SK, Leigh IM, Lane EB, Garrod DR, Eady RAJ. Mutations in the plakophilin 1 gene result in ectodermal dysplasia/skin fragility syndrome. Nature Genetics. 1997;17:240-4.

88. South AP, Wan H, Stone MG, Dopping-Hepenstal PJ, Purkis PE, Marshall JF, Leigh IM, Eady RA, Hart IR, McGrath JA. Lack of plakophilin 1 increases keratinocyte migration and reduces desmosome stability. J Cell Sci. 2003;116(Pt 16):3303-14. Epub 2003/07/04. doi: 10.1242/jcs.00636. PubMed PMID: 12840072.

89. Tucker DK, Stahley SN, Kowalczyk AP. Plakophilin-1 protects keratinocytes from pemphigus vulgaris IgG by forming calcium-independent desmosomes. J Invest Dermatol. 2014;134(4):1033-43. Epub 2013/09/24. doi: 10.1038/jid.2013.401. PubMed PMID: 24056861; PMCID: PMC3961504.

90. Gurjar M, Raychaudhuri K, Mahadik S, Reddy D, Atak A, Shetty T, Rao K, Karkhanis MS, Gosavi P, Sehgal L, Gupta S, Dalal SN. Plakophilin3 increases desmosome assembly, size and stability by increasing expression of desmocollin2. Biochem Biophys Res Commun. 2018;495(1):768-74. Epub 2017/11/18. doi: 10.1016/j.bbrc.2017.11.085. PubMed PMID: 29146182.

91. Simons K, Ehehalt R. Cholesterol, lipid rafts, and disease. Journal of Clinical Investigation. 2002;110(5):597-603. doi: 10.1172/jci0216390.

92. Saaf AM, Tengvall-Linder M, Chang HY, Adler AS, Wahlgren CF, Scheynius A, Nordenskjold M, Bradley M. Global expression profiling in atopic eczema reveals reciprocal expression of inflammatory and lipid genes. PLoS One. 2008;3(12):e4017. Epub 2008/12/25. doi: 10.1371/journal.pone.0004017. PubMed PMID: 19107207; PMCID: PMC2603322.

93. Mathay C, Pierre M, Pittelkow MR, Depiereux E, Nikkels AF, Colige A, Poumay Y. Transcriptional Profiling after Lipid Raft Disruption in Keratinocytes Identifies Critical Mediators of Atopic Dermatitis Pathways. Journal of Investigative Dermatology. 2011;131(1):46-58. doi: 10.1038/jid.2010.272.

94. Eggers SD, Keswani SC, Melli G, Cornblath DR. Clinical and genetic description of a family with Charcot-Marie-Tooth disease type 1B from a transmembrane MPZ mutation. Muscle Nerve. 2004;29(6):867-9. Epub 2004/06/02. doi: 10.1002/mus.20034. PubMed PMID: 15170620.

95. Plotkowski ML KS, Phillips ML, Partridge AW, Deber CM, Bowie JU. Transmembrane domain of myelin protein zero can form dimers- possible implications for myelin construction. Biochemistry. 2007;46(43):12164-73. doi: 10.1021/bi701066h. PubMed PMID: 17915947.

96. Han X, Mihailescu M, Hristova K. Neutron diffraction studies of fluid bilayers with transmembrane proteins: structural consequences of the achondroplasia mutation. Biophys J. 2006;91(10):3736-47. Epub 2006/09/05. doi: 10.1529/biophysj.106.092247. PubMed PMID: 16950849; PMCID: PMC1630470.

97. Arielly SS, Ariel M, Yehuda R, Scigelova M, Yehezkel G, Khalaila I. Quantitative analysis of caveolin-rich lipid raft proteins from primary and metastatic colorectal cancer clones. J Proteomics. 2012;75(9):2629-37. Epub 2012/04/10. doi: 10.1016/j.jprot.2012.03.011. PubMed PMID: 22484058.

98. Staubach S, Muller S, Pekmez M, Hanisch FG. Classical Galactosemia: Insight into Molecular Pathomechanisms by Differential Membrane Proteomics of Fibroblasts under Galactose Stress. J Proteome Res. 2017;16(2):516-27. Epub 2017/01/12. doi: 10.1021/acs.jproteome.6b00658. PubMed PMID: 28075131.

99. Erne B, Sansano S, Frank M, Schaeren-Wiemers N. Rafts in adult peripheral nerve myelin contain major structural myelin proteins and myelin and lymphocyte protein (MAL) and CD59 as specific markers. Journal of Neurochemistry. 2002;82:550-62.

100. Fasano A, Amoresano A, Rossano R, Carlone G, Carpentieri A, Liuzzi GM, Pucci P, Riccio P. The different forms of PNS myelin P0 protein within and outside lipid rafts. J Neurochem. 2008;107(1):291-301. Epub 2008/08/06. doi: 10.1111/j.1471-4159.2008.05598.x. PubMed PMID: 18680558.

101. Harder T, Scheiffele P, Verkade P, Simons K. Lipid domain structure of the plasma membrane revealed by patching of membrane components. The Journal of Cell Biology. 1998;141(4):929-42.

102. Gumbiner B, Stevenson B, Grimaldi A. The role of the cell adhesion molecule uvomorulin in the formation and maintenance of the epithelial junctional complex. The Journal of Cell Biology. 1988;107:1575-87. doi: 10.1083/jcb.107.4.1575.

103. Watabe-Uchida M, Uchida N, Imamura Y, Nagafuchi A, Fujimoto K, Uemura T, Vermeulen S, Roy Fv, Adamson ED, Takeichi M. alpha-catenin-vinculin interaction functions to organize the apical junctional complex in epithelial cells. The Journal of Cell Biology. 1998;142(3). doi: 10.1083/jcb.142.3.847.

104. Lewis JE, Jensen PJ, Wheelock MJ. Cadherin Function Is Required for Human Keratinocytes to Assemble Desmosomes and Stratify in Response to Calcium. Journal of Investigative Dermatology. 1994;102(6):870-7. doi: 10.1111/1523-1747.ep12382690.

105. Vasioukhin V, Bauer C, Degenstein L, Wise B, Fuchs E. Hyperproliferation and defects in epithelial polarity upon conditional ablation of a-catenin in skin. Cell. 2001;104:605-17.

106. Choi HJ, Gross JC, Pokutta S, Weis WI. Interactions of plakoglobin and beta-catenin with desmosomal cadherins: basis of selective exclusion of alpha- and beta-catenin from desmosomes. J Biol Chem. 2009;284(46):31776-88. Epub 2009/09/18. doi: 10.1074/jbc.M109.047928. PubMed PMID: 19759396; PMCID: PMC2797248.

107. Shafraz O, Rubsam M, Stahley SN, Caldara AL, Kowalczyk AP, Niessen CM, Sivasankar S. E-cadherin binds to desmoglein to facilitate desmosome assembly. Elife. 2018;7. Epub 2018/07/13. doi: 10.7554/eLife.37629. PubMed PMID: 29999492; PMCID: PMC6066328.

108. Lowndes M, Rakshit S, Shafraz O, Borghi N, Harmon RM, Green KJ, Sivasankar S, Nelson WJ. Different roles of cadherins in the assembly and structural integrity of the desmosome complex. J Cell Sci. 2014;127(Pt 10):2339-50. Epub 2014/03/13. doi: 10.1242/jcs.146316. PubMed PMID: 24610950; PMCID: PMC4021477.

109. Burdett ID, Sullivan KH. Desmosome assembly in MDCK cells: transport of precursors to the cell surface occurs by two phases of vesicular traffic and involves major changes in centrosome and Golgi location during a Ca(2+) shift. Exp Cell Res. 2002;276(2):296-309. Epub 2002/05/25. doi: 10.1006/excr.2002.5509. PubMed PMID: 12027459.

110. Ruiz P, Brinkmann V, Ledermann B, Behrend M, Grund C, Thalhammer C, Vogel F, Birchmeier C, Gunthert U, Franke WW, Birchmeier W. Targeted mutation of PG in mice reveals essential functions of desmosomes in the embryonic heart. The Journal of Cell Biology. 1996;135(1):215-25.

111. Kowalczyk AP, Palka HL, Luu HH, Nilles LA, Anderson JE, Wheelock MJ, Green KJ. Posttranslational regulation of plakoglobin expression: influence of the desmosomal cadherins on plakoglobin metabolic stability. The Journal of Biological Chemistry. 1994;269(49):31214-23.

112. Roberts BJ, Johnson KE, McGuinn KP, Saowapa J, Svoboda RA, Mahoney MG, Johnson KR, Wahl JK, 3rd. Palmitoylation of plakophilin is required for desmosome assembly. J Cell Sci. 2014;127(Pt 17):3782-93. Epub 2014/07/09. doi: 10.1242/jcs.149849. PubMed PMID: 25002405; PMCID: PMC4150063.

113. Kljuic A, Bazzi H, Sundberg JP, Martinez-Mir A, O'Shaughnessy R, Mahoney MG, Moise Levy, Montagutelli X, Ahmad W, Aita VM, Gordon D, Uitto J, Whiting D, Ott J, Fischer S, Gilliam TC, Jahoda CAB, Morris RJ, Panteleyev AA, Nguyen VT, Christiano AM. Desmoglein 4 in hair follicle differentiation and epidermal adhesion: evidence from inherited hypotrichosis and acquired pemphigus vulgaris. Cell. 2003;113:249-60.

114. Bornsleager EA, Corcoran CM, Stappenbeck TS, Green KJ. Breaking the Connection: Displacement of the Desmosomal Plaque Protein Desmoplakin from Cell-Cell Interfaces Disrupts Anchorage of Intermediate Filament Bundles and Alters Intercellular Junction Assembly. The Journal of Cell Biology. 1996;134(4):985-1001.

115. Setzer SV, Calkins CC, Garner J, Summers S, Green KJ, Kowalczyk AP. Comparative analysis of armadillo family proteins in the regulation of a431 epithelial cell junction assembly, adhesion and migration. J Invest Dermatol. 2004;123(3):426-33. Epub 2004/08/12. doi: 10.1111/j.0022-202X.2004.23319.x. PubMed PMID: 15304078.

116. Boukamp P, Petrussevska RT, Breitkreutz D, Hornung J, Markham A, Fusenig NE. Normal keratinization in a spontaneously immortalized aneuploid human keratinocyte cell line. The Journal of Cell Biology. 1988;106:761-71.

117. Pokutta S, Weis WI. Structure and mechanism of cadherins and catenins in cell-cell contacts. Annu Rev Cell Dev Biol. 2007;23:237-61. Epub 2007/06/02. doi: 10.1146/annurev.cellbio.22.010305.104241. PubMed PMID: 17539752.

118. Lingwood D, Simons K. Detergent resistance as a tool in membrane research. Nat Protoc. 2007;2(9):2159-65. Epub 2007/09/15. doi: 10.1038/nprot.2007.294. PubMed PMID: 17853872.

119. Huen AC, Park JK, Godsel LM, Chen X, Bannon LJ, Amargo EV, Hudson TY, Mongiu AK, Leigh IM, Kelsell DP, Gumbiner BM, Green KJ. Intermediate filament-membrane attachments function synergistically with actin-dependent contacts to regulate intercellular adhesive strength. J Cell Biol. 2002;159(6):1005-17. Epub 2002/12/25. doi: 10.1083/jcb.200206098. PubMed PMID: 12499357; PMCID: PMC2173978.

120. Hartlieb E, Rotzer V, Radeva M, Spindler V, Waschke J. Desmoglein 2 compensates for desmoglein 3 but does not control cell adhesion via regulation of p38 mitogen-activated protein kinase in keratinocytes. J Biol Chem. 2014;289(24):17043-53. Epub 2014/05/02. doi: 10.1074/jbc.M113.489336. PubMed PMID: 24782306; PMCID: PMC4059146.

121. Walter E, Vielmuth F, Wanuske MT, Seifert M, Pollmann R, Eming R, Waschke J. Role of Dsg1- and Dsg3-Mediated Signaling in Pemphigus Autoantibody-Induced Loss of Keratinocyte Cohesion. Front Immunol. 2019;10:1128. Epub 2019/06/11. doi: 10.3389/fimmu.2019.01128. PubMed PMID: 31178865; PMCID: PMC6543754.

122. Wanuske MT, Brantschen D, Schinner C, Studle C, Walter E, Hiermaier M, Vielmuth F, Waschke J, Spindler V. Clustering of desmosomal cadherins by desmoplakin is essential for cell-cell adhesion. Acta Physiol (Oxf). 2021;231(4):e13609. Epub 2020/12/24. doi: 10.1111/apha.13609. PubMed PMID: 33354837.

123. Baddam SR, Arsenovic PT, Narayanan V, Duggan NR, Mayer CR, Newman ST, Abutaleb DA, Mohan A, Kowalczyk AP, Conway DE. The Desmosomal Cadherin Desmoglein-2 Experiences Mechanical Tension as Demonstrated by a FRET-Based Tension Biosensor Expressed in Living Cells. Cells. 2018;7(7). Epub 2018/06/29. doi: 10.3390/cells7070066. PubMed PMID: 29949915; PMCID: PMC6070948.

124. Bruce MA, Butte MJ. Real-time GPU-based 3D Deconvolution. Optics Express. 2013;21:4766-73.

125. Zimmer SE, Kowalczyk AP. The desmosome as a model for lipid raft driven membrane domain organization. Biochim Biophys Acta Biomembr. 2020;1862(9):183329. Epub 2020/05/08. doi: 10.1016/j.bbamem.2020.183329. PubMed PMID: 32376221.

126. Broussard JA, Jaiganesh A, Zarkoob H, Conway DE, Dunn AR, Espinosa HD, Janmey PA, Green KJ. Scaling up single-cell mechanics to multicellular tissues - the role of the

intermediate filament-desmosome network. J Cell Sci. 2020;133(6). Epub 2020/03/18. doi: 10.1242/jcs.228031. PubMed PMID: 32179593; PMCID: PMC7097224.

127. Brooke MA, Nitoiu D, Kelsell DP. Cell-cell connectivity: desmosomes and disease. J Pathol. 2012;226(2):158-71. Epub 2011/10/13. doi: 10.1002/path.3027. PubMed PMID: 21989576.

128. Nitoiu D, Etheridge SL, Kelsell DP. Insights into Desmosome Biology from Inherited Human Skin Disease and Cardiocutaneous Syndromes. Cell Communication & Adhesion. 2014;21(3):129-40. doi: 10.3109/15419061.2014.908854.

129. Samuelov L, Sprecher E. Inherited desmosomal disorders. Cell and Tissue Research. 2014;360(3):457-75. doi: 10.1007/s00441-014-2062-y.

130. Lee JYW, McGrath JA. Mutations in genes encoding desmosomal proteins: spectrum of cutaneous and extracutaneous abnormalities. Br J Dermatol. 2020. Epub 2020/06/28. doi: 10.1111/bjd.19342. PubMed PMID: 32593191.

131. Hennies H-C, Kuster W, Mischke D, Reis A. Localization of a locus for the striated form of PPK to chromosome 18q near the desmosomal cadherin gene cluster. Human Molecular Genetics. 1995;4:1015-20.

132. Has C, Jakob T, He Y, Kiritsi D, Hausser I, Bruckner-Tuderman L. Loss of desmoglein 1 associated with palmoplantar keratoderma, dermatitis and multiple allergies. Br J Dermatol. 2015;172(1):257-61. Epub 2014/07/22. doi: 10.1111/bjd.13247. PubMed PMID: 25041099.

133. Stahley SN, Bartle EI, Atkinson CE, Kowalczyk AP, Mattheyses AL. Molecular organization of the desmosome as revealed by direct stochastic optical reconstruction microscopy. J Cell Sci. 2016;129(15):2897-904. Epub 2016/08/10. doi: 10.1242/jcs.185785. PubMed PMID: 27505428; PMCID: PMC5004873.

134. Stahley SN, Warren MF, Feldman RJ, Swerlick RA, Mattheyses AL, Kowalczyk AP. Super-Resolution Microscopy Reveals Altered Desmosomal Protein Organization in Tissue from Patients with Pemphigus Vulgaris. J Invest Dermatol. 2016;136(1):59-66. Epub 2016/01/15. doi: 10.1038/JID.2015.353. PubMed PMID: 26763424; PMCID: PMC4730957.

135. Nelson MPaWJ. Regulation of desmosome assembly in epithelial cells- kinetics of synthesis, transport, and stabilization of dsgI, a major protein of the membrane core domain. The Journal of Cell Biology. 1989;109:163-77. doi: 10.1083/jcb.109.1.163.

136. Kim DE, Chivian D, Baker D. Protein structure prediction and analysis using the Robetta server. Nucleic Acids Res. 2004;32(Web Server issue):W526-31. Epub 2004/06/25. doi: 10.1093/nar/gkh468. PubMed PMID: 15215442; PMCID: PMC441606.

137. Akbar A, Prince C, Payne C, Fasham J, Ahmad W, Baple EL, Crosby AH, Harlalka GV, Gul A. Novel nonsense variants in SLURP1 and DSG1 cause palmoplantar keratoderma in Pakistani families. BMC Med Genet. 2019;20(1):145. Epub 2019/08/25. doi: 10.1186/s12881-019-0872-1. PubMed PMID: 31443639; PMCID: PMC6708247.

138. Abi Zamer B, Mahfood M, Saleh B, Al Mutery AF, Tlili A. Novel mutation in the DSG1 gene causes autosomal-dominant striate palmoplantar keratoderma in a large Syrian family. Ann Hum Genet. 2019;83(6):472-6. Epub 2019/06/14. doi: 10.1111/ahg.12335. PubMed PMID: 31192455.

139. Parks GD, Lamb RA. Role of NH2-terminal positively charged residues in estabishing membrane protein topology. The Journal of Biological Chemistry. 1993;268:19101-9.

140. Reddy T, Manrique S, Buyan A, Hall BA, Chetwynd A, Sansom MS. Primary and secondary dimer interfaces of the fibroblast growth factor receptor 3 transmembrane domain: characterization via multiscale molecular dynamics simulations. Biochemistry. 2014;53(2):323-32. Epub 2014/01/09. doi: 10.1021/bi401576k. PubMed PMID: 24397339; PMCID: PMC4871223.

141. Elazar A, Weinstein J, Biran I, Fridman Y, Bibi E, Fleishman SJ. Mutational scanning reveals the determinants of protein insertion and association energetics in the plasma membrane. Elife. 2016;5. Epub 2016/01/30. doi: 10.7554/eLife.12125. PubMed PMID: 26824389; PMCID: PMC4786438.

142. Partridge AW, Therien AG, Deber CM. Missense mutations in TMD- phenotypic propensity of polar residues for human disease. Proteins. 2004;54:648-56.

143. Ojemalm K, Higuchi T, Lara P, Lindahl E, Suga H, von Heijne G. Energetics of side-chain snorkeling in transmembrane helices probed by nonproteinogenic amino acids. Proc Natl Acad Sci U S A. 2016;113(38):10559-64. Epub 2016/09/08. doi: 10.1073/pnas.1606776113. PubMed PMID: 27601675; PMCID: PMC5035864.

144. Schow EV, Freites JA, Cheng P, Bernsel A, von Heijne G, White SH, Tobias DJ. Arginine in membranes: the connection between molecular dynamics simulations and translocon-mediated insertion experiments. J Membr Biol. 2011;239(1-2):35-48. Epub 2010/12/04. doi: 10.1007/s00232-010-9330-x. PubMed PMID: 21127848; PMCID: PMC3030942.

145. Jaud S, Fernandez-Vidal M, Nilsson I, Meindl-Beinker NM, Hubner NC, Tobia DJ, Heijne Gv, White SH. Insertion of short transmembrane helices by the Sec61 translocon. PNAS. 2009;106:11588-93.

146. Hessa T, Kim H, Bihlmaier K, Lundin C, Boekel J, Anderson H, Nilsson I, White SH, Heijne Gv. Recognition of transmembrane helices by the ER translocon. Nature. 2005;433:377-81.

147. Hessa T, Meindl-Beinker NM, Bernsel A, Kim H, Sato Y, Lerch-Bader M, Nilsson I, White SH, von Heijne G. Molecular code for transmembrane-helix recognition by the Sec61 translocon. Nature. 2007;450(7172):1026-30. Epub 2007/12/14. doi: 10.1038/nature06387. PubMed PMID: 18075582.

148. Dorairaj S, Allen TW. On the thermodyanimc stability of a charged arginine side chain in a transmembrane helix. PNAS. 2007;104:4943-8.

149. Lorent JH, Levental KR, Ganesan L, Rivera-Longsworth G, Sezgin E, Doktorova M, Lyman E, Levental I. Plasma membranes are asymmetric in lipid unsaturation, packing and protein shape. Nat Chem Biol. 2020. Epub 2020/05/06. doi: 10.1038/s41589-020-0529-6. PubMed PMID: 32367017.

150. Wan H, Dopping-Hepenstal P, Gratian M, Stone M, McGrath J, Eady R. Desmosomes exhibit site-specific features in human palm skin. Experimental Dermatology. 2003;12:378-88.

151. Hammers CM, Stanley JR. Desmoglein-1, differentiation, and disease. J Clin Invest. 2013;123(4):1419-22. Epub 2013/03/26. doi: 10.1172/JCI69071. PubMed PMID: 23524961; PMCID: PMC3613937.

152. The PyMOL Molecular Graphics System VS, LLC.

153. Daniotti JL, Pedro MP, Valdez Taubas J. The role of S-acylation in protein trafficking. Traffic. 2017. doi: 10.1111/tra.12510.

154. Green KJ, Roth-Carter Q, Niessen CM, Nichols SA. Tracing the Evolutionary Origin of Desmosomes. Curr Biol. 2020;30(10):R535-R43. Epub 2020/05/20. doi: 10.1016/j.cub.2020.03.047. PubMed PMID: 32428495; PMCID: PMC7310670.

155. Gonzalez Montoro A, Bigliani G, Valdez Taubas J. The shape of the transmembrane domain is a novel endocytosis signal for single-spanning membrane proteins. J Cell Sci. 2017;130(22):3829-38. Epub 2017/10/04. doi: 10.1242/jcs.202937. PubMed PMID: 28972131.

156. Bywater RP, Thomas D, Vriend G. A sequence and structural study of transmembrane helices. Journal of Computer-Aided Molecular Design. 2001;15:533-52.

157. Ulmschneider MB, Sansom MSP. Amino acid distributions in integral membrane protein structures. Biochimica et Biophysica Acta. 2001;1512:1-14.

158. Sansom MS, Weinstein H. Hinges, swivels, and switches- the role of prolines in signaling via transmebrane a-helices. Trends in Pharmacological Sciences. 2000;21:445-51.

159. Jacob J, Duclohier H, Cafiso DS. The role of proline and glycine in determining the backbone flexibility of a channel-forming peptide. Biophysical Journal. 1999;76:1367-76.

160. Kami K, Chidgey M, Dafforn T, Overduin M. The desmoglein-specific cytoplasmic region is intrinsically disordered in solution and interacts with multiple desmosomal protein partners. J Mol Biol. 2009;386(2):531-43. Epub 2009/01/13. doi: 10.1016/j.jmb.2008.12.054. PubMed PMID: 19136012.

161. Levitt M. Conformation preferences of amino acids in globular proteins. American Chemical Society. 1978;17(20):4277-85.

162. Cordes FS, Bright JN, Sansom MSP. Proline-induced Distortions of Transmembrane Helices. Journal of Molecular Biology. 2002;323(5):951-60. doi: 10.1016/s0022-2836(02)01006-9.

163. Baker JA, Wong WC, Eisenhaber B, Warwicker J, Eisenhaber F. Charged residues next to transmembrane regions revisited: "Positive-inside rule" is complemented by the "negative inside depletion/outside enrichment rule". BMC Biol. 2017;15(1):66. Epub 2017/07/26. doi: 10.1186/s12915-017-0404-4. PubMed PMID: 28738801; PMCID: PMC5525207.

164. Yohannan S, Yang D, Faham S, Boulting G, Whitelegge J, Bowie JU. Proline substitutions are not easily accommodated in a membrane protein. J Mol Biol. 2004;341(1):1-6. Epub 2004/08/18. doi: 10.1016/j.jmb.2004.06.025. PubMed PMID: 15312757.

165. Lu KP, Finn G, Lee TH, Nicholson LK. Prolyl cis-trans isomerization as a molecular timer. Nat Chem Biol. 2007;3(10):619-29. Epub 2007/09/19. doi: 10.1038/nchembio.2007.35. PubMed PMID: 17876319.

166. Stewart DE, Sarkar A, Wampler JE. Occurence and role of cis peptide bonds in protein structures. Journal of Molecular Biology. 1990;214(1):253-60.

167. Pal D, Chakrabarti P. Cis peptide bonds in proteins- residues involved, their conformations, interactions, and locations. Journal of Molecular Biology. 1999;294:2710288.

168. Zondlo NJ. Aromatic-proline interactions: electronically tunable CH/pi interactions. Acc Chem Res. 2013;46(4):1039-49. Epub 2012/11/15. doi: 10.1021/ar300087y. PubMed PMID: 23148796; PMCID: PMC3780429.

169. Thomas KM, Naduthambi D, Zondlo NJ. Electronic control of amide cis-trans isomerizm via the aromatic-prolyl interaction. Journal of American Chemical Society. 2006;128(7):2216-7. Epub 2005/10/07. doi: 10.1002/bip.20382. PubMed PMID: 16208767.

170. Lang K, Scmid FX, Fischer G. Catalysis of protein folding by prolyl isomerase. Nature. 1987;329:268-70.

171. Lawen A. Biosynthesis of cyclosporins and other natural peptidyl prolyl cis/trans isomerase inhibitors. Biochim Biophys Acta. 2015;1850(10):2111-20. Epub 2014/12/17. doi: 10.1016/j.bbagen.2014.12.009. PubMed PMID: 25497210.

172. Hennig L, Christner C, Kipping M, Schelbert B, Rυcknagel KP, Grabley S, Kullertz G, Fischer G. Selective inactivation of parvulin-like peptidyl-prolyl cis-trans isomerases by juglone. Biochemistry. 1998;37:5953-60.

173. Gothel SF, Marahiel MA. Peptidyl-prolyl cis-trans isomerases, a superfamily of ubiquitous folding catalysts. Cellular and Molecular Life Sciences. 1999;55:423-36.

174. Rudd KE, Sofia HJ, Koonin EV, III GP, Lazar S, Rouviere PE. A new family of peptidyl-prolyl isomerases. Trends Biochem Sci. 1995;20(1):12-4.

175. Badu-Nkansah KA, Lechler T. Proteomic analysis of desmosomes reveals novel components required for epidermal integrity. Mol Biol Cell. 2020;31(11):1140-53. Epub 2020/04/03. doi: 10.1091/mbc.E19-09-0542. PubMed PMID: 32238101; PMCID: PMC7353166.

176. Uhlen M, Fagerberg L, Hallstrom BM, Lindskog C, Oksvold P, Mardinoglu A, Sivertsson A, Kampf C, Sjostedt E, Asplund A, Olsson I, Edlund K, Lundberg E, Navani S, Szigyarto CA, Odeberg J, Djureinovic D, Takanen JO, Hober S, Alm T, Edqvist PH, Berling H, Tegel H, Mulder J, Rockberg J, Nilsson P, Schwenk JM, Hamsten M, von Feilitzen K, Forsberg M, Persson L, Johansson F, Zwahlen M, von Heijne G, Nielsen J, Ponten F. Proteomics. Tissue-based map of the human proteome. Science. 2015;347(6220):1260419. Epub 2015/01/24. doi: 10.1126/science.1260419. PubMed PMID: 25613900.

177. Thul PJ, Akesson L, Wiking M, Mahdessian D, Geladaki A, Ait Blal H, Alm T, Asplund A, Bjork L, Breckels LM, Backstrom A, Danielsson F, Fagerberg L, Fall J, Gatto L, Gnann C, Hober S, Hjelmare M, Johansson F, Lee S, Lindskog C, Mulder J, Mulvey CM, Nilsson P, Oksvold P, Rockberg J, Schutten R, Schwenk JM, Sivertsson A, Sjostedt E, Skogs M, Stadler C, Sullivan DP, Tegel H, Winsnes C, Zhang C, Zwahlen M, Mardinoglu A, Ponten F, von Feilitzen K, Lilley KS, Uhlen M, Lundberg E. A subcellular map of the human proteome. Science. 2017;356(6340). Epub 2017/05/13. doi: 10.1126/science.aal3321. PubMed PMID: 28495876.

178. Fink A, Sal-Man N, Gerber D, Shai Y. Transmembrane domains interactions within the membrane milieu: principles, advances and challenges. Biochim Biophys Acta. 2012;1818(4):974-83. Epub 2011/12/14. doi: 10.1016/j.bbamem.2011.11.029. PubMed PMID: 22155642.

179. UniProt C. UniProt: the universal protein knowledgebase in 2021. Nucleic Acids Res. 2021;49(D1):D480-D9. Epub 2020/11/26. doi: 10.1093/nar/gkaa1100. PubMed PMID: 33237286; PMCID: PMC7778908.

180. Crooks GE, Hon G, Chandonia JM, Brenner SE. WebLogo: a sequence logo generator. Genome Res. 2004;14(6):1188-90. Epub 2004/06/03. doi: 10.1101/gr.849004. PubMed PMID: 15173120; PMCID: PMC419797.

181. Schneider TD, Stephens RM. Sequence logos- a new way to display consensus sequences. Nucleic Acids Research. 1990;18(20):6097-100.

182. Contreras FX, Ernst AM, Haberkant P, Bjorkholm P, Lindahl E, Gonen B, Tischer C, Elofsson A, von Heijne G, Thiele C, Pepperkok R, Wieland F, Brugger B. Molecular recognition of a single sphingolipid species by a protein's transmembrane domain. Nature. 2012;481(7382):525-9. Epub 2012/01/11. doi: 10.1038/nature10742. PubMed PMID: 22230960.

183. Bjorkholm P, Ernst AM, Hacke M, Wieland F, Brugger B, von Heijne G. Identification of novel sphingolipid-binding motifs in mammalian membrane proteins. Biochim Biophys Acta. 2014;1838(8):2066-70. Epub 2014/05/07. doi: 10.1016/j.bbamem.2014.04.026. PubMed PMID: 24796501.

184. Fantini J, Di Scala C, Evans LS, Williamson PT, Barrantes FJ. A mirror code for protein-cholesterol interactions in the two leaflets of biological membranes. Sci Rep. 2016;6:21907. Epub 2016/02/27. doi: 10.1038/srep21907. PubMed PMID: 26915987; PMCID: PMC4768152.

185. Barrett PJ, Song Y, Horn WDV, Hustedt EJ, Schafer JM, Hadziselimovic A, Peel AJ, Sanders CR. The amyloid precursor protein has a flexible transmembrane domain and binds cholesterol. Science. 2012;336(6085):1168-71. doi: 10.1126/science.1219988.

186. Ng SY, Lee LT, Chow BK. Receptor oligomerization: from early evidence to current understanding in class B GPCRs. Front Endocrinol (Lausanne). 2012;3:175. Epub 2013/01/15. doi: 10.3389/fendo.2012.00175. PubMed PMID: 23316183; PMCID: PMC3539651.

187. Otmar Huber RK, and Dieter Langosch. Mutations affecting transmembrane segment interactions impair adhesiveness of E-cadherin. Journal of Cell Science. 1999;112:4415-23. PubMed PMID: 10564659.

188. Megan L. Plotkowski SK, Martin L. Phillips, Anthony W. Partridge, Charles M. Deber, and James U. Bowie. Transmembrane domain of myelin protein zero can form dimers: possible implications for myelin construction. Biochemistry. 2007;46:12164-73.

189. Teese MG, Langosch D. Role of GxxxG Motifs in Transmembrane Domain Interactions. Biochemistry. 2015;54(33):5125-35. Epub 2015/08/06. doi: 10.1021/acs.biochem.5b00495. PubMed PMID: 26244771.

190. Gurezka R, Laage R, Brosig B, Langosch D. A heptad motif of leucine residues found in membrane proteins can drive self-assembly of artifical transmembrane segments. The Journal of Biological Chemistry. 1999;274(14):9265-70.

191. Sal-Man N, Gerber D, Shai Y. The identification of a minimal dimerization motif QXXS that enables homo- and hetero-association of transmembrane helices in vivo. J Biol Chem. 2005;280(29):27449-57. Epub 2005/05/25. doi: 10.1074/jbc.M503095200. PubMed PMID: 15911619.

192. Sal-Man N, Gerber D, Shai Y. The composition rather than position of polar residues (QxxS) drives aspartate receptor transmembrane domain dimerization in Vivo. Biochemistry. 2004;43:2309-13.

193. Sal-Man N, Gerber D, Shai Y. Proline localized to the interaction interface can mediate self-association of transmembrane domains. Biochim Biophys Acta. 2014;1838(9):2313-8. Epub 2014/05/21. doi: 10.1016/j.bbamem.2014.05.006. PubMed PMID: 24841754.

194. Gurezka R, Langosch D. In vitro selection of membrane-spanning leucine zipper protein-protein interaction motifs using POSSYCCAT. J Biol Chem. 2001;276(49):45580-7. Epub 2001/10/05. doi: 10.1074/jbc.M105362200. PubMed PMID: 11585820.

195. Russ WP, Engelman DM. TOXCAT- a measure of transmembrane helix association in a biological membrane. Proc Natl Acad Sci U S A. 1999;96:863-8.

196. Su PC, Berger BW. Identifying key juxtamembrane interactions in cell membranes using AraC-based transcriptional reporter assay (AraTM). J Biol Chem. 2012;287(37):31515-26. Epub 2012/07/24. doi: 10.1074/jbc.M112.396895. PubMed PMID: 22822084; PMCID: PMC3438984.

197. Chen LY, Yang-Yen HF, Tsai CC, Thio CL, Chuang HL, Yang LT, Shen LF, Song IW, Liu KM, Huang YT, Liu FT, Chang YJ, Chen YT, Yen JJY. Protein Palmitoylation by ZDHHC13 Protects Skin against Microbial-Driven Dermatitis. J Invest Dermatol. 2017;137(4):894-904. Epub 2016/12/27. doi: 10.1016/j.jid.2016.12.011. PubMed PMID: 28017833.

198. Liu KM, Chen YJ, Shen LF, Haddad ANS, Song IW, Chen LY, Chen YJ, Wu JY, Yen JJY, Chen YT. Cyclic Alopecia and Abnormal Epidermal Cornification in Zdhhc13-Deficient Mice Reveal the Importance of Palmitoylation in Hair and Skin Differentiation. J Invest Dermatol. 2015;135(11):2603-10. Epub 2015/06/30. doi: 10.1038/jid.2015.240. PubMed PMID: 26121212.

199. Woodley KT, Collins MO. S-acylated Golga7b stabilises DHHC5 at the plasma membrane to regulate cell adhesion. EMBO Rep. 2019;20(10):e47472. Epub 2019/08/14. doi: 10.15252/embr.201847472. PubMed PMID: 31402609; PMCID: PMC6776912.

200. Liu JS, Fan LL, Li JJ, Xiang R. Whole-Exome Sequencing Identifies a Novel Mutation of Desmocollin 2 in a Chinese Family With Arrhythmogenic Right Ventricular Cardiomyopathy. Am J Cardiol. 2017;119(9):1485-9. Epub 2017/03/04. doi: 10.1016/j.amjcard.2017.01.011. PubMed PMID: 28256248.

201. Brodehl A, Stanasiuk C, Anselmetti D, Gummert J, Milting H. Incorporation of desmocollin-2 into the plasma membrane requires N-glycosylation at multiple sites. FEBS Open Bio. 2019;9(5):996-1007. Epub 2019/04/04. doi: 10.1002/2211-5463.12631. PubMed PMID: 30942563; PMCID: PMC6487837.

202. Nekrasova OE, Amargo EV, Smith WO, Chen J, Kreitzer GE, Green KJ. Desmosomal cadherins utilize distinct kinesins for assembly into desmosomes. J Cell Biol. 2011;195(7):1185-203. Epub 2011/12/21. doi: 10.1083/jcb.201106057. PubMed PMID: 22184201; PMCID: PMC3246898.

203. Shafraz O, Xie B, Yamada S, Sivasankar S. Mapping transmembrane binding partners for E-cadherin ectodomains. Proc Natl Acad Sci U S A. 2020;117(49):31157-65. Epub 2020/11/25. doi: 10.1073/pnas.2010209117. PubMed PMID: 33229577; PMCID: PMC7733791.

204. Baumgartner W, Wendeler MW, Weth A, Koob R, Drenckhahn D, Gessner R. Heterotypic trans-interaction of LI- and E-cadherin and their localization in plasmalemmal microdomains. J Mol Biol. 2008;378(1):44-54. Epub 2008/03/18. doi: 10.1016/j.jmb.2008.02.023. PubMed PMID: 18342884.

205. Lewis JE, Wahl JK, Sass KM, Jensen PJ, Johnson KR, Wheelock MJ. Cross-talk between adherens junctions and desmosomes depends on plakoglobin. The Journal of Cell Biology. 1997;136(4):919-34.

206. Chum T, Glatzová D, Kvíčalová Z, Malínský J, Brdička T, Cebecauer M. The role of palmitoylation and transmembrane domain in sorting of transmembrane adaptor proteins. Journal of Cell Science. 2016;129(15):3053-. doi: 10.1242/jcs.194209.

207. Michels C, Aghdam SY, Niessen CM. Cadherin-mediated regulation of tight junctions in stratifying epithelia. Ann N Y Acad Sci. 2009;1165:163-8. Epub 2009/06/23. doi: 10.1111/j.1749-6632.2009.04443.x. PubMed PMID: 19538302.

208. Shigetomi K, Ono Y, Inai T, Ikenouchi J. Adherens junctions influence tight junction formation via changes in membrane lipid composition. J Cell Biol. 2018;217(7):2373-81. Epub 2018/05/04. doi: 10.1083/jcb.201711042. PubMed PMID: 29720382; PMCID: PMC6028530.

209. Van Itallie CM, Gambling TM, Carson JL, Anderson JM. Palmitoylation of claudins is required for efficient tight-junction localization. J Cell Sci. 2005;118(Pt 7):1427-36. Epub 2005/03/17. doi: 10.1242/jcs.01735. PubMed PMID: 15769849.

210. Heiler S, Mu W, Zoller M, Thuma F. The importance of claudin-7 palmitoylation on membrane subdomain localization and metastasis-promoting activities. Cell Commun Signal. 2015;13:29. Epub 2015/06/10. doi: 10.1186/s12964-015-0105-y. PubMed PMID: 26054340; PMCID: PMC4459675.

211. Rajagopal N, Irudayanathan FJ, Nangia S. Palmitoylation of Claudin-5 Proteins Influences Their Lipid Domain Affinity and Tight Junction Assembly at the Blood-Brain Barrier Interface. J Phys Chem B. 2019;123(5):983-93. Epub 2019/01/11. doi: 10.1021/acs.jpcb.8b09535. PubMed PMID: 30629442.

212. Yokoyama S, Tachibana K, Nakanishi H, Yamamoto Y, Irie K, Mandai K, Nagafuchi A, Monden M, Takai Y. a-Catenin-indepedent recruitment of ZO-1 to nectin-based cell-cell adhesion sites through afadin. Molecular Biology of the Cell. 2001;12:1595-609.

213. Ooshio T, Kobayashi R, Ikeda W, Miyata M, Fukumoto Y, Matsuzawa N, Ogita H, Takai Y. Involvement of the interaction of afadin with ZO-1 in the formation of tight junctions in Madin-Darby canine kidney cells. J Biol Chem. 2010;285(7):5003-12. Epub 2009/12/17. doi: 10.1074/jbc.M109.043760. PubMed PMID: 20008323; PMCID: PMC2836104.

214. Sacco PA, McGranahan TM, Wheelock MJ, Johnson KR. Identification of plakoglobin domains required for association with N-cadherin and alpha-catenin. The Journal of Biological Chemistry. 1995;270(34):20201-6.

215. Wahl JK, Sacco PA, McGranahan-Sadler TM, Sauppe LM, Wheelock MJ, Johnson KR. Plakoglobin domains that define its association with the desmosomal cadherins and the classical cadherins: identification of unique and shared domains. Journal of Cell Science. 1996;109:1143-54.

216. Palka HL, Green KJ. Roles of plakoglobin end domains in desmosome assembly. Journal of Cell Science. 1997;110:2359-71.

217. Chitaev NA, Averbakh AZ, Troyanovsky RB, Troyanovsky SM. Molecular organization of the desmoglein-plakoglobin complex. Journal of Cell Science. 1998;111:1941-9.

218. Kowalczyk AP, Bornslaeger EA, Borgwardt JE, Palka HL, Dhaliwal AS, Corcoran CM, Denning MF, Green KJ. The amino-terminal domain of desmoplakin binds to plakoglobin and

clusters desmosomal cadherin-plakoglobin complexes. The Journal of Cell Biology. 1997;139(3):773-84.

219. Loranger A, Gilbert S, Brouard JS, Magin TM, Marceau N. Keratin 8 modulation of desmoplakin deposition at desmosomes in hepatocytes. Exp Cell Res. 2006;312(20):4108-19. Epub 2006/11/28. doi: 10.1016/j.yexcr.2006.09.031. PubMed PMID: 17126832.

220. Kroger C, Loschke F, Schwarz N, Windoffer R, Leube RE, Magin TM. Keratins control intercellular adhesion involving PKC-alpha-mediated desmoplakin phosphorylation. J Cell Biol. 2013;201(5):681-92. Epub 2013/05/22. doi: 10.1083/jcb.201208162. PubMed PMID: 23690176; PMCID: PMC3664716.

221. Bar J, Kumar V, Roth W, Schwarz N, Richter M, Leube RE, Magin TM. Skin fragility and impaired desmosomal adhesion in mice lacking all keratins. J Invest Dermatol. 2014;134(4):1012-22. Epub 2013/10/15. doi: 10.1038/jid.2013.416. PubMed PMID: 24121403.

222. Watt FM, Mattey DL, Garrod DR. Calcium-induced reorganization of desmosomal components in cultured human keratinocytes. The Journal of Cell Biology. 1984;99:2211-5.

223. Garrod DR, Berika MY, Bardsley WF, Holmes D, Tabernero L. Hyper-adhesion in desmosomes: its regulation in wound healing and possible relationship to cadherin crystal structure. J Cell Sci. 2005;118(Pt 24):5743-54. Epub 2005/11/24. doi: 10.1242/jcs.02700. PubMed PMID: 16303847.

224. Kimura TE, Merritt AJ, Garrod DR. Calcium-independent desmosomes of keratinocytes are hyper-adhesive. J Invest Dermatol. 2007;127(4):775-81. Epub 2006/12/30. doi: 10.1038/sj.jid.5700643. PubMed PMID: 17195016.

225. Hobbs RP, Green KJ. Desmoplakin regulates desmosome hyperadhesion. J Invest Dermatol. 2012;132(2):482-5. Epub 2011/10/14. doi: 10.1038/jid.2011.318. PubMed PMID: 21993560; PMCID: PMC3461275.

226. Wallis S, Lloyd S, Wise I, Ireland G, Fleming TP, Garrod D. The alpha isoform of protein kinase C is involved in signaling the response of desmosomes to wounding in cultured epithelial cells. Molecular Biology of the Cell. 2000;11:1077-92.

227. Sheu H-M, Kitajima Y, Yaoita H. Involvement of protein kinase C in translocation of desmoplakins from cytosol to plasma membrane during desmosome formation in human squamous cell carcinoma cells grown in low to normal calcium concentration. Experimental Cell Research. 1989;185:176-90.

228. Hengel Jv, Gohon L, Bruyneel E, Vermeulen S, Cornelissen M, Mareel M, Roy Fv. Protein kinase C activation upregulates intercellular adhesion of alpha-catenin-negative human colon cancer cell variants via induction of desmosomes. The Journal of Cell Biology. 1997;137(5):1103-16.

229. Bartle EI, Rao TC, Beggs RR, Dean WF, Urner TM, Kowalczyk AP, Mattheyses AL. Protein exchange is reduced in calcium-independent epithelial junctions. J Cell Biol.

2020;219(6). Epub 2020/05/14. doi: 10.1083/jcb.201906153. PubMed PMID: 32399559; PMCID: PMC7265307.

230. Bartle EI, Urner TM, Raju SS, Mattheyses AL. Desmoglein 3 Order and Dynamics in Desmosomes Determined by Fluorescence Polarization Microscopy. Biophys J. 2017;113(11):2519-29. Epub 2017/12/07. doi: 10.1016/j.bpj.2017.09.028. PubMed PMID: 29212005; PMCID: PMC5768488.

231. Calay D, Vind-Kezunovic D, Frankart A, Lambert S, Poumay Y, Gniadecki R. Inhibition of Akt signaling by exclusion from lipid rafts in normal and transformed epidermal keratinocytes. J Invest Dermatol. 2010;130(4):1136-45. Epub 2010/01/08. doi: 10.1038/jid.2009.415. PubMed PMID: 20054340.

232. Jans R, Atanasova G, Jadot M, Poumay Y. Cholesterol depletion upregulates involucrin expression in epidermal keratinocytes through activation of p38. J Invest Dermatol. 2004;123(3):564-73. Epub 2004/08/12. doi: 10.1111/j.0022-202X.2004.23221.x. PubMed PMID: 15304097.

233. Lambert S, Ameels H, Gniadecki R, Herin M, Poumay Y. Internalization of EGF receptor following lipid rafts disruption in keratinocytes is delayed and dependent on p38 MAPK activation. J Cell Physiol. 2008;217(3):834-45. Epub 2008/08/30. doi: 10.1002/jcp.21563. PubMed PMID: 18727093.

234. Giltaire S, Lambert S, Poumay Y. HB-EGF synthesis and release induced by cholesterol depletion of human epidermal keratinocytes is controlled by extracellular ATP and involves both p38 and ERK1/2 signaling pathways. J Cell Physiol. 2011;226(6):1651-9. Epub 2011/03/18. doi: 10.1002/jcp.22496. PubMed PMID: 21413023.

235. Mathay C, Giltaire S, Minner F, Bera E, Herin M, Poumay Y. Heparin-binding EGF-like growth factor is induced by disruption of lipid rafts and oxidative stress in keratinocytes and participates in the epidermal response to cutaneous wounds. J Invest Dermatol. 2008;128(3):717-27. Epub 2007/10/12. doi: 10.1038/sj.jid.5701069. PubMed PMID: 17928891.

236. Lambert S, Vind-Kezunovic D, Karvinen S, Gniadecki R. Ligand-independent activation of the EGFR by lipid raft disruption. J Invest Dermatol. 2006;126(5):954-62. Epub 2006/02/04. doi: 10.1038/sj.jid.5700168. PubMed PMID: 16456534.